University of Padova
Department of Information Engineering

Ph.D. School on Information Engineering

Information and Communication Science and Technologies (I.C.T.)

XXIII Cycle

Spatio-temporal Spectrum Reuse based on Channel Gain Cartography

Emiliano Dall'Anese

Ph.D. School Director:

Prof. M. Bertocco

Advisor:

Prof. S. Pupolin

Co-Advisor:

Prof. G. B. Giannakis

Academic Year 2010–2011

Padova, December 2010.

to my parents, Giulia, and Nikki

ai miei genitori, Giulia, e Nikki

Abstract

During the last decade, the perceived scarcity of spectrum resources along with the proliferation of new wireless technologies have motivated a substantial research effort on dynamic spectrum management. Although a fixed frequency assignment policy has guiltily led to an alarming spectrum crowding belief, a noticeable underutilization of the allocated frequency bands has been revealed by extensive spectrum occupancy measurements. Therefore, a dynamic re-utilization of the licensed frequencies would be a breakthrough toward a mitigation of the troublesome inefficiency in the spectrum management, aggressively answering to the unceasing demand of resources for new wireless services.

Prominent in this context is the hierarchical spectrum access, an emerging model that envisages secondary users (a.k.a. cognitive radios) aiming to access to the frequency bands of the licensed systems (a.k.a. primary users) in a dynamical and nonintrusive manner. Envisioned as autonomous entities endowed with learning and decisional capabilities, secondary devices accomplish spectrum sensing and dynamical radio resource allocation tasks, thus enabling an opportunistic access to portions of the spectrum under the primary-secondary hierarchy.

The consequent continuous need for a concrete situational awareness required by the cognitive radios demands for innovative signal processing algorithms for high-resolution primary users' activity monitoring, efficient transmission opportunity exploitation and, most importantly, accurate characterization of the surrounding RF propagation environment. Due to the lack of explicit coordination between the two networks, as envisaged in the cognitive radio paradigm, learning the features of the propagation environment is conceivably critical for adaptation of operational system parameters and obligatory protection of the licensed primary system.

To strike the foregoing sensing and control objectives reliably, a significant departure from a one-dimensional view of the RF environment, conventionally attained by point-to-point feedback strategies to acquire channel coefficients as well as interference levels on a per-link basis, is advocated. Toward this direction the present Thesis introduces the concept of channel gain cartography, a groundbreak-

ing geostatistics-inspired application that enables a portrayal of the RF environment impinging upon arbitrary locations in space. The most appealing feature of the proposed tool consists in the non-trivial capability of inferring the channel gain between arbitrary transmitter-receiver locations, based on the only measurements taken among collaborating cognitive radios. Such ability in estimating any-to-any channel gains may open the door to aggressive resource allocation techniques, thus leading to markedly higher spectral efficiency - and finds well-motivated applications not only in the cognitive radio context.

With an accurate RF environment description close at hand, the Thesis presents a primary system's state tracker based on a parsimonious model accounting for the reasonable sparse activity of the primary sources - due to well-known mutual interference concerns - in the monitored geographical area. Motivated by recent advances in sparse linear regression, where the ℓ_1-norm places itself as a cornerstone for lassoing the non-zero support of the estimand, a sparsity-cognizant state tracker is developed in both centralized and distributed formats. As a byproduct ensued from the parsimonious model, the tracker possesses localization and primary transmission power estimation abilities, which lead to a capability of estimating the actual power spectral density map of the primary system, a continuously-updated portrayal of the aggregate primary power impinging upon the whole monitored geographical region. Detection of the so called spectrum spatial holes is efficiently attainable, thus enhancing the spatial re-use of the primary frequency bands.

Due to the aforementioned lack of explicit support from the primary system, sensing algorithms often face difficulty in acquiring secondary-to-primary users channels. Moreover, the sensing algorithms cannot detect silent licensed receivers, which nevertheless have to be obligatorily protected. Based on primary coverage map and channel gain cartography, the approach pursued here is to exploit statistical knowledge of the secondary-to-primary channels, where the combined effect of shadow fading as well as small-scale fading is accounted for, to maximize a given secondary network utility function under chance constraints that ensure protection to any potential licensed user. Albeit a non-convex interference-constrained network utility maximization problem is derived, Karush-Kuhn-Tucker solutions are provably obtained by the proposed algorithms.

Error-corrupted measurements and missing and/or outdated channel gain estimates may undoubtedly compromise the accomplishment of the power control task. To overcome this issue, a novel probabilistic approach encompassing channel knowledge uncertainty on both secondary-to-secondary and secondary-to-primary links is also presented.

The foregoing technical findings are fully corroborated by numerical tests.

Sommario

Durante l'ultimo decennio, la proliferazione di nuove tecnologie wireless, unitamente all'apparente scarsità di risorse spettrali disponibili, ha motivato una considerevole attività di ricerca rivolta a tecniche di gestione dinamica dello spettro. Sebbene una allocazione statica dello spettro abbia colpevolmente indotto alla percezione di un preoccupante sovraffollamento delle bande disponibili, un sostanziale sottoutilizzo di tali frequenze è stato rilevato durante campagne di misurazione dell'occupazione effettiva di bande di frequenza ad uso esclusivo. Un riutilizzo dinamico di tali frequenze potrebbe essere un passo in avanti fondamentale per risolvere l'attuale sistematica inefficienza nella gestione dello spettro e, quindi, rispondere alla continua richiesta di risorse spettrali per nuovi sistemi wireless.

In questo contesto si posiziona in maniera prominente il modello ad accesso gerarchico, modello che prevede utenti secondari (chiamati anche cognitive radio) che accedono alle bande di frequenza allocate agli utenti licenziatari (chiamati comunemente utenti primari) in maniera dinamica e non intrusiva. Immaginati come entità autonome con capacità decisionali e di apprendimento dell'ambiente di propagazione, gli utenti secondari sono in grado di riutilizzare porzioni dello spettro in maniera opportunistica, rispettando la gerarchia tra sistemi licenziatari e sistemi secondari. Operazioni necessarie per tale accesso opportunistico sono il sensing dello spettro e l'allocazione dinamica delle risorse radio disponibili.

Il conseguente bisogno di una continua cognizione situazionale da parte degli utenti secondari richiede soluzioni algoritmiche innovative per monitorare l'attività degli utenti primari in maniera affidabile, utilizzare efficientemente le porzioni di spettro quando libere, e acquisizione di un'accurata caratterizzazione dell'ambiente di propagazione. Infatti, data la mancanza di una cooperazione esplicita tra sistemi primario e secondario, il continuo apprendimento delle caratteristiche dell'ambiente di propagazione è di fondamentale importanza per l'adattamento dei parametri di sistema e la protezione obbligatoria del sistema primario.

Per compiere in maniera affidabile sensing e allocazione dinamica delle risorse disponibili è richiesto un significativo scostamento dalla visione uni-dimensionale

dell'ambiente di propagazione, la quale si basa sulle tecniche classiche di stima di canale e acquisizione dei livelli di interferenza via feedback su collegamenti punto-punto. In questa direzione, la presente tesi introduce il concetto di cartografia del guadagno di canale, una tecnica innovativa con origini dalla geostatistica che permette l'acquisizione di una descrizione completa dell'ambiente di propagazione percepito in punti arbitrari di una regione geografica. La caratteristica principale di tale tecnica consiste nella capacità di stimare il guadagno di canale tra coppie arbitrarie trasmettitore-ricevitore, partendo da delle misurazioni effettuate sui soli link tra cognitive radio cooperanti.

Con un'accurata descrizione dell'ambiente di propagazione a portata di mano, nella tesi viene introdotto un algoritmo per la stima della potenza trasmissiva degli utenti licenziatari attivi e la loro localizzazione. L'algoritmo è basato su un modello di sistema parsimonioso che tiene in considerazione la sparsità nel dominio spaziale di utenti primari attivi, sparsità che è strettamente legata a fenomeni ben noti di interferenza mutua. La stima della potenza trasmissiva degli utenti primari, della loro posizione geografica e, infine, del loro atlante del guadagno di canale, permettono la ricostruzione dell'area di copertura del sistema primario e, conseguentemente, la rivelazione delle aree geografiche in cui le frequenze primarie sono inutilizzate. In questo caso, l'atlante del guadagno di canale permette si superare la classica semplificazione circolare e tempo invariante dell'area di copertura.

Data la mancanza di una cooperazione esplicita tra i due sistemi, la stima dei canali di comunicazione tra utenti primari e secondari non puó essere effettuata; inoltre, gli algoritmi di sensing classici possono rivelare la presenza di trasmettitori primari ma non dei ricevitori primari, i quali devono essere obbligatoriamente protetti. Per superare tali ostacoli, e garantire la protezione degli utenti primari da interferenza causata dai trasmettitori secondari, l'approccio seguito nella tesi prevede l'utilizzo della stima dell'area di copertura e della descrizione statistica dei canali tra utenti primari e secondari, in modo tale da garantire che la probabilità di interferenza sia tenuta sotto una certa soglia in tutte le posizioni geografiche in cui ricevitori primari possono risiedere. Anche se il problema di massimizzazione della funzione di utilità della rete secondaria, sotto vincoli probabilistici che limitano l'interferenza causata al sistema primario, risulta essere non convesso, l'algoritmo proposto nella tesi dimostra una sicura convergenza a un punto di minimo (almeno) locale. Inoltre, in un contesto come quello ad accesso gerarchico, anche i canali tra gli utenti secondari possono non essere stimati correttamente. Un nuovo approccio comprendente vincoli probabilistici sia sull'interferenza arrecata al sistema primario che sugli eventi di outage sui collegamenti tra utenti secondari è quindi proposto.

Tutti i risultati ricavati nella tesi sono corroborati via simulazioni numeriche.

Contents

List of Figures

List of Tables

Chapter 1

Introduction

The conventional license-based fixed frequency assignment policy has led to an alarming spectrum crowding belief and, thus, an apparent scarcity of spectral resources for next-generation wireless systems. Nonetheless, a substantial underutilization of a large swath of licensed bands was revealed in recent spectrum occupancy measurements, thus indicating that the culprit for such perceived scarcity of spectral resources is the exclusive-use spectrum management policy rather than the physical lack of usable frequencies.

To mitigate such cumbersome inefficiency in the current management of the licensed spectrum, and in a tentative that strives for making some room in the spectrum allocation chart for emerging wireless technologies, new spectrum management policies and access techniques have been the subject of research efforts in the last decade or so. The underlying idea behind the flurry of exciting activities envisions an improvement of the spectrum utilization upon permitting a conceivable dynamical access to the licensed bands on either a negotiated or an opportunistic basis, but without compromising the transmission opportunities granted to the licensed users.

The present thesis focuses on the hierarchical access model, probably the most appreciated model thank to an envisaged coexistence of licensed and secondary users without the demand for new network infrastructures or new spectrum rights regulations. As the secondary users are envisioned as entities endowed with learning and decisional capabilities, able to opportunistically and dynamically reuse the under-utilized primary bands in

an autonomous and non-intrusive manner, several new challenges have to be addressed compared to conventional wireless networking setups. A comprehensive description of the hierarchical access model along with its main critical challenges are provided in chapter 2. Also, chapter 2 explains the ambitious vision that motivated the research activities subject of the ensuing parts as well as the main contribution of the present dissertation.

With the motivation provided in chapter 2 in mind, chapter 3 collects innovative large-scale channel gain estimation algorithms that permit acquisition of a global, multidimensional view of the RF ambient, with a significant departure from classical channel estimation techniques. The proposed tools will be shown to provide dramatic benefits in the hierarchical access setup, but may find applications also in several other contexts. Then, chapters 4 and 5 present collaborative and adaptive signal processing algorithms that accomplish the objectives of layered sensing and a novel power allocation technique, which cope with the impossibility of estimating the channels between primary and secondary users. All the chapters are self-contained, in the sense that comparison with prior art, formal problem statement and solution approach are meticulously provided, in each chapter.

The technical findings collected in the present thesis were carried out during part of my Ph.D. at the Department of Information Engineering at the University of Padova, under the supervision of Prof. Silvano Pupolin. They are also a result of the collaboration with Prof. Georgios B. Giannakis, who is also my co-supervisor, and the with other members of the SPiNCOM research group during my stay at the University of Minnesota.

1.1 Acknowledgements

First, I would like to thank my supervisor Prof. Silvano Pupolin for his continual support; he allowed me to work quite independently, but he provided encouragement and invaluable guidance at the right times. I am indebted to Prof. Georgios B. Giannakis; his boundless energy, devotion to his research activity and loyalty to his students have been inspirational.

I am grateful to Seung-Jun Kim for the harmonious collaboration and the never-ending rewarding discussions in front of the whiteboard. Thank

to Antonio Assalini for the productive collaboration on some works that are not reported in this thesis. I'm grateful to Daniele Angelosante, Stefano Rinauro, Gonzalo Mateos, Alfonso Cano, Donatello Materassi, Marco Rotoloni and Davide Chiarotto for the lively discussions about several research topics and, most importantly, for their truly friendship.

There is a number of other people I also wish to thank including Antonio G. Marques, Nikolaos Gatsis, Hao Zhu, Vassilis Kekatos, Ketan Rajawat, Juan-Andres Bazerque, Yannis Schizas, Shahrokh Farahmand, Eric Msechu, Pedro Forero, Brian Baingana, Morteza Mardani, Guobing Li, Tomaso Erseghe, Davide Zennaro and Nihar Jindal.

Chapter 2

Spatio-temporal Spectrum Reuse: Principles

Although a fixed frequency assignment policy has led to an alarming spectrum crowding belief, a substantial underutilization of the licensed frequency bands has been revealed by extensive spectrum occupancy measurements. To alleviate such cumbersome inefficiency in the management of the spectrum and make a swath of frequencies available for emerging wireless services, a considerable research effort has focused on dynamic spectrum re-utilization techniques. Prominent in this context is the hierarchical spectrum access, where cognitive radios aim to make a spatio-temporal re-use of the licensed bands in an autonomous and non-intrusive manner. To this end, cognitive radio devices have to accomplish to spectrum sensing and dynamical radio resource allocation tasks for transmission opportunity detection and exploitation. Although many issues in technical, regulatory and economical aspects still need to be addressed, research efforts have made to devise innovative signal processing algorithms able to cope with new challenges entailed by a practical implementation of the hierarchical access model.

2.1 Motivation for Dynamic Spectrum Access

Traditionally, frequency assignment policy has regulated allocation of portions of the spectrum in a fixed manner, where non-overlapping swaths of

bandwidth were granted to existing wireless systems for exclusive use. This rigid spectrum-licensing policy has the vivid merit of ruling out mutual interference concerns among heterogeneous systems but, however, it has guiltily led to an alarming perception of scarcity of available spectrum resources for emerging wireless technologies. Such belief is certainly strengthened when it comes to look for available frequencies in both the overly-crowded U.S. frequency allocation chart and its European counterpart.

Nonetheless, a substantial underutilization of a large amount of licensed frequency bands was revealed in recent extensive spectrum occupancy measurements, thus indicating that the current utilization of the spectrum is grossly inefficient [1]; in other words, measurements pointed out that at any given time instant and geographical location, a consistent amount of licensed spectrum lies idle. Surprisingly, the culprit for such scarcity of spectral resources is then the exclusive-use spectrum management policy rather than the physical lack of usable frequencies.

Examples of test-validated evidences of spectrum underutilization comprise the frequency occupancy measurement campaign performed in Chicago, Washington, D.C., and New York City [2] in the licensed bands between 30MHz and $3,000$MHz; a significant amount of exclusive-use spectrum was found to be scarcely occupied, with temporary idle frequencies that sometimes span even contiguous spectrum blocks. Likewise, frequent availability of licensed spectrum was revealed by analyzing data collected in some European locations such as, e.g., Aachen, Germany [3], Amsterdam, The Netherlands [4] and Barcelona, Spain [5].

To alleviate such cumbersome inefficiency in the management of the licensed spectrum, and in a tentative that strives for addressing the unceasing demand for spectrum resources for emerging wireless technologies, a blast of research activities have been devoted for devising new spectrum management policies and access techniques. The underlying idea envisions an improvement of the spectrum utilization upon permitting a conceivable *dynamical* access to the licensed bands on either a negotiated or an opportunistic basis, but without compromising the transmission opportunities granted to the licensed users [6, 7].

Although the fast proliferation of spectrum leasing and re-use techniques

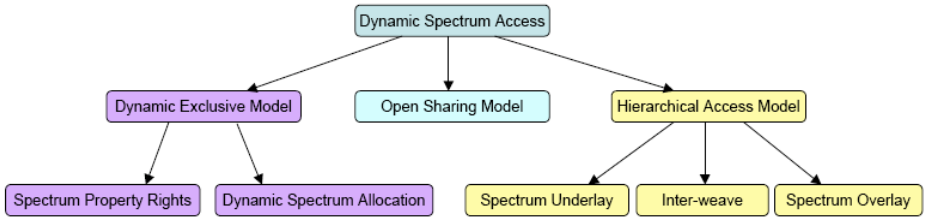

Figure 2.1: A taxonomy of dynamic spectrum access models.

had led to a large amount of technical terms coined so far, dynamic spectrum access (DSA) strategies can be mainly categorized into three basic models, namely [6]:

i. dynamic exclusive use model;

ii. open sharing model;

iii. hierarchical access model.

Dynamic exclusive use model maintains a rigid allocation policy, as spectrum bands are still licensed to wireless systems for exclusive use. However, such method introduces a flexibility in the management of the spectrum that entails a trading or leasing of the licensed bands by means of spectrum property rights [8, 9] or dynamic spectrum allocation [10]. The approach based on spectrum property permits licensed systems to lease and trade portions of their frequency bands. Clearly, more emphasis is given on the economy and market side, as leasing and trading may be done for pure profit. However, sharing is not mandatory, and it is freely up to the licensed systems. Dynamic spectrum allocation was brought forth by the European Union funded DRiVE project [10]. It aims to enable multimedia services in a heterogeneous multi-radio environment in a spectrum-efficient manner. Essentially, by exploiting spatial and temporal traffic statistics of different wireless services, spectrum is dynamically allocated in time and space to the targeted services, but still for exclusive use.

It is thus clear that the dynamic exclusive use model introduces a flexibility in the management of the spectrum, making somehow room for new wireless technologies. However, since the exclusive use policy still governs

the spectrum utilization, the aforementioned approaches hardly address the need for an improved efficiency in the spectrum occupation, because of the bursty nature of wireless traffic and the intermittent spectrum usage still entailed by some technologies.

Motivated by the actual co-existence of multiple wireless services operating in, e.g., the unlicensed industrial, scientific, and medical (ISM) frequency band, in the open sharing model peer users use a common portion of the spectrum by properly managing the interference they would cause to each other [11, 12]. This model, which falls also under the spectrum commons tag, adheres to classical interference management problems and is thus far from pure economy and market concerns. However, if applied to the nowadays scenario, it would require explicit coordination among current licensed systems and devices that aim to re-use the primary frequencies; in fact, such collaboration is essential for limiting mutual interference and managing the access to the wireless medium. Thus, incorporating the open sharing model in the current allocation policy may be hard in practice, as licensed systems may refuse to spend computational energies in cooperating with other devices without getting any advantage out of that.

Probably the most prominent model so far, hierarchical spectrum access model envisages secondary users aiming to access to the frequency bands of the licensed systems, also referred to as primary users (PUs), in a dynamical and nonintrusive manner [13, 14]. Dynamical because of the opportunistic nature that entails a prompt exploitation of transmission opportunities in the time, frequency and spatial domains, thus requiring agility in accessing to different portions of the spectrum in different instants and locations; nonintrusive in the sense that no harmful interference is caused to the PUs. Hierarchical spectrum access model has the well-appreciated merit of allowing coexistence of licensed users and secondary users without requiring new infrastructures or new regulations of the primary system.

Secondary devices, also referred to as cognitive radios (CRs), access to portions of the spectrum under the primary-secondary hierarchy without requiring any sort of explicit cooperation with the PUs. Differently from software-defined radios, which supports multiple air interfaces and protocols, CRs are envisioned as autonomous entities endowed with learning and

decisional capabilities; this context-aware intelligence along with the capability of adapting the operational system parameters to the communication environment, allow autonomous detection of the transmission opportunities, or "spectrum holes", and dynamical radio resource exploitation, thus enabling an opportunistic access to portions of the spectrum and performance optimization under given interference constraints.

Several approaches to spectrum sharing under the primary-secondary hierarchy have been proposed so far, as explained in the next section.

2.2 Hierarchical spectrum access model

In the hierarchical spectrum access model secondary users access to the licensed spectrum a dynamical and nonintrusive manner. Ideally, a primary channel can be considered as an opportunity by the CRs if it is not currently used by any PU or if the interference that would be caused to the licensed users could be safely kept under a predetermined limit. Clearly, the interference limit is set by the PU system according to its quality of system (QoS) requirements.

Depending on the dimension(s) where the transmission opportunity is available and on the specific interference constraints, the classification of the access techniques provided next is generally considered.

2.2.1 Inter-Weave, Overlay, and Underlay Access

Although there is sometimes a compound of confusion about their actual distinguishing features, three approaches have been proposed as the basis for sharing licensed spectrum under the primary-secondary hierarchy, namely (see, e.g., [15, 16, 17]):

iii.1. inter-weave;

iii.2. overlay;

iii.3. underlay.

The inter-weave model is essentially based on the idea of on opportunistic re-use the spectrum in the spatial domain; in other words, CRs can

utilize the primary spectrum in geographical areas where primary activity is absent. Exploitation of the so called "spatial spectrum holes" is attracting an increasing interest, since many current licensed systems like, e.g., TV broadcasting and cellular systems, show a non-contiguous and non-uniform spatial coverage due to self-interference concerns and infrastructure limitations. A pictorial example is portrayed in Fig. 2.3(b), where "CR 1" can ideally serve some of the secondary users since no PU activity is present in its proximity. Clearly, transmission power has to be properly calibrated, so that overlaps among the coverage regions of "CR 1" and "PU 1" and "PU 2" are avoided; conversely, if regions overlapped, "CR 1" would have harmed the primary system.

From this simple example, it is immediate to understand that actual implementation of the inter-weave model involves challenges related to the estimation of the actual spatial spectrum hole; such ambitious challenges were not present in conventional peer-to-peer wireless setups. Due to a lack of explicit coordination between PU and CR systems, inter-weave model calls for innovative signal processing algorithms for high-resolution PU sources localization and PU transmission power estimation. Calibration of the CR transmission power is, at a first glance, not an issue here, as transmit power should be limited by the CR sensing range (detection distance). However, as discussed in section 2.3, transmit power must be carefully set in order to avoid harmful interference to the PU system, which may unexpectedly happen due to fading propagation effects not accounted for.

In a sense, the approach governing the inter-weave model in the spatial domain is mirrored in the time domain by the overlay model. This model, firstly known under the name of spectrum pooling, exploits PU inactivity in time and, clearly, in frequency [16]. It does not impose any particular restriction on the transmission power of CRs, as long as transmissions end before a new burst of PU data. Take, for example, "CR 2" in Fig. 2.3(b); lying inside the coverage region of "PU 2", "CR 2" is restricted to transmit data only during the periods where "PU 2" is silent.

Besides detecting the presence of PU activity in the nearby area, overlay access model requires the non-trivial acquisition of the statistics of the PU transmissions. In fact, the sensing module mounted in the CR plat-

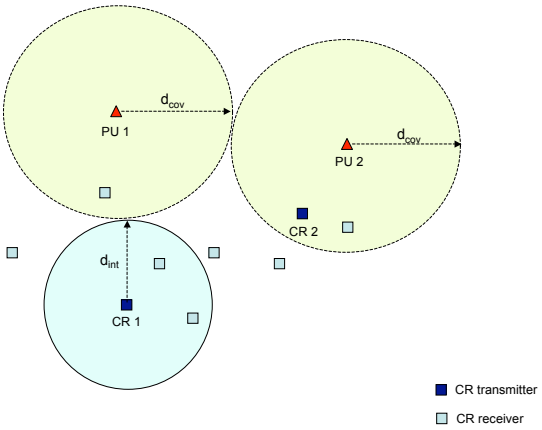

Figure 2.2: Exemplification of spectrum opportunities.

form cannot listen to the channel - determining the presence of ongoing PU transmissions - while the transmission module is actively operating; thus, a characterization of the PU activity is essential for calibrating the duration of the CR transmissions and thus avoid overlaps between PU and CR communications in time.

In its first conception, underlay access envisaged CRs to operate below the noise floor of the PUs, entailing an undercurrent of CR communications without PUs being aware of. Thus, CRs would operate under severe spectral mask constraints, contributing to a minor increase of the PU noise floor. This was essentially the underlaying idea behind the recently proposed cognitive ultrawideband (UWB) system [18]. Taking a look to Fig. 2.3(b), it is clear that both "CR 1" and "CR 2" can ideally continuously transmit no matter when PUs are present or not in their area. Note, however, that "CR 1" confines itself to have a lower communication rate with its intended receivers, being the PU inactivity not accounted for in the power allocation process.

Closer in spirit to traditional wireless networks, constraints on the interference took the place of the receiver noise floor in recent extensions of the underlay model [17]; CR and PU now can coexist in the same band,

location and time as long as the interference to PUs remains tolerable, i.e., below a prescribed interference threshold. This vision introduces a handful of challenging issues comprising a proper statistical modeling of the aggregate interference that CRs would cause to the PUs and localization of the PU receivers.

2.3 Motivation: a Multi-Dimensional Vision

As mentioned in the preceding discussion, inter-weave and overlay strategies aim to exploit the transmission opportunities in the spatial and time domain, respectively, whereas the underlay concept involves a more complicated communication scenario with more emphasis on the interference avoidance aspect.

Ideally, a primary channel can be considered as an opportunity if it is not currently used by PUs or if communications among CRs can happen with the interference that would be caused to the licensed users kept below a predetermined limit. The concept of spectrum opportunity is however more involved than that it may appear at a first glance. Demystifying the sharp cut among frequency, time, and space domains, it is thinkable that for an aggressive and full opportunistic re-use of the licensed resources under the primary-secondary hierarchy, a multi-dimensional nature of the spectrum hole should be envisaged, with interference concerns incorporated as well. In a sense, considering one dimension individually is not sufficient (or, at least, not optimal), as transmission opportunities or interference hitches may appear in another dimension. CRs should fill the spectrum gap in space, time and frequency simultaneously, with protection of the incumbent PU system systematically guaranteed.

Just to make an elucidative example, suppose that a set of CRs reveal no PU activity at a given time instant in their proximity, i.e., in the area determined by their detection radii. Thus, CRs may ideally send some bursts of data in an overlay setup. However, in practice, CRs can neither set an indiscriminately high transmission power nor restrict their coverage region to be contained in (or equal to) their detection area. In fact, sensing algorithm can detect primary transmitters within the detection distance

but cannot detect silent licensed receivers, which nevertheless have to be obligatorily protected; thus, a naïve implementation of the overlay model based on the detection radius would potentially harm PU receivers. Learning the PU power spectral density (PSD) distribution in space, rather then having cognition of the only PU transmitters' state, is thus essential in order to detect the regions where PU receivers may potentially reside; thus, PU system can be protected by limiting the interference. In some sense, interweave, overlay, and underlay setups should be merged together, leading to a technique that conceivably fills the spectrum holes jointly in time, frequency and space, under the obligatory constraints on the interference caused to any primary receiver.

Critical for the spectrum opportunity detection and the succeeding opportunity exploitation is the characterization of the radio frequency (RF) propagation environment that surrounds primary and secondary systems. As no collaboration among primary and secondary systems is envisaged and, thus, PU-to-CR channels and interference levels cannot be acquired via conventional point-to-point feedback on a per-link basis, a continuous learning the RF ambient in an autonomous manner is of paramount importance. This allows a significant departure from a simple and inaccurate model based on the only deterministic path loss and, thus, a reliable detection of the PU activities in time and space. Also, no matter whether instantaneous or mean interference is concerned, cognition of the channel states actually enforces interference constraints, which may be unduly violated when it comes to adopt a path loss-only propagation model.

Take, for example, the setup in Fig. 2.3(a), where the PSD map of a PU source is portrayed relying on a path loss-based model. Assuming that the interference threshold for the PUs is set to -60dB, one can notice that a CR transmitter is allowed to communicate with all the CR receivers since they lie outside the PU coverage region. However, the true coverage region is significantly different from a simple disk-shaped time-invariant area, as propagation impairments provide shadow and multi-path fading phenomena. This can be noticed in Fig. 2.3(b), where a realization of the actual PU coverage region is portrayed and where one can notice that the CR transmitter can actually serve only one receiver; then, following a path loss-only

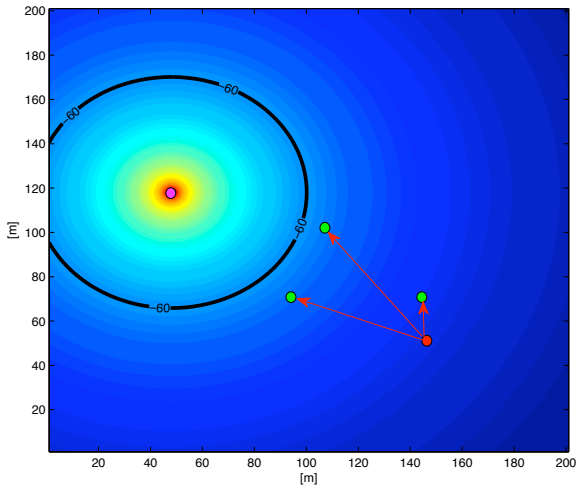

(a) Path loss-only propagation model.

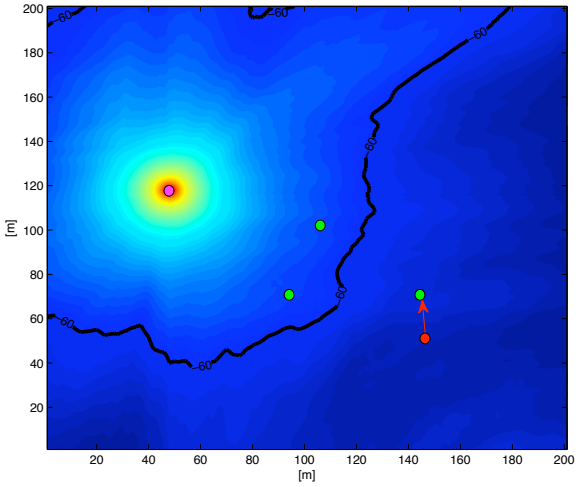

(b) Channel gain atlas.

Figure 2.3: Spatio-temporal spectrum opportunity at a given instant.

model, CR system would interfere PU receivers.

The aforementioned multi-dimensional vision of the transmission opportunities along with the lack of explicit coordination among primary and secondary systems demand for a continuous situational awareness for the CR system. This, in turn, calls for large-scale signal processing algorithms, complemented by collaborative and adaptive sensing and control platforms, to accomplish to the objectives of layered sensing and interference-limited opportunistic spectrum access. Innovative large-scale algorithms enabling a meticulous and autonomous RF propagation learning and, thus, a significant departure from conventional per-link channel gain and interference level acquisition are also advocated.

In a tentative to address the aforementioned ambitious challenges involved by a hierarchical spectrum access with no cooperation among primary and secondary systems, the present thesis offers the following contribution.

2.4 Contribution of the Thesis

The contribution of the present thesis is threefold: RF propagation environment learning, large-scale spectrum sensing, and interference-limited power control are considered throughout the ensuing chapters. Inside each subject, motivation are renewed and main novelties are stressed next.

1. *Introduction of the channel gain cartography concept.* Due to lack of collaboration mechanisms between PU and CR systems, estimating the CR-to-PU channels requires considerable effort, especially when prior information about the PU signalling scheme is nor available. More challenging is acquiring channel between CRs and passive PU receivers, which do not transmit RF energy but just listen. The problem addressed in this work entails tracking the spatio-temporal evolution of channel gains (CGs) in a given geographical region through a collaborative network of CRs. Based on the CG measurements obtained among the CRs, it is proposed a large-scale algorithm that allows estimation of the actual CGs of wireless links from *any* point to *any* other point in space. The non-trivial capability of estimating

the channel gain between arbitrary transmitter-receiver locations enables a significant departure from the classical one-dimensional view of the propagation environment, with a consistent global-view of the RF ambient viewed from arbitrary points in space. As shown throughout the thesis, the so called CR maps or atlases improve the spectrum sensing performance and enable a coverage region reconstruction and a reliable interference-constrained power allocation. Beyond the CR context, the vision is to use such CG atlas for cross-layer design and assessment of the system-level performance of wireless networks and to enhance hand-off, localization, routing, and resource allocation. To address scalability and robustness concerns, a distributed consensus-based algorithm is also derived.

2. *Sparsity-aware spectrum sensing and PSD maps.* Spectrum opportunities identification in an autonomous manner is performed via spectrum sensing. Based on a parsimonious model accounting for PU mutual interference concerns, and motivated by recent advances in sparse linear regression, a collaborative sparsity-cognizant state tracker is developed in centralized and distributed formats. The appealing features of the proposed algorithms consist in the PU transmission power estimation and PU localization capabilities. With these information close at hand, CRs can reconstruct the actual power spectral density (PSD) map of the primary system by employing the PU CG map. Thus, detection of the spatio-temporal spectrum spatial holes is efficiently attainable, enhancing the re-use of the primary frequency bands.

3. *Chance-constrained power allocation under channel gain uncertainty.* In a conventional power allocation problem, channels among devices can be accurately acquired via training and, based on those estimates, a given network utility function is to be maximized. In the cognitive radio context, actual protection of the PU receivers encounters the nuisance impossibility of estimating the CR-to-PU receiver channel gains. One way to estimate the potential PU receiver locations, and eventually their channel gains, is to rely on the idea of channel gain cartography. Based on location information of the (potential)

PU receivers and, possibly, an estimate of the PU receivers CG maps, the approach pursued in the present thesis is to exploit the statistical channel knowledge of the CR-to-PU channels. As PU protection constraints must be enforced with high reliability, probabilistic constraints will be imposed in order to guarantee that the interference power experienced by PU receivers falls below a tolerable level with a given high probability. Acquisition of instantaneous CR-to-CR channel state information is rendered challenging by, e.g., mobility of the nodes, fast variation of the CR environment, and prolonged occupancy of the primary bands. To address this case, a robust network utility maximization problem is considered, where per-CR link probability of outage constraints are enforced.

Chapter 3

The Concept of Channel Gain Cartography

The present chapter introduces the concept of channel gain cartography*, a groundbreaking geostatistics-inspired application that enables a portrayal of the RF environment impinging upon arbitrary locations in space. The most appealing feature of the proposed tool consists in the non-trivial capability of inferring the channel gain between arbitrary transmitter-receiver locations, based on the only measurements taken among a set of collaborating devices. The vision is to use such channel gain atlas for cross-layer design and assessment of the system-level performance of wireless networks and to enhance hand-off, localization, routing, spectrum sensing, and resource allocation.*

3.1 Preliminaries and motivation

Conventional acquisition of channel coefficients and interference levels on a per-link basis might become inadequate for emerging wireless technologies, as a continuous need for a concrete situational awareness is unrelentingly demanded to accomplish layered sensing and dynamical spectrum control. Innovative signal processing algorithms enabling a significant departure from such a one-dimensional view of the propagation environment are thus advocated [19], [20], [21].

Critical to this departure is characterizing the spatio temporal evolution

of wireless fading links. The fast-varying small-scale fading process is due to multi-path propagation effects, and is roughly uncorrelated across time and when samples are taken on the order of few carrier wavelengths apart [22]. The medium-scale fading, or shadowing, arises from attenuation and diffraction of propagating signals owing to obstructions such as hills, buildings, and trees. Shadowing is more challenging to characterize statistically, especially when correlations among different locations and time instants are accounted for.

Well-established correlation models for shadow fading are available for cellular networks, in which mobile terminals are assumed to move with constant velocity [23]. An extension involving one mobile and two base stations was proposed in [24], and multi-hop relay scenarios were studied in [25]. The main limitation of Gudmundson's correlation model [23] consists in completely neglecting possible cross-correlations among links that do not have any communication ending point in common; hence, it is rarely applicable to model shadowing (cross-) correlations in ad hoc networks. The importance of shadowing correlation in analyzing performance of wireless ad hoc networks was pointed out in [26], which introduced a model to capture shadowing (spatial) correlation among any wireless links in the deployment area. An experimentally validated parametric model for nomadic as well as distributed channels was reported in [27]; spatio-temporal shadowing correlation was also analyzed for the different propagation scenarios.

Answering to the advocated departure from a one-dimensional view of the RF environment, the problem addressed here entails tracking the spatio-temporal evolution of channel gains (CGs) in a given geographical region through a collaborative network of CRs. Based on the CG measurements obtained among the radios, it is desired to predict the actual CGs from *any* point in space to the radios, which are henceforth termed *local CG maps*; as well as the CGs of wireless links from *any* point to *any* other point in space (i.e., links that do not have communication ending points in common with the CR-to-CR links), which constitute what is hereafter termed as *global CG map*. See Fig. 3.1 for a schematic representation.

The vision is to use such atlas for cross-layer design and assessment of the system-level performance of wireless networks [28], [29], [30]; also, maps may

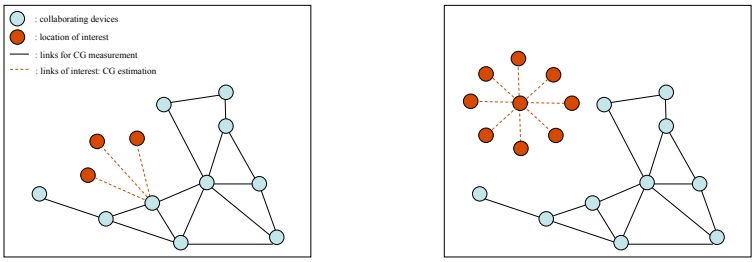

(a) Local map (b) Global map

Figure 3.1: Channel gain maps.

play an instrumental role to enhance hand-off, localization, and routing. In CR networks, CG maps can provide vital information for spectrum sensing and resource allocation tasks [31], [32].

Efforts to model and estimate a spatial description of the RF environment are growing. The ambient RF power spectrum was viewed as a random field in [33], [34], and the Kriging spatial interpolation technique [35] was adopted to estimate the spatial power spectral density (PSD). Kriging is a linear spatial interpolator that was originally developed for the mining industry, but has now found a wide range of application areas including earth and environmental sciences and engineering [35], [36], [37]. Assuming that the PSD map is confined to a low-dimensional subspace, [38] devised a distributed projection algorithm to reduce observation noise. In [39], the PSD map was estimated by exploiting the underlying sparsity inherent to the system model and a simple path loss-only channel model. The spline interpolation technique was employed in [40] to accommodate shadowing effects and to estimate potentially time-varying PSD maps.

The overarching contribution of the present work is to introduce the concept of CG cartography and develop algorithmic solutions for effectively reconstructing the desired maps starting from the CR-to-CR CG measurements [31], [41]. Going into the details of the framework, first, the shadowing correlation model of [26] is judiciously extended to accommodate temporal variations of the shadow fading. Time-varying CG maps are then tracked by adapting to the problem at hand the Kriged Kalman filtering (KKF),

a tool with widely appreciated merits in spatial statistics and geo-sciences used for estimating time-varying random fields. A distributed KKF, which involves message passing only among one-hop neighboring nodes, is then developed to address scalability and robustness concerns about the centralized algorithm. Specifically, distributed Kalman filtering (KF) is developed to track the mean field of the shadow fading process in space and time; and a distributed Kriging interpolator is derived to interpolate a spatially colored yet temporally white shadow fading component. The present work is the first to model the spatio-temporal correlation of *any-to-any* CGs, and develop corresponding estimation algorithms in both centralized and distributed set-ups.

Numerical tests verify that the collaborative approach significantly enhances the accuracy of CG map estimation over a non-collaborative alternative.

3.2 Channel gain model

Consider a radio link from position $\mathbf{x}$ to position $\mathbf{y}$ at time t, where $\mathbf{x}$ and $\mathbf{y}$ are arbitrary points in a geographical area $\mathcal{A} \subset \mathbb{R}^2$. Let $\dot{g}_{\mathbf{x}\to\mathbf{y}}(t)$ denote the instantaneous channel gain of link $\mathbf{x} \to \mathbf{y}$ at time t, which can be expressed as [42, Ch. 2]

$$\dot{g}_{\mathbf{x}\to\mathbf{y}}(t) = g_{0,\mathbf{x}\to\mathbf{y}} \cdot ||\mathbf{x}-\mathbf{y}||_2^{-\eta} \cdot s_{\mathbf{x}\to\mathbf{y}}(t) \cdot |h_{\mathbf{x}\to\mathbf{y}}(t)|^2 \tag{3.1}$$

where $g_{0,\mathbf{x}\to\mathbf{y}}$ collects the antenna and other propagation gains [42, Ch. 2], η is the path loss exponent, $s_{\mathbf{x}\to\mathbf{y}}(t)$ the shadow fading, and $|h_{\mathbf{x}\to\mathbf{y}}(t)|^2$ the squared envelope of the small-scale fading. Denote as $\dot{G}_{\mathbf{x}\to\mathbf{y}}(t)$ the instantaneous channel gain expressed in dB, i.e., $\dot{G}_{\mathbf{x}\to\mathbf{y}}(t) := 10\log_{10}\dot{g}_{\mathbf{x}\to\mathbf{y}}(t)$.

Shadowing $s_{\mathbf{x}\to\mathbf{y}}(t)$ has been experimentally shown to be accurately modeled by a log-Normal-distributed first-order spatial autoregressive process [26],[27] whereas a Nakagami-m distributed multipath fading [43], independent of $s_{\mathbf{x}\to\mathbf{y}}(t)$, is assumed here. Nakagami-m distribution offers a closer match to empirical data than Rayleigh or Ricean distribution [44]. However, it is well known that Nakagami-m distribution boils down to Rayleigh and Ricean distributed fading by properly choosing the parameter $m > 1/2$ [42,

Ch. 2]. Independent realizations of the small-scale fading over different links are assumed.

It is first essential to provide a statistical characterization of the composite shadowed Nakagami fading, which will henceforth be denoted as $a_{\mathbf{x}\to\mathbf{y}} := s_{\mathbf{x}\to\mathbf{y}} \cdot |h_{\mathbf{x}\to\mathbf{y}}|^2$. Furthermore, let $A_{\mathbf{x}\to\mathbf{y}} := 10\log_{10} a_{\mathbf{x}\to\mathbf{y}}$ be the composite fading expressed in dB. Upon denoting the mean and the variance of the Gaussian-distributed shadowing component $S_{\mathbf{x}\to\mathbf{y}} := 10\log_{10} s_{\mathbf{x}\to\mathbf{y}}$ in dB as $\mu_{S_{\mathbf{x}\to\mathbf{y}}}$ and $\sigma^2_{S_{\mathbf{x}\to\mathbf{y}}}$, respectively, the probability density function (*p.d.f.*) of random variable (r.v.) $a_{\mathbf{x}\to\mathbf{y}}$ is given by the Gamma-log-normal density

$$f_{a_{\mathbf{x}\to\mathbf{y}}}(a) = \int_0^\infty \left(\frac{m}{u}\right)^m \frac{a^{m-1}}{\Gamma(m)} e^{-\frac{ma}{u}} \cdot \frac{1}{\sqrt{2\pi}\kappa\sigma_{S_{\mathbf{x}\to\mathbf{y}}} u} e^{-\frac{\left(10\log_{10}(u)-\mu_{S_{\mathbf{x}\to\mathbf{y}}}\right)^2}{2\sigma^2_{S_{\mathbf{x}\to\mathbf{y}}}}} du \tag{3.2}$$

where $\kappa := \frac{1}{10}\ln 10$, and $\Gamma(\cdot)$ is the Gamma function. It is known that this can be well-approximated by the log-normal density as [42, Ch. 2]

$$f_{a_{\mathbf{x}\to\mathbf{y}}}(a) \approx \frac{1}{\sqrt{2\pi}\kappa\sigma_{A_{\mathbf{x}\to\mathbf{y}}} a} e^{-\frac{\left(10\log_{10}(a)-\mu_{A_{\mathbf{x}\to\mathbf{y}}}\right)^2}{2\sigma^2_{A_{\mathbf{x}\to\mathbf{y}}}}} \tag{3.3}$$

where $\mu_{A_{\mathbf{x}\to\mathbf{y}}}$ and $\sigma^2_{A_{\mathbf{x}\to\mathbf{y}}}$ are given by

$$\mu_{A_{\mathbf{x}\to\mathbf{y}}} = \kappa^{-1}\left(-\ln m - C + \sum_{m'=1}^{m-1} \frac{1}{m'}\right) + \mu_{S_{\mathbf{x}\to\mathbf{y}}} \tag{3.4}$$

$$\sigma^2_{A_{\mathbf{x}\to\mathbf{y}}} = \kappa^{-2}\zeta(2,m) + \sigma^2_{S_{\mathbf{x}\to\mathbf{y}}} \tag{3.5}$$

respectively. Here, $C \approx 0.5772$ is the Euler's constant and $\zeta(\cdot,\cdot)$ the Hurwitz's zeta function, i.e., $\zeta(a,b) = \sum_{k=0}^{+\infty} \frac{1}{(k+b)^a}$, $a, b > 1$. Under (3.3), the channel gain $\dot{g}_{\mathbf{x}\to\mathbf{y}}(t)$ turns out to be (approximated as) log-Normal (cf. (3.6)). For future use, denote as $\mu_{G_{\mathbf{x}\to\mathbf{y}}}$ and $\sigma_{G_{\mathbf{x}\to\mathbf{y}}}$ mean and standard deviation, respectively, of the Gaussian-distributed channel gain $\dot{G}_{\mathbf{x}\to\mathbf{y}}(t)$.

The approximation in (3.3) is quite accurate in the propagation scenarios of practical interest, but starts deteriorating when $m = 1$ (Rayleigh fading) and $\sigma_{S_{\mathbf{x}\to\mathbf{y}}} < 6$ dB [45]. The approximation was used in [46] in a cellular network context, and more recently for interference modeling in CR networks [47]. The overarching advantage of approximation (3.3) consists in

offering the possibility of sidestepping the hurdle represented by the nuisance lack of mathematical tractability of (3.2). In this way, approximate analysis can be readily and elegantly carried out in a log-Normal domain - in a Gaussian domain when quantities are expressed in dB. Such statistical description will be meticulously employed in the ensuing chapters, especially when the challenging system coverage region estimation and power allocation problems will be faced.

The Bayesian inference framework proposed next for reconstructing local/global CG maps requires knowledge of (only) the averaged CG function, which can be written as [cf. (3.1)]

$$g_{\mathbf{x}\to\mathbf{y}}(t) := g_{0,\mathbf{x}\to\mathbf{y}} \cdot ||\mathbf{x}-\mathbf{y}||_2^{-\eta} \cdot s_{\mathbf{x}\to\mathbf{y}}(t)\,. \tag{3.6}$$

Note that $g_{\mathbf{x}\to\mathbf{y}}(t)$ is modeled as a log-Normal r.v., being the path loss $g_{0,\mathbf{x}\to\mathbf{y}} \cdot ||\mathbf{x}-\mathbf{y}||_2^{-\eta}$ a constant and $s_{\mathbf{x}\to\mathbf{y}}(t)$ log-Normal [26], [27]. The corresponding quantity expressed in dB - which is Gaussian distributed - is given by

$$G_{\mathbf{x}\to\mathbf{y}}(t) = G_{0,\mathbf{x}\to\mathbf{y}} - 10\eta \log_{10}(\|\mathbf{x}-\mathbf{y}\|_2) + S_{\mathbf{x}\to\mathbf{y}}(t)\,. \tag{3.7}$$

where $G_{0,\mathbf{x}\to\mathbf{y}} := 10\log_{10} g_{0,\mathbf{x}\to\mathbf{y}}$. Since shadowing and small-scale fading are characterized by a different coherence time [27], measuring $g_{\mathbf{x}\to\mathbf{y}}(t)$ is possible upon observing the channel for an amount of time sufficient for averaging out the effect of $h_{\mathbf{x}\to\mathbf{y}}(t)$; see, for example, [48].

Before proceeding with the explanation of the powerful channel gain map estimation machinery, it is necessary to setup a suitable spatio-temporal model for the shadow fading - the subject of the ensuing section.

3.2.1 Dynamic shadow fading model

While small-scale fading is roughly uncorrelated across time and when distance among links is on the order of few carrier wavelengths apart, a challenge in statistical modeling of shadowing lies in accurately characterizing its spatio-temporal correlation. In an effort to establish a shadowing correlation model suitable for ad hoc network scenarios, the concept of *spatial loss field* was introduced in [26]. The spatial loss field essentially captures the obstructions in the area where the network is deployed. The shadowing

effects experienced by individual links in the network are then modeled by line integrals of this common field. The resulting shadow fading correlation matches field measurements, as well as the conventional correlation models in the literature [26]. The scope of this approach is considerably broadened here by incorporating the temporal dynamics as well.

Let $\ell(\mathbf{x}, t)$ denote the spatial loss field at location $\mathbf{x} \in \mathcal{A}$ at time $t \in \mathbb{N}$, which is assumed to be Gaussian [26]. The spatio-temporal dynamics of the spatial loss field are characterized by the following relations (see also [49])

$$\ell(\mathbf{x}, t) = \bar{\ell}(\mathbf{x}, t) + \tilde{\ell}(\mathbf{x}, t) \tag{3.8}$$

$$\bar{\ell}(\mathbf{x}, t) = \int_{\mathcal{A}} w(\mathbf{x}, \mathbf{u}) \bar{\ell}(\mathbf{u}, t-1) d\mathbf{u} + \eta(\mathbf{x}, t) \tag{3.9}$$

where $\bar{\ell}(\mathbf{x}, t)$ represents the component that is colored both in space and time through the filter $w(\mathbf{x}, \mathbf{u})$ capturing the interaction of loss $\bar{\ell}$ at position $\mathbf{x}$ at time t, with the loss $\bar{\ell}$ at position $\mathbf{u}$ at time $t-1$; $\tilde{\ell}(\mathbf{x}, t)$ and $\eta(\mathbf{x}, t)$ are spatially colored yet temporally white zero-mean Gaussian stationary random fields. Process $\eta(\mathbf{x}, t)$ captures unmodeled dynamics uncorrelated with $\tilde{\ell}(\mathbf{u}, \tau)$, $\forall \mathbf{u}, \tau$. Moreover, $\mathbb{E}\{\tilde{\ell}(\mathbf{x}, t)\bar{\ell}(\mathbf{u}, t)\} = \mathbb{E}\{\eta(\mathbf{x}, t)\bar{\ell}(\mathbf{u}, t-1)\} = 0$ for all $\mathbf{x}$, $\mathbf{u}$ and t. For stability, the filter $w(\mathbf{x}, \mathbf{u})$ must satisfy the condition $\left| \int_{\mathcal{A}} w(\mathbf{x}, \mathbf{u}) d\mathbf{u} \right| < 1, \ \forall \mathbf{x}$.

Using the loss function ℓ, the shadow fading process in dB for the link $\mathbf{x} \to \mathbf{y}$ is modeled as (see also [26])

$$S_{\mathbf{x}\to\mathbf{y}}(t) = \frac{1}{\|\mathbf{x} - \mathbf{y}\|_2^{\frac{1}{2}}} \int_{\mathbf{x}\to\mathbf{y}} \ell(\mathbf{u}, t) d\mathbf{u} \tag{3.10}$$

which, after using (3.8), yields

$$S_{\mathbf{x}\to\mathbf{y}}(t) = \bar{S}_{\mathbf{x}\to\mathbf{y}}(t) + \tilde{S}_{\mathbf{x}\to\mathbf{y}}(t) \tag{3.11}$$

where

$$\bar{S}_{\mathbf{x}\to\mathbf{y}}(t) := \frac{1}{\|\mathbf{x} - \mathbf{y}\|_2^{\frac{1}{2}}} \int_{\mathbf{x}\to\mathbf{y}} \bar{\ell}(\mathbf{u}, t) d\mathbf{u} \tag{3.12}$$

$$\tilde{S}_{\mathbf{x}\to\mathbf{y}}(t) := \frac{1}{\|\mathbf{x} - \mathbf{y}\|_2^{\frac{1}{2}}} \int_{\mathbf{x}\to\mathbf{y}} \tilde{\ell}(\mathbf{u}, t) d\mathbf{u}. \tag{3.13}$$

Remark 3.2.1. In a recent measurement campaign in the 2.4 GHz band for nomadic as well as mobile channels, it was confirmed that shadow fading, when expressed in dB, can be accurately modeled by a Gaussian-distributed first-order spatio-temporal autoregressive process [27]. An analogy can be drawn between the shadow fading model developed here and the model experimentally confirmed by [27], as follows: $\bar{S}_{\mathbf{x}\to\mathbf{y}}(t)$ captures the static shadowing component (both the obstruction-based as well as the multipath-based static shadowing), and the spatially correlated dynamic shadowing component; while $\tilde{S}_{\mathbf{x}\to\mathbf{y}}(t)$ represents the time-varying shadowing component possessing spatial structure but no temporal correlation. The lack of temporal structure may be due to a low sampling frequency, compared to the time scale of the small-scale movements in the environment, which cause dynamic shadowing. Note that when $w(\mathbf{x},\mathbf{u}) \equiv 0$, i.e., in the absence of temporal structure, the model described in this section reduces precisely to the one in [26]. □

3.2.2 Finite dimensional state-space model

The state-space model described by (3.8) and (3.9) is infinite-dimensional. A standard approach to reduce its dimensionality and render it computationally tractable from a signal processing perspective is to employ a basis-expansion representation [49], [50]. If $\{\psi_k(\cdot)\}_{k=1}^{\infty}$ denotes a complete orthonormal basis defined on the two-dimensional domain $\mathcal{A}$, then, $\bar{\ell}(\cdot)$ and $w(\cdot)$ can be expressed as

$$\bar{\ell}(\mathbf{x},t) = \sum_{k=1}^{\infty} \alpha_k(t)\psi_k(\mathbf{x}) \tag{3.14}$$

$$w(\mathbf{x},\mathbf{u}) = \sum_{k=1}^{\infty} \beta_k(\mathbf{x})\psi_k(\mathbf{u}) \tag{3.15}$$

where $\{\alpha_k(t)\}$ and $\{\beta_k(\mathbf{x})\}$ are the basis-expansion coefficients for $\bar{\ell}(\cdot)$ and $w(\cdot)$, respectively.

To obtain a finite-dimensional approximation, consider retaining only the K dominant terms in the expansions. Upon defining the $K \times 1$ vectors $\boldsymbol{\alpha}(t) := [\alpha_1(t) \ \ldots \ \alpha_K(t)]^T$, $\boldsymbol{\beta}(\mathbf{x}) := [\beta_1(\mathbf{x}) \ \ldots \ \beta_K(\mathbf{x})]^T$, and $\boldsymbol{\psi}(\mathbf{x}) := [\psi_1(\mathbf{x}) \ \ldots \ \psi_K(\mathbf{x})]^T$ and exploiting the orthonormality of the basis, (3.9)

can be written as

$$\boldsymbol{\psi}^T(\mathbf{x})\boldsymbol{\alpha}(t) = \boldsymbol{\beta}^T(\mathbf{x})\boldsymbol{\alpha}(t-1) + \eta(\mathbf{x},t). \tag{3.16}$$

Now, consider N_r positions $\{\mathbf{x}_r \in \mathcal{A}\}_{r=1}^{N_r}$ where measurements of $\bar{\ell}$ are available. Upon defining the $(N_r \times K)$-matrices $\mathbf{B} := [\boldsymbol{\beta}(\mathbf{x}_1) \ \ldots \ \boldsymbol{\beta}(\mathbf{x}_{N_r})]^T$ and $\boldsymbol{\Psi} := [\boldsymbol{\psi}(\mathbf{x}_1) \ \ldots \ \boldsymbol{\psi}(\mathbf{x}_{N_r})]^T$, and the $(N_r \times 1)$-dimensional vector $\boldsymbol{\eta}(t) := [\eta(\mathbf{x}_1,t) \ \ldots \ \eta(\mathbf{x}_{N_r},t)]^T$, the state evolution observed at the N_r sampling positions can be expressed as [cf. (3.16)]

$$\boldsymbol{\Psi}\boldsymbol{\alpha}(t) = \mathbf{B}\boldsymbol{\alpha}(t-1) + \boldsymbol{\eta}(t). \tag{3.17}$$

Thus, selecting $N_r \geq K$ and assuming that $\boldsymbol{\Psi}^T\boldsymbol{\Psi}$ is non-singular, one obtains the following state evolution equation

$$\boldsymbol{\alpha}(t) = \mathbf{T}\boldsymbol{\alpha}(t-1) + \boldsymbol{\Psi}^\dagger\boldsymbol{\eta}(t) \tag{3.18}$$

where $\boldsymbol{\Psi}^\dagger := (\boldsymbol{\Psi}^T\boldsymbol{\Psi})^{-1}\boldsymbol{\Psi}^T$ is the pseudo-inverse of $\boldsymbol{\Psi}$ and $\mathbf{T} := \boldsymbol{\Psi}^\dagger\mathbf{B}$ is the state transition matrix.

Note, furthermore, that by plugging (3.14) into (3.12), the shadowing component $\bar{S}_{\mathbf{x}\to\mathbf{y}}(t)$ can be further expressed as

$$\bar{S}_{\mathbf{x}\to\mathbf{y}}(t) = \sum_{k=1}^{\infty} \underbrace{\left[\frac{1}{\|\mathbf{x}-\mathbf{y}\|_2^{1/2}} \int_{\mathbf{x}\to\mathbf{y}} \psi_k(\mathbf{u})d\mathbf{u}\right]}_{:=\phi_{\mathbf{x}\to\mathbf{y},k}} \alpha_k(t) \tag{3.19}$$

$$\approx \boldsymbol{\phi}_{\mathbf{x}\to\mathbf{y}}^T\boldsymbol{\alpha}(t) \tag{3.20}$$

where only K terms have been retained in (3.20), and the entries of the basis coefficients vactor $\boldsymbol{\phi}_{\mathbf{x}\to\mathbf{y}} := [\phi_{\mathbf{x}\to\mathbf{y},1} \ \ldots \ \phi_{\mathbf{x}\to\mathbf{y},K}]^T$ depend only on the spatial coordinates $\mathbf{x}$ and $\mathbf{y}$.

Next, the spatial correlation model for $\tilde{S}_{\mathbf{x}\to\mathbf{y}}(t)$ is established. To do this, the spatial correlation for $\tilde{\ell}(\mathbf{x},t)$ need to be first modeled.

3.2.3 Spatial correlation model

Given $\boldsymbol{\alpha}(t)$, $\bar{S}_{\mathbf{x}\to\mathbf{x}_r}(t)$ represents the deterministic time-varying mean of the shadowing $S_{\mathbf{x}\to\mathbf{x}_r}(t)$, which is referred to as *trend* in the spatial statistics parlance [51]. Likewise, conditioned on $\boldsymbol{\alpha}(t)$, $\bar{\ell}(\mathbf{x},t)$ corresponds to the trend

of the spatial loss field $\ell(\mathbf{x}, t)$. Noting that [26] models spatial loss effects as a zero-mean random field reveals that the modeling and analysis of [26] actually hold for the *de-trended* zero-mean random field $\tilde{\ell}(\mathbf{x}, t)$ in the present context. This justifies modeling $\tilde{\ell}(\mathbf{x}, t)$ the same way [26] modeled the spatial loss field.

Thus, the covariance of the de-trended spatial loss field $\tilde{\ell}(\mathbf{x}, t)$ at time t can be modeled as

$$C_{\tilde{\ell}}(\mathbf{x}, \mathbf{y}) := \mathbb{E}\{\tilde{\ell}(\mathbf{x}, t)\tilde{\ell}(\mathbf{y}, t)\} = \frac{\sigma^2_{\tilde{S}}}{d_{\tilde{\ell}}} \exp\left(-\frac{\|\mathbf{x} - \mathbf{y}\|_2}{d_{\tilde{\ell}}}\right) \tag{3.21}$$

where $\sigma^2_{\tilde{S}}$ is the variance of $\tilde{S}_{\mathbf{x}\to\mathbf{y}}(t)$, and $d_{\tilde{\ell}}$ denotes the coherence distance of the $\tilde{\ell}$-field. Correspondingly, the cross-correlation of $\tilde{S}_{\mathbf{x}\to\mathbf{y}}(t)$ and $\tilde{S}_{\mathbf{u}\to\mathbf{v}}(t)$ for arbitrary links $\mathbf{x} \to \mathbf{y}$ and $\mathbf{u} \to \mathbf{v}$, respectively, is given by [cf. (3.13) and (3.21)]

$$C_{\tilde{S}}(\mathbf{x} \to \mathbf{y}, \mathbf{u} \to \mathbf{v}) := \mathbb{E}\{\tilde{S}_{\mathbf{x}\to\mathbf{y}}(t)\tilde{S}_{\mathbf{u}\to\mathbf{v}}(t)\} \tag{3.22}$$

$$= \frac{\sigma^2_{\tilde{S}}}{d_{\tilde{\ell}}\|\mathbf{x} - \mathbf{y}\|_2^{\frac{1}{2}}\|\mathbf{u} - \mathbf{v}\|_2^{\frac{1}{2}}} \int_{\mathbf{x}\to\mathbf{y}} \int_{\mathbf{u}\to\mathbf{v}} \exp\left(-\frac{\|\mathbf{x}_1 - \mathbf{x}_2\|_2}{d_{\tilde{\ell}}}\right) d\mathbf{x}_1^T d\mathbf{x}_2 \tag{3.23}$$

which can be evaluated numerically.

3.3 Map tracking via Kriged Kalman filtering

Time-varying channel gain maps are tracked via KKF. In its essential parts, KKF is constituted by a Kalman filter (KF), which is in charge for tracking the spatio-temporal evolution of the trend field $\bar{S}_{\mathbf{x}\to\mathbf{y}}$, augmented with a Kriging linear spatial interpolator for the estimation of $\tilde{S}_{\mathbf{x}\to\mathbf{y}}(t)$. The latter was originally developed for the mining industry, but has now found a wide range of application areas including earth and environmental sciences and engineering.

From the model set forth in Sec. 3.2, it is clear that estimating the shadowing $S_{\mathbf{x}\to\mathbf{y}}(t)$ can benefit from fusing the observations of all sensing devices indexed by $r \in \{1, 2, \ldots, N_r\}$, thanks to the existence of an underlying spatial loss field. To this end, it is necessary to set up a measurement model, which is the subject of the next section.

3.3.1 Measurement model

Consider a network of N_r sensors, whose geographical positions $\{\mathbf{x}_r\}_{r=1}^{N_r}$ are known to one another. In order to estimate the gains of the sensor-to-sensor channels, training signals transmitted by the sensors will be exploited. The training signals are generally present in the data packets to aid synchronization and channel estimation at the intended receivers. For simplicity, it is assumed that the sensors transmit unit-power training packets in a time-division multiple access (TDMA)-fashion. Suppose sensor $j \neq r$ transmits a training signal for sensor r to acquire an estimate of $G_{\mathbf{x}_j \to \mathbf{x}_r}(t)$ by simply measuring the received power. Using (3.6), it is then possible to obtain a noisy version of $S_{\mathbf{x}_j \to \mathbf{x}_r}(t)$ modeled as [31]

$$\breve{S}_{\mathbf{x}_j \to \mathbf{x}_r}(t) = S_{\mathbf{x}_j \to \mathbf{x}_r}(t) + \epsilon_{\mathbf{x}_j \to \mathbf{x}_r}(t) \tag{3.24}$$

where $\epsilon_{\mathbf{x}_j \to \mathbf{x}_r}(t)$ denotes zero-mean Gaussian measurement noise resulting from averaging out small-scale fading and interference [48]. From (3.20), this measurement can be re-expressed as

$$\breve{S}_{\mathbf{x}_j \to \mathbf{x}_r}(t) = \boldsymbol{\phi}_{\mathbf{x}_j \to \mathbf{x}_r}^T \boldsymbol{\alpha}(t) + \tilde{S}_{\mathbf{x}_j \to \mathbf{x}_r}(t) + \epsilon_{\mathbf{x}_j \to \mathbf{x}_r}(t). \tag{3.25}$$

Suppose that each sensor r can measure the received powers from the transmissions of the set $\mathcal{M}_r$ of sensors, where $\mathcal{M}_r \subset \{1, 2, \ldots, N_r\} \backslash \{r\}$. Specifically, denote as d_{comm} the sensors' communication range and assume that $\mathcal{M}_r$ is given by $\mathcal{M}_r = \{j, j \neq r : \|\mathbf{x}_j - \mathbf{x}_r\|_2 \leq d_{\text{comm}}\}$. Let M_r be the cardinality of the set $\mathcal{M}_r$, and $M := \sum_{r=1}^{N_r} M_r$. Define $\boldsymbol{\Phi}_r$ to be the $(M_r \times K)$-matrix obtained by stacking the vectors $\boldsymbol{\phi}_{\mathbf{x}_j \to \mathbf{x}_r}^T$, $j \in \mathcal{M}_r$, in the order of increasing j. Likewise, define the $(M_r \times 1)$-vectors $\breve{\mathbf{S}}_r(t)$, $\tilde{\mathbf{S}}_r(t)$ and $\boldsymbol{\epsilon}_r(t)$ through appropriate vectorizations of $\breve{S}_{\mathbf{x}_j \to \mathbf{x}_r}(t)$, $\tilde{S}_{\mathbf{x}_j \to \mathbf{x}_r}(t)$, and $\epsilon_{\mathbf{x}_j \to \mathbf{x}_r}(t)$, $j \in \mathcal{M}_r$, respectively. Then, the vector $\breve{\mathbf{S}}_r(t)$ acquired by sensor r at time t is

$$\breve{\mathbf{S}}_r(t) = \boldsymbol{\Phi}_r \boldsymbol{\alpha}(t) + \tilde{\mathbf{S}}_r(t) + \boldsymbol{\epsilon}_r(t). \tag{3.26}$$

Also, by pooling measurements from all sensors to an $(M \times 1)$-super-vector $\breve{\mathbf{S}}(t)$, one can write

$$\breve{\mathbf{S}}(t) = \boldsymbol{\Phi} \boldsymbol{\alpha}(t) + \tilde{\mathbf{S}}(t) + \boldsymbol{\epsilon}(t) \tag{3.27}$$

where $\boldsymbol{\Phi} := [\boldsymbol{\Phi}_1^T \ \ldots \ \boldsymbol{\Phi}_{N_r}^T]^T$, $\tilde{\mathbf{S}}(t) := [\tilde{\mathbf{S}}_1^T(t) \ \ldots \ \tilde{\mathbf{S}}_{N_r}^T(t)]^T$, and finally $\boldsymbol{\epsilon}(t) := [\boldsymbol{\epsilon}_1^T(t) \ \ldots \ \boldsymbol{\epsilon}_{N_r}^T(t)]^T$.

3.3.2 Kriged Kalman filtering

In a centralized setting, KKF collects all measurements to a central processor to perform KKF. Given the state equation (3.18) and the measurement equation (3.27), the minimum mean-square error (MMSE) estimate of the state vector $\boldsymbol{\alpha}(t)$ at time t can be obtained via ordinary KF. Define $\mathbf{C}_{\tilde{S}} := \text{cov}\{\tilde{\mathbf{S}}(t)\}$, $\mathbf{C}_{\epsilon} := \text{cov}\{\boldsymbol{\epsilon}(t)\}$, $\mathbf{C}_{\eta} := \text{cov}\{\boldsymbol{\eta}(t)\}$, and $\boldsymbol{\Sigma} := \mathbf{C}_{\tilde{S}} + \mathbf{C}_{\epsilon}$. Also, let $\breve{\mathbf{S}}_{1:t}$ denote the $(M \times t)$-matrix containing the cumulative measurements $\{\breve{\mathbf{S}}(\tau)\}_{\tau=1}^{t}$.

Upon defining $\hat{\boldsymbol{\alpha}}(t|t-1) := \mathbb{E}\{\boldsymbol{\alpha}(t)|\breve{\mathbf{S}}_{1:t-1}\}$, $\hat{\boldsymbol{\alpha}}(t|t) := \mathbb{E}\{\boldsymbol{\alpha}(t)|\breve{\mathbf{S}}_{1:t}\}$, $\mathbf{P}(t|t-1) := \text{cov}\{\boldsymbol{\alpha}(t)|\breve{\mathbf{S}}_{1:t-1}\}$, and $\mathbf{P}(t|t) := \text{cov}\{\boldsymbol{\alpha}(t)|\breve{\mathbf{S}}_{t}\}$, the KF equations in the information form are given by [52, Ch. 3]

$$\mathbf{P}(t|t-1) = \mathbf{T}\mathbf{P}(t-1|t-1)\mathbf{T}^T + \boldsymbol{\Psi}^{\dagger}\mathbf{C}_{\eta}{\boldsymbol{\Psi}^{\dagger}}^T \tag{3.28}$$

$$\hat{\boldsymbol{\alpha}}(t|t-1) = \mathbf{T}\hat{\boldsymbol{\alpha}}(t-1|t-1) \tag{3.29}$$

$$\mathbf{P}(t|t) = \left[\boldsymbol{\Phi}^T\boldsymbol{\Sigma}^{-1}\boldsymbol{\Phi} + \mathbf{P}^{-1}(t|t-1)\right]^{-1} \tag{3.30}$$

$$\hat{\boldsymbol{\alpha}}(t|t) = \hat{\boldsymbol{\alpha}}(t|t-1) + \mathbf{P}(t|t)\boldsymbol{\Phi}^T\boldsymbol{\Sigma}^{-1}\left[\breve{\mathbf{S}}(t) - \boldsymbol{\Phi}\hat{\boldsymbol{\alpha}}(t|t-1)\right]. \tag{3.31}$$

The Kalman filter-estimate $\hat{\boldsymbol{\alpha}}_r(t|t)$ can thus be used to track the dynamic component $\bar{S}_{\mathbf{x}\to\mathbf{y}}(t)$ through $\mathbb{E}\{\bar{S}_{\mathbf{x}\to\mathbf{y}}(t)|\breve{\mathbf{S}}_{1:t}\} = \boldsymbol{\phi}_{\mathbf{x}\to\mathbf{y}}^T\hat{\boldsymbol{\alpha}}_r(t|t)$. Note that the line integral that transforms the spatial loss field to shadow fading has been absorbed into $\boldsymbol{\phi}_{\mathbf{x}\to\mathbf{y}}$ for the "trend" part via (3.19)–(3.20), and the cross-correlation structure for $\tilde{S}_{\mathbf{x}\to\mathbf{y}}$ is directly modeled via (3.22)–(3.23). Therefore, the model fits well into the KKF framework delineated in [31] and [50]. That is, since the peculiarities of adopting the spatial loss field model have been completely absorbed by the state space model, and the measurements are jointly Gaussian with the shadowing field, the following proposition in [31] and [50] adapted here for the collective measurements applies. It reveals that the KF-based trend estimate augmented by Kriging spatial interpolation yields the desired estimate of the shadowing field.

Proposition 3.3.1. *Conditioned on the measurements $\breve{\mathbf{S}}_{1:t}$, the shadow fading process $S_{\mathbf{x}\to\mathbf{y}}(t)$ for any $\mathbf{x}, \mathbf{y} \in \mathcal{A}$, is Gaussian distributed with mean and*

variance given, respectively, by

$$\begin{aligned}\hat{S}_{\mathbf{x}\to\mathbf{y}}(t) &:= \mathbb{E}\{S_{\mathbf{x}\to\mathbf{y}}(t)|\breve{\mathbf{S}}_{1:t}\} \\ &= \boldsymbol{\phi}_{\mathbf{x}\to\mathbf{y}}^T\hat{\boldsymbol{\alpha}}(t|t) + \mathbf{c}_{\tilde{S}}^T(\mathbf{x},\mathbf{y})\boldsymbol{\Sigma}^{-1}\left[\breve{\mathbf{S}}(t) - \boldsymbol{\Phi}\hat{\boldsymbol{\alpha}}(t|t)\right] \qquad (3.32)\end{aligned}$$

$$\begin{aligned}\mathrm{var}\{S_{\mathbf{x}\to\mathbf{y}}(t)|\breve{\mathbf{S}}_{1:t}\} &= \sigma_{\tilde{S}}^2 - \mathbf{c}_{\tilde{S}}^T(\mathbf{x},\mathbf{y})\boldsymbol{\Sigma}^{-1}\mathbf{c}_{\tilde{S}}(\mathbf{x},\mathbf{y}) \\ &\quad + \left[\boldsymbol{\phi}_{\mathbf{x}\to\mathbf{y}}^T - \mathbf{c}_{\tilde{S}}^T(\mathbf{x},\mathbf{y})\boldsymbol{\Sigma}^{-1}\boldsymbol{\Phi}\right]\mathbf{P}(t|t)\left[\boldsymbol{\phi}_{\mathbf{x}\to\mathbf{y}} - \boldsymbol{\Phi}^T\boldsymbol{\Sigma}^{-1}\mathbf{c}_{\tilde{S}}(\mathbf{x},\mathbf{y})\right] \qquad (3.33)\end{aligned}$$

where $\mathbf{c}_{\tilde{S}}(\mathbf{x},\mathbf{y}) := \mathbb{E}\{\tilde{\mathbf{S}}(t)\tilde{S}_{\mathbf{x}\to\mathbf{y}}(t)\}$.

Proof: See section 3.6.1. □

Note that (3.32) provides the MMSE estimate $\hat{S}_{\mathbf{x}\to\mathbf{y}}(t)$ of the shadow fading process $S_{\mathbf{x}\to\mathbf{y}}(t)$ at any $\mathbf{x},\mathbf{y}$ and t, using only the preselected bases in $\boldsymbol{\Phi}$ and the estimates $\breve{\mathbf{S}}_{1:t}$ acquired at the sensors.

Given the KKF estimate $\hat{S}_{\mathbf{x}\to\mathbf{y}}(t)$, the CG map estimate $\hat{G}_{\mathbf{x}\to\mathbf{y}}(t)$ for an arbitrary $\mathbf{x},\mathbf{y}\in\mathcal{A}$ can be readily constructed by adding back the deterministic (and known) path loss component as [cf. (3.6)]

$$\hat{G}_{\mathbf{x}\to\mathbf{y}}(t) = G_{0,\mathbf{x}\to\mathbf{y}} - 10\eta\log_{10}(\|\mathbf{x}-\mathbf{y}\|_2) + \hat{S}_{\mathbf{x}\to\mathbf{y}}(t). \qquad (3.34)$$

Remark 3.3.2. Besides the MMSE estimate $\hat{S}_{\mathbf{x}\to\mathbf{y}}(t)$ of the shadow fading $S_{\mathbf{x}\to\mathbf{y}}(t)$, the KKF carries out the conditional variance $\mathrm{var}\{S_{\mathbf{x}\to\mathbf{y}}(t)|\breve{\mathbf{S}}_{1:t}\}$. Hence, sufficient information for computing the conditional distribution of the shadow fading is available, being $G_{\mathbf{x}\to\mathbf{y}}(t)$ Gaussian. The distribution of $G_{\mathbf{x}\to\mathbf{y}}(t)$ and, hence, of $\dot{G}_{\mathbf{x}\to\mathbf{y}}(t)$ (see (3.2), where in this case $\sigma^2_{S_{\mathbf{x}\to\mathbf{y}}} = \mathrm{var}\{S_{\mathbf{x}\to\mathbf{y}}(t)|\breve{\mathbf{S}}_{1:t}\}$) may provide vital information for spectrum sensing and resource allocation tasks. □

3.3.3 Handling measurement losses

In a challenging scenario such as the hierarchical spectrum access, training signals need to respect the PU-CR hierarchy. Thus measurements cannot be acquired if the PUs are continuously active over an extended period of time. Measurement misses may also occur when the control channel is congested.

In case of missing measurements, i.e., vector $\breve{\mathbf{S}}(t)$ is not collected, the KKF update must be performed open-loop. Specifically, if the measurement

is missing at time t, the prediction step of Kalman filtering is the same as in (3.28)–(3.29), but the correction step in (3.30)–(3.31) is replaced by [53]

$$\mathbf{P}(t|t) = \mathbf{P}(t|t-1) \tag{3.35}$$

$$\hat{\boldsymbol{\alpha}}_r(t|t) = \hat{\boldsymbol{\alpha}}_r(t|t-1)\,. \tag{3.36}$$

Then, the KKF estimate at time t then becomes

$$\hat{S}_{\mathbf{x}\to\mathbf{y}}(t) = \boldsymbol{\phi}^T_{\mathbf{x}\to\mathbf{y}}\hat{\boldsymbol{\alpha}}_r(t|t) \tag{3.37}$$

$$\text{var}\{S_{\mathbf{x}\to\mathbf{y}}(t)|\check{\mathbf{S}}_r(t)\} = \sigma^2_{\tilde{S}} + \boldsymbol{\phi}^T_{\mathbf{x}\to\mathbf{y}}\mathbf{P}(t|t)\boldsymbol{\phi}_{\mathbf{x}\to\mathbf{y}}. \tag{3.38}$$

It should be noted that under proper stability conditions, the measurement losses over an extended period will eventually bring the KKF estimate $\hat{S}_{\mathbf{x}\to\mathbf{y}}(t)$ down to 0. In this case, the KKF-based model falls back to the path loss-only model [cf. (3.6)]. This is a nice safety feature ensuring that the proposed algorithms perform no worse than the alternatives which account only for path-loss effects. Note also that it is natural to initialize the CG map estimates with the path-loss-only map.

3.3.4 Estimation of model parameters

The KKF is optimal when exact knowledge of the model covariances $\mathbf{C}_\epsilon$, $\mathbf{C}_\eta$ and $\mathbf{C}_{\tilde{S}}$ as well as the state transition matrix $\mathbf{T}$ is available. Also, the cross-covariance $C_{\tilde{S}}(\mathbf{x}\to\mathbf{y}, \mathbf{u}\to\mathbf{v})$ for arbitrary points $\mathbf{x}, \mathbf{y}, \mathbf{u}$, and $\mathbf{v}$ is required to perform the Kriging interpolation in Proposition 3.3.1.

In this work, an empirical Bayesian approach is pursued to estimate the required parameters in (3.18) and (3.27) from the data, and use them in the KKF recursions. In [49], the standard method of moments was employed to obtain the necessary estimates. This approach is adopted here for simplicity. To estimate $\sigma^2_{\tilde{S}}$ and $d_{\tilde{\ell}}$ in (3.21), an exhaustive search over the $(\sigma^2_{\tilde{S}}, d_{\tilde{\ell}})$-space will be performed.

Estimation of model covariances Supposing that the measurement noise $\epsilon_{\mathbf{x}_j\to\mathbf{x}_r}(t)$ is white in space and time, it follows that $\mathbf{C}_\epsilon = \sigma^2_\epsilon\mathbf{I}_M$, where σ^2_ϵ can be obtained during the calibration process of the measurement device. The estimate $\hat{\mathbf{C}}_{\check{S}}$ of $\mathbf{C}_{\check{S}} := \text{cov}\{\check{\mathbf{S}}(t)\}$ is readily found using

the sample covariance of the data $\check{\mathbf{S}}(t)$ (assuming ergodicity of $S_{\mathbf{x}\to\mathbf{y}}(t)$). Then, the estimate of $\mathbf{C}_S := \mathrm{cov}\{\mathbf{S}(t)\}$ is obtained as $\hat{\mathbf{C}}_S = \hat{\mathbf{C}}_{\check{S}} - \mathbf{C}_\epsilon$. Since $\bar{\mathbf{S}}(t)$ belongs to the subspace spanned by the columns of matrix $\mathbf{\Phi}$, it is possible to estimate $\mathbf{C}_{\bar{S}}$ by a projection operation as

$$\hat{\mathbf{C}}_{\bar{S}} = \mathbf{\Phi}\mathbf{\Phi}^\dagger \hat{\mathbf{C}}_S \mathbf{\Phi}^{\dagger T}\mathbf{\Phi}^T. \tag{3.39}$$

Similarly, $\hat{\mathbf{C}}_{\tilde{S}}$ can be obtained as

$$\hat{\mathbf{C}}_{\tilde{S}} = (\mathbf{I}_M - \mathbf{\Phi}\mathbf{\Phi}^\dagger)\hat{\mathbf{C}}_{\check{S}}(\mathbf{I}_M - \mathbf{\Phi}\mathbf{\Phi}^\dagger)^T. \tag{3.40}$$

With $\hat{\mathbf{C}}_{\tilde{S}}$ close at hand, it is now possible to estimate the model parameters $\sigma^2_{\tilde{S}}$ and $d_{\tilde{\ell}}$ inherent to $\tilde{S}_{\mathbf{x}\to\mathbf{y}}(t)$; see (3.21). An exhaustive search over the $(\sigma^2_{\tilde{S}}, d_{\tilde{\ell}})$-space can be performed, which entails finding the couple of parameters $(\sigma^2_{\tilde{S}}, d_{\tilde{\ell}})$ that minimize the quadratic quadratic cost $||\hat{\mathbf{C}}_{\tilde{s}} - \mathbf{C}_{\tilde{s}}(\sigma^2_{\tilde{s}}, d_{\tilde{\ell}})||_2^2$, where the entries $\mathbf{C}_{\tilde{S}}(\sigma^2_{\tilde{s}}, d_{\tilde{\ell}})$ are numerically computed via (3.23).

Before estimating $\mathbf{C}_\eta$, observe that the KKF recursion (3.29) requires only an estimate of the product $\mathbf{\Psi}^\dagger \mathbf{C}_\eta \mathbf{\Psi}^{\dagger T}$, and not an estimate of $\mathbf{C}_\eta$ in isolation. Define $\mathbf{C}_\alpha := \mathrm{cov}\{\boldsymbol{\alpha}(t)\}$ and $\mathbf{C}^{(1)}_\alpha := \mathbb{E}\{\boldsymbol{\alpha}(t)\boldsymbol{\alpha}^T(t-1)\}$. Then, note that $\mathbf{C}_{\bar{S}} = \mathbf{\Phi}\mathbf{C}_\alpha\mathbf{\Phi}^T$, and that $\mathbf{C}^{(1)}_{\check{S}} := \mathbb{E}\{\check{\mathbf{S}}_{1:t}\check{\mathbf{S}}^T(t-1)\}$ is given by [cf. (3.27)]

$$\mathbf{C}^{(1)}_{\check{S}} = \mathbb{E}\left\{\left[\mathbf{\Phi}\boldsymbol{\alpha}(t) + \tilde{\mathbf{S}}(t) + \boldsymbol{\epsilon}(t)\right]\cdot\left[\mathbf{\Phi}\boldsymbol{\alpha}(t-1) + \tilde{\mathbf{S}}(t-1) + \boldsymbol{\epsilon}(t-1)\right]^T\right\} \tag{3.41}$$

$$= \mathbf{\Phi}\mathbf{C}^{(1)}_\alpha\mathbf{\Phi}^T. \tag{3.42}$$

Thus, $\mathbf{C}_\alpha = \mathbf{\Phi}^\dagger\mathbf{C}_{\bar{S}}\mathbf{\Phi}^{\dagger T}$ and $\mathbf{C}^{(1)}_\alpha = \mathbf{\Phi}^\dagger\mathbf{C}^{(1)}_{\check{S}}\mathbf{\Phi}^{\dagger T}$ hold; hence, [cf. (3.18)]

$$\begin{aligned}
&\mathbf{\Psi}^\dagger\mathbf{C}_\eta\mathbf{\Psi}^{\dagger T}\\
&= \mathbb{E}\left\{[\boldsymbol{\alpha}(t) - \mathbf{T}\boldsymbol{\alpha}(t-1)]\,[\boldsymbol{\alpha}(t) - \mathbf{T}\boldsymbol{\alpha}(t-1)]^T\right\} &(3.43)\\
&= \mathbf{\Phi}^\dagger\mathbf{C}_{\bar{S}}\mathbf{\Phi}^{\dagger T} - \mathbf{\Phi}^\dagger\mathbf{C}^{(1)}_{\check{S}}\mathbf{\Phi}^{\dagger T}\mathbf{T}^T - \mathbf{T}\mathbf{\Phi}^\dagger_r\mathbf{C}^{(1)}_{\check{S}}\mathbf{\Phi}^\dagger + \mathbf{T}\mathbf{\Phi}^\dagger\mathbf{C}_{\bar{S}}\mathbf{\Phi}^{\dagger T}\mathbf{T}^T. &(3.44)
\end{aligned}$$

Matrix $\mathbf{\Psi}^\dagger\mathbf{C}_\eta\mathbf{\Psi}^{\dagger T}$ can now be estimated by plugging into (3.44) the expression for $\hat{\mathbf{C}}_{\bar{S}}$ found as in (3.39), and the estimate $\hat{\mathbf{C}}^{(1)}_{\check{S}}$ obtained via sample averaging.

Estimation of the state transition matrix To estimate the state transition matrix $\mathbf{T}$, note first that [cf. (3.17) and (3.27)]

$$\begin{aligned}\mathbf{C}_{\check{S}}^{(1)} &= \mathbb{E}\{[\mathbf{B}\boldsymbol{\alpha}(t-1)+\boldsymbol{\eta}(t)+\tilde{\mathbf{S}}(t)+\boldsymbol{\epsilon}(t)] \\ &\quad \cdot [\boldsymbol{\Phi}\boldsymbol{\alpha}(t-1)+\boldsymbol{\eta}(t-1)+\tilde{\mathbf{S}}(t-1)+\boldsymbol{\epsilon}(t-1)]^T\} \qquad (3.45)\\ &= \mathbf{B}\boldsymbol{\Phi}^{\dagger}\mathbf{C}_{\bar{S}}\boldsymbol{\Phi}^{\dagger T}\boldsymbol{\Phi}^T \qquad (3.46)\end{aligned}$$

where the relation $\mathbf{C}_{\alpha} = \boldsymbol{\Phi}^{\dagger}\mathbf{C}_{\bar{S}}\boldsymbol{\Phi}^{\dagger T}$ is again used to get (3.46). Thus, an estimate of matrix $\mathbf{B}$ is obtained as

$$\hat{\mathbf{B}} = \hat{\mathbf{C}}_{\check{S}}^{(1)}\boldsymbol{\Phi}^{\dagger T}[\boldsymbol{\Phi}^{\dagger}\hat{\mathbf{C}}_{\bar{S}}\boldsymbol{\Phi}^{\dagger T}]^{-1} \qquad (3.47)$$

and $\hat{\mathbf{T}} = \boldsymbol{\Phi}^{\dagger}\hat{\mathbf{B}}$.

Recall that $\boldsymbol{\Psi}$ (and hence $\boldsymbol{\Phi}$) is formed using pre-selected basis functions. One such basis can be constructed easily for a rectangular area $\mathcal{A}$ using the set of Legendre polynomials in two variables [54, Ch. 2].

Table 3.1 summarizes the overall algorithm for tracking the CG map $G_{\mathbf{x}\to\mathbf{y}}(t)$ across time t, for any arbitrary points of interest $\mathbf{x}, \mathbf{y}$ in the geographical area $\mathcal{A}$.

3.4 Distributed Kriged Kalman filtering

In certain cases, a distributed algorithm may be more desirable since it does not require all the measurements to be collected at a single processor, but rather performs consensus-based in-network processing. Moreover, a centralized algorithm may face scalability and robustness concerns because the fusion center constitutes an isolated point of failure. These considerations motivated the development next to perform the KKF operation in a distributed fashion.

3.4.1 Distributed Kalman Filtering

Consider the computation of the KF recursion (3.28)–(3.31). Recall that matrices $\mathbf{T}$, $\boldsymbol{\Sigma}$ and $\boldsymbol{\Psi}^{\dagger}\mathbf{C}_{\eta}\boldsymbol{\Psi}^{\dagger T}$ are known to all sensors (at least an estimate of them). The prediction step in (3.28)–(3.29) can be performed locally at each node, provided that $\hat{\boldsymbol{\alpha}}(t-1|t-1)$ and $\mathbf{P}(t-1|t-1)$ are available. However, to

Acquisition of observation $\breve{\mathbf{S}}(t)$
During time interval $[t, t+1)$ in the j-th slot, sensor $j \neq r$ transmits a training signal with power $p_j(t)$ in a TDMA fashion.
Sensor r measures the received power $\pi_r^{(j)}(t)$ in slot $j \neq r$ and computes the channel gain estimate by $\hat{g}_{\mathbf{x}_j \to \mathbf{x}_r}(t) = \pi_r^{(j)}(t)/p_j(t)$.
Compute $\hat{G}_{\mathbf{x}_j \to \mathbf{x}_r}(t) = 10 \log_{10} \hat{g}_{\mathbf{x}_j \to \mathbf{x}_r}(t)$.
Compute $\breve{S}_{\mathbf{x}_j \to \mathbf{x}_r}(t) = \hat{G}_{\mathbf{x}_j \to \mathbf{x}_r}(t) - G_{0,\mathbf{x}_j \to \mathbf{x}_r} + 10\eta \log_{10} \|\mathbf{x}_r - \mathbf{x}_j\|_2$.
Collect $\breve{S}_{\mathbf{x}_j \to \mathbf{x}_r}(t)$, $j \in \mathcal{M}_r$ and form $\breve{\mathbf{S}}_r(t)$.
Collect $\breve{\mathbf{S}}_r(t)$, $r = 1, \ldots, N_r$ and form $\breve{\mathbf{S}}_{1:t}$.
Model parameter estimation
Obtain $\hat{\mathbf{C}}_{\breve{S}}$ and $\hat{\mathbf{C}}_{\breve{S}}^{(1)}$ from sample covariances.
Compute $\hat{\mathbf{C}}_S = \hat{\mathbf{C}}_{\breve{S}} - \mathbf{C}_\epsilon$.
Obtain $\hat{\mathbf{C}}_{\bar{S}}$ from (3.39) and $\hat{\mathbf{C}}_{\tilde{S}}$ from (3.40).
Compute $\sigma_{\tilde{S}}^2$ and d_ℓ by least squares model fitting.
Compute $\hat{\mathbf{B}}$ from (3.47) and set $\hat{\mathbf{T}} = \mathbf{\Phi}^\dagger \hat{\mathbf{B}}$.
Obtain an estimate of $\mathbf{\Psi}^\dagger \mathbf{C}_\eta \mathbf{\Psi}^{\dagger T}$ from (3.44).
Map tracking via KKF
1: Initialize $t = 0$
2: If $\breve{\mathbf{S}}(t)$ is not available, update KF open-loop by (3.28)–(3.29) and (3.36)–(3.35). Compute the KKF estimate $\hat{S}_{\mathbf{x} \to \mathbf{y}}(t)$ by (3.37). Go to Step 4.
3: If $\breve{\mathbf{S}}(t)$ is available, update KF by (3.28)–(3.31). Compute the KKF estimate $\hat{S}_{\mathbf{x} \to \mathbf{y}}(t)$ by (3.33).
4: Compute estimate $\hat{G}_{\mathbf{x} \to \mathbf{y}}(t)$ by (3.34).
5: Increment t and go to Step 2.

Table 3.1: Summary of the centralized map tracking algorithm.

perform the correction step in (3.31), the measurements from other sensors are required. To reduce the substantial message-passing overhead associated with globally sharing (i.e., flooding) the measurements in each update step, a distributed algorithm is desired. To this end, consider the innovation process

$$\mathbf{y}(t) := \breve{\mathbf{S}}(t) - \mathbf{\Phi}\hat{\boldsymbol{\alpha}}(t|t-1) \tag{3.48}$$

and define a $(K \times 1)$-vector

$$\boldsymbol{\chi}(t) := \mathbf{\Phi}^T \mathbf{\Sigma}^{-1} \mathbf{y}(t). \tag{3.49}$$

It is clear from (3.31) that if $\boldsymbol{\chi}(t)$ were available at each sensor, the Kalman steps in (3.28)–(3.31) could be performed locally at individual sensors.

Distributed computation of $\boldsymbol{\chi}(t)$ was considered in [55], using the standard consensus averaging algorithm. In [56], the consensus problem was re-cast as a convex optimization problem, which was then solved in a distributed manner by a set of "bridge" nodes based on the alternating direction method of multipliers (ADMoM) [57, p. 253]. This latter approach has the additional benefit of improved robustness to communication and quantization noise [56]. However, the distributed KF algorithm developed here does not require election of bridge nodes; each sensor needs to exchange information only with its single-hop neighbors. Note that a similar approach was taken in [31] to obtain a distributed solution for a sparse regression problem.

To distribute $\boldsymbol{\chi}(t)$, consider re-writing it as a sum of N_r terms, each of which contains only local information. Let $\mathbf{H}_r$ denote the $(K \times M_r)$-matrix formed by the $\left(\sum_{r'=1}^{r-1} M_{r'} + 1\right)$-st to the $(\sum_{r'=1}^{r} M_{r'})$-th columns of $\mathbf{\Phi}^T \mathbf{\Sigma}^{-1}$. Using $\mathbf{H}_r$ and $\mathbf{y}_r(t) := \breve{\mathbf{S}}_r(t) - \mathbf{\Phi}_r \boldsymbol{\alpha}(t|t-1)$, it is possible to express $\boldsymbol{\chi}(t)$ as

$$\boldsymbol{\chi}(t) = \sum_{r=1}^{N_r} \mathbf{H}_r \mathbf{y}_r(t). \tag{3.50}$$

A key observation is that (3.50) is equivalent to

$$\boldsymbol{\chi}(t) = \arg\min_{\boldsymbol{\chi}} \sum_{r=1}^{N_r} \|\boldsymbol{\chi} - N_r \mathbf{H}_r \mathbf{y}_r(t)\|_2^2. \tag{3.51}$$

To show the equivalence between (3.50) and (3.51), rewrite (3.51) as

$$\boldsymbol{\chi}(t) = \arg\min_{\boldsymbol{\chi}} \sum_{r=1}^{N_r} \left[\boldsymbol{\chi}^T\boldsymbol{\chi} - 2N_r\boldsymbol{\chi}^T\mathbf{H}_r\mathbf{y}_r(t) + N_r^2\|\boldsymbol{\chi}^T\mathbf{H}_r\mathbf{y}_r(t)\|_2^2\right] \tag{3.52}$$

$$= \arg\min_{\boldsymbol{\chi}} \left[\boldsymbol{\chi}^T\boldsymbol{\chi} - 2\boldsymbol{\chi}^T\sum_{r=1}^{N_r}\mathbf{H}_r\check{\mathbf{y}}_r(t)\right]. \tag{3.53}$$

The solution of the unconstrained problem (3.53) can be readily obtained in closed-form and it coincides with (3.50).

To distribute (3.50), introduce local copies of $\boldsymbol{\chi}(t)$ per sensor, and denote them as $\boldsymbol{\chi}_r(t)$, $r = 1, 2, \ldots, N_r$. Denote as $\mathcal{N}_r$ the set of one-hop neighboring nodes of sensor r; note that $\mathcal{M}_r$ and $\mathcal{M}_r$ might be in general different, especially if detection radius (for CG measurement) and communication range (for packet exchange) are different. Then, (3.51) can be re-formulated as the following constrained optimization problem:

$$\{\boldsymbol{\chi}_r(t)\}_{r=1}^{N_r} = \arg\min_{\{\boldsymbol{\chi}_r\}} \sum_{r=1}^{N_r} \|\boldsymbol{\chi}_r - N_r\mathbf{H}_r\mathbf{y}_r(t)\|_2^2 \tag{3.54}$$

$$\text{subject to } \boldsymbol{\chi}_r = \boldsymbol{\chi}_\varrho, \quad \forall \varrho \in \mathcal{N}_r, \quad r = 1, \ldots, N_r \tag{3.55}$$

where the constraints in (3.55) enforce the local copies of $\boldsymbol{\chi}(t)$ to coincide within the set of one-hop neighbors $\mathcal{N}_r$ of node r, $\forall r \in \{1, 2, \ldots, N_r\}$. Under the assumption that the network remains connected, i.e., there exist (possibly multi-hop) paths from any node to any other node in the network, the constraints in (3.55) ensure global consensus on $\boldsymbol{\chi}_r(t)$, $\forall\, r = 1, \ldots, N_r$.

Employing the ADMoM, one can show that the following iterative algorithm attains the solution to (3.54)–(3.55):

$$\boldsymbol{\zeta}_r^{(j)}(t) = \boldsymbol{\zeta}_r^{(j-1)}(t) + c\left(|\mathcal{N}_r|\boldsymbol{\chi}_r^{(j)}(t) - \sum_{\varrho\in\mathcal{N}_r}\boldsymbol{\chi}_\varrho^{(j)}(t)\right) \tag{3.56}$$

$$\boldsymbol{\chi}_r^{(j+1)}(t) = (1 + c|\mathcal{N}_r|)^{-1} \cdot \left[N_r\mathbf{H}_r\mathbf{y}_r(t) - \frac{1}{2}\boldsymbol{\zeta}_r^{(j)}(t) + \frac{c}{2}\left(|\mathcal{N}_r|\boldsymbol{\chi}_r^{(j)}(t) + \sum_{\varrho\in\mathcal{N}_r}\boldsymbol{\chi}_\varrho^{(j)}(t)\right)\right] \tag{3.57}$$

where $\boldsymbol{\zeta}_r^{(j)}(t)$ denotes the Lagrange multiplier corresponding to (3.55) updated at sensor r during the KF iteration indexed by t; superscript j indexes

consensus iterations; $c > 0$ is a constant that can be chosen arbitrarily; and $|\mathcal{N}_r|$ denotes the cardinality of the set $\mathcal{N}_r$.

At iteration j, sensor r needs to collect from its neighbors the current estimates $\{\boldsymbol{\chi}_\varrho^{(j)}(t)\}_{\varrho\in\mathcal{N}_r}$ to update the auxiliary vector $\boldsymbol{\zeta}_r^{(j)}(t)$ via (3.56), and to subsequently compute $\boldsymbol{\chi}_r^{(j+1)}(t)$ via (3.57). Derivation of (3.56)–(3.57) as well as the proof of the convergence result stated in the following proposition are deferred to in section (3.6.2)

Proposition 3.4.1. *Assume that the network of sensors is connected and the links are bi-directional; i.e., $\varrho \in \mathcal{N}_r$ implies $r \in \mathcal{N}_\varrho$. By performing the updates in* (3.56)–(3.57) *at each sensor $r = 1, 2, \ldots, N_r$, iteratively for $j = 1, 2, \ldots$, the local copies $\boldsymbol{\chi}_r(t)$ for all r converge and coincide with $\boldsymbol{\chi}(t)$ of* (3.51) *as $j \to \infty$, for any positive c, and initialization $\{\boldsymbol{\chi}_r^{(1)}(t)\}$ and $\{\boldsymbol{\zeta}_r^{(0)}(t)\}$.* □

After reaching consensus on $\boldsymbol{\chi}(t)$ and, thus, performing step (3.31), $\bar{S}_{\mathbf{x}\to\mathbf{y}}(t)$ can be readily estimated by [cf. (3.20)]

$$\mathbb{E}\{\bar{S}_{\mathbf{x}\to\mathbf{x}_r}(t)|\breve{\mathbf{S}}_{1:t}\} = \boldsymbol{\phi}_{\mathbf{x}\to\mathbf{x}_r}^T\hat{\boldsymbol{\alpha}}(t|t). \tag{3.58}$$

3.4.2 Distributed Kriging

To obtain $\tilde{S}_{\mathbf{x}\to\mathbf{y}}(t)$ in (3.32) locally per sensor, it is first noted from (3.31) that

$$\mathbf{c}_{\tilde{S}}^T(\mathbf{x},\mathbf{y})\boldsymbol{\Sigma}^{-1}\left[\breve{\mathbf{S}}(t) - \boldsymbol{\Phi}\hat{\boldsymbol{\alpha}}(t|t)\right] = \mathbf{c}_{\tilde{S}}^T(\mathbf{x},\mathbf{y})\boldsymbol{\Sigma}^{-1}\mathbf{y}(t) - \mathbf{c}_{\tilde{S}}^T(\mathbf{x},\mathbf{y})\boldsymbol{\Sigma}^{-1}\boldsymbol{\Phi}\mathbf{P}(t|t)\boldsymbol{\chi}(t). \tag{3.59}$$

Thus, one only needs to obtain $\xi(t) := \mathbf{c}_{\tilde{S}}^T(\mathbf{x},\mathbf{y})\boldsymbol{\Sigma}^{-1}\mathbf{y}(t)$ in a distributed manner. Upon denoting the $(M_r \times 1)$ vector collecting the $\left(\sum_{r'=1}^{r-1} M_{r'} + 1\right)$-st to the $(\sum_{r'=1}^{r} M_{r'})$-th entries of $\mathbf{c}_{\tilde{S}}^T(\mathbf{x},\mathbf{y})\boldsymbol{\Sigma}^{-1}$ into the vector $\boldsymbol{\sigma}_r^T$, it follows that the scalar quantity $\xi(t)$ can be rewritten as [cf. (3.50)]

$$\xi(t) = \sum_{r=1}^{N_r} \boldsymbol{\sigma}_r^T\mathbf{y}_r(t). \tag{3.60}$$

Therefore, in the same manner used to derive (3.56)–(3.57), a distributed algorithm can be devised to obtain $\xi(t)$ per sensor via (3.56)–(3.57) with

$\boldsymbol{\chi}_r^{(j)}(t)$ and $\mathbf{H}_r$ replaced by $\xi_r^{(j)}(t)$ and $\boldsymbol{\sigma}_r^T$, respectively. Specifically, consider the constrained optimization problem

$$\{\xi_r(t)\}_{r=1}^{N_r} = \arg\min_{\{\xi_r\}} \sum_{r=1}^{N_r} (\xi_r - \boldsymbol{\sigma}_r^T \mathbf{y}_r(t))^2 \tag{3.61}$$

$$\text{subject to } \xi_r = \xi_\varrho, \quad \forall \varrho \in \mathcal{N}_r, \quad r = 1, \ldots, N_r \tag{3.62}$$

where $\{\xi_r(t)\}_{r=1}^{N_r}$ are local copies of $\xi(t)$ and, again, the constraints in (3.62) enforce the local copies of $\xi(t)$ to coincide within the set of one-hop neighbors $\mathcal{N}_r$ of node r, $\forall r \in \{1, 2, \ldots, N_r\}$ - and, hence, in the entire network under the assumption of network connectivity.

Employing the ADMoM to iteratively solve (3.61)–(3.62), one can show that the following steps can be derived and are to be performed at each iteration j:

$$\nu_r^{(j)}(t) = \nu_r^{(j-1)}(t) + c_\xi \left(|\mathcal{N}_r| \xi_r^{(j)}(t) - \sum_{\varrho \in \mathcal{N}_r} \xi_\varrho^{(j)}(t) \right) \tag{3.63}$$

$$\begin{aligned} \xi_r^{(j+1)}(t) = {} & (1 + c_\xi |\mathcal{N}_r|)^{-1} \\ & \cdot \left[N_r \boldsymbol{\sigma}_r^T \mathbf{y}_r(t) - \frac{1}{2} \nu_r^{(j)}(t) + \frac{c_\xi}{2} \left(|\mathcal{N}_r| \xi_r^{(j)}(t) + \sum_{\varrho \in \mathcal{N}_r} \xi_\varrho^{(j)}(t) \right) \right] \end{aligned} \tag{3.64}$$

where $\nu_r^{(j)}(t)$ denotes the Lagrange multiplier corresponding to (3.62) and $c_\xi > 0$. Through and through similar to proposition 3.4.1, convergence of iterations (3.63)–(3.64) can be stated.

Proposition 3.4.2. *Under network connectivity and link bidirectional links assumptions, by performing the updates in* (3.63)–(3.64) *at each sensor* $r = 1, 2, \ldots, N_r$, *iteratively for* $j = 1, 2, \ldots$, *the local copies* $\xi_r(t)$ *for all* r *converge and coincide with* $\xi(t)$ *of* (3.61) *as* $j \to \infty$, *for any positive* c_ξ, *and initialization* $\{\xi_r^{(1)}(t)\}$ *and* $\{\nu_r^{(0)}(t)\}$. □

Note, finally, that iterations (3.56)–(3.57) and (3.63)–(3.64) can be computed in parallel. Table 3.2 summarizes the overall distributed algorithm.

Acquisition of local observation $\breve{\mathbf{S}}_r(t)$
During time interval $[t, t+1)$ in the j-th slot, sensor $j \neq r$ transmits a training signal with power $p_j(t)$ in a TDMA fashion. Sensor r measures the received power $\pi_r^{(j)}(t)$ in slot $j \neq r$ and computes the channel gain estimate by $\hat{g}_{\mathbf{x}_j \to \mathbf{x}_r}(t) = \pi_r^{(j)}(t)/p_j(t)$. Compute $\hat{G}_{\mathbf{x}_j \to \mathbf{x}_r}(t) = 10 \log_{10} \hat{g}_{\mathbf{x}_j \to \mathbf{x}_r}(t)$. Compute $\breve{S}_{\mathbf{x}_j \to \mathbf{x}_r}(t) = \hat{G}_{\mathbf{x}_j \to \mathbf{x}_r}(t) - G_{0,\mathbf{x}_j \to \mathbf{x}_r} + 10\eta \log_{10} \|\mathbf{x}_r - \mathbf{x}_j\|_2$. Collect $\breve{S}_{\mathbf{x}_j \to \mathbf{x}_r}(t)$, $j \in \mathcal{M}_r$ and form $\breve{\mathbf{S}}_r(t)$.
Map tracking via distributed KKF
At each sensor r: 1: Initialize $t = 0$ 2: If $\breve{\mathbf{S}}(t)$ is not available update KF open-loop locally by (3.28)–(3.29) and (3.36)–(3.35). Compute the KKF estimate $\hat{S}_{\mathbf{x} \to \mathbf{y}}(t)$ by (3.37). Go to Step 4. 3: If $\breve{\mathbf{S}}(t)$ is available Initialize $\{\boldsymbol{\chi}_r^{(0)}(t)\}$, $\{\boldsymbol{\zeta}_r^{(0)}(t)\}$ $\{\xi_r^{(1)}(t)\}$, and $\{\nu_r^{(0)}(t)\}$. for $j = 1, 2, \ldots, N_I$, at each sensor r: collect $\{\boldsymbol{\chi}_\varrho^{(j)}(t)\}_{\varrho \in \mathcal{N}_r}$ update $\boldsymbol{\zeta}_r^{(j)}(t)$ via (3.56) compute $\boldsymbol{\chi}_r^{(j+1)}(t)$ via (3.57) collect $\{\xi_\varrho^{(j)}(t)\}_{\varrho \in \mathcal{N}_r}$ update $\{\nu_r^{(j)}(t)$ via (3.63) compute $\xi_r^{(j+1)}(t)$ via (3.64) transmit $\xi_r^{(j+1)}(t)$ and $\xi_r^{(j+1)}$ Compute the KKF estimate $\hat{S}_{\mathbf{x} \to \mathbf{y}}(t)$ by (3.33). 4: Compute estimate $\hat{G}_{\mathbf{x} \to \mathbf{y}}(t)$ by (3.34). 5: Increment t and go to Step 2.

Table 3.2: Summary of the distributed map tracking algorithm.

3.5 Numerical results

Numerical tests were performed to assess the performance of the proposed algorithms. A geographical area of 200m $\times$ 200m was considered, where 40 sensors were randomly deployed. Two networks were considered: first, the nodes collaborating were $N_r = 20$ and were positioned at the locations marked with black circles in Fig. 3.2. Then, sensor positioned at the locations marked with grey circles were added in order to attain a network comprising $N_r = 40$ nodes.

The path loss parameters were set to $G_{0,\mathbf{x}\to\mathbf{y}} = 0$ dB for each $\mathbf{x}, \mathbf{y}$, and $\eta = 3$. The variance of the CG measurement noise $\epsilon_{\mathbf{x}_j\to\mathbf{x}_r}(t)$ was set to 10 [48]. For the basis expansion, $K = 15$ Legendre polynomials [54, Ch. 2] were used. The shadow fading was generated via the model set forth in section 3.2.1, with $w(\mathbf{x}, \mathbf{u}) = w_0 \exp(\|\mathbf{x} - \mathbf{u}\|_2/d_w)$, where $w_0 = 7.3 \times 10^{-3}$ and $d_w = 50$m were used, and the covariance of $\eta(\mathbf{x}, t)$ was set to $\mathbb{E}\{\eta(\mathbf{x}_1, t)\eta(\mathbf{x}_2, \tau)\} = \sigma_\eta^2 \exp(\|\mathbf{x}_1 - \mathbf{x}_2\|_2/d_\eta)\delta(t - \tau)$, with $\sigma_\eta = 0.25$ and $d_\eta = 30$m. The model parameters for $\tilde{\ell}(\mathbf{x}, t)$ were set to $\sigma_{\tilde{s}} = 0.5$ dB and $d_{\tilde{\ell}} = 30$m. The generated shadow fading had mean 0dB and standard deviation 10dB. The parameters of the state-space model were estimated from the generated shadowing, as discussed in Sec. 3.3.4.

To assess the map tracking performance of the proposed algorithm, the CG estimation errors were averaged over the 35 links from each of the uniformly spread grid points, denoted by the squares in Fig. 3.2, to the grid position $\mathbf{x}_g$ at $(149, 83)$; as well as over 20 independent shadowing realizations. It was assumed that two sensors could communicate only if they were within a given communication range d_{comm}; i.e., $\mathcal{M}_r = \{j | j \neq r, \|\mathbf{x}_r - \mathbf{x}_j\| \leq d_{\text{comm}}\}$. Thus, d_{comm} essentially limits the number of CG measurements that each sensor can obtain. Fig. 3.3(a) depicts the root-mean-square-errors (RMSEs) of:

i) the centralized KKF proposed in this work;

ii) the distributed KKF;

iii) the non-collaborative KKF at sensor $r = 1$ (see Fig. 3.2), in which the sensor uses only its local CG measurements to run the KKF recursions;

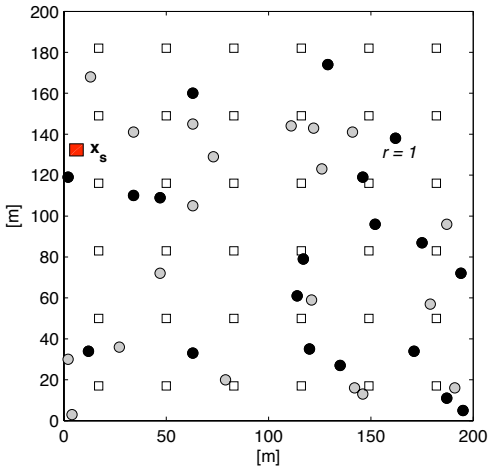

Figure 3.2: CG map estimation. Simulation scenario.

hence, no collaboration among nodes is involved;

iv) the path loss-only map.

The value of d_{comm} was varied in $[50, 200]$m and it was assume to be the same to construct $\{\mathcal{M}_r\}$ and $\{\mathcal{N}_r\}$. 15 iterations of the KKF were performed. For the distributed KKF, 100 consensus iterations were performed per time t. Figs. 3.3(b) presents the same set of trajectories corresponding to the set-up $N_r = 40$.

It is seen from Fig.s 3.3(a) and 3.3(b) that the proposed collaborative algorithm clearly outperforms the non-collaborative alternative. This happens because the non-collaborative algorithm uses only M_1 local CG measurements, whereas the collaborative KKF makes use of all $M = \sum_{r=1}^{N_r} M_r$ measurements through consensus iterations. Certainly, it would be challenging for the non-collaborative algorithm to predict the shadow fading for a transmitter that is far from CR 1 due to the lack of informative measurements, while the collaborative algorithm can extract a single coherent view of the global shadowing field. As d_{comm} increases, the non-collaborative approach performs considerably better due to the increased number of measurements, but still remains inferior to the collaborative approach.

It is also noted that when d_{comm} is very small, the performance of the distributed algorithm degrades slightly compared to the centralized algorithm,

as a larger number of hops would be necessary to achieve full consensus. This effect is negligible when $N_r = 40$, where full consensus is achieved even for small communication radii.

After having assessed the average estimation performance of the KKF, consider next a location of interest $\mathbf{x}_s$, marked with a red square in Fig. 3.2, and its (true) channel gain map at a given time instant depicted in Fig. 3.4. Clearly, the channel gain map peaks at the location $\mathbf{x}_s$ due to the path loss effect; however, the spatially inhomogeneous shadowing component renders the overall CG map non-isotropic. Also, consider discretizing the monitored area $\mathcal{A}$ by using a finer grid; specifically, use 40^2 uniformly spread grid points - 5m of spacing among points.

It is of interest to reconstruct the current channel gain map, i.e., estimate the channel gain of links between the grid points and the position $\mathbf{x}_s$. Fig. 3.5 reports the portrayal of the channel gain map inherent to $\mathbf{x}_s$ collaboratively carried out by the sensor network. The communication range was set to $d_{\text{comm}} = 150$m, $N_r = 20$ (first network configuration) and 100 consensus iterations were performed in both the distributed KF and the distributed Kriging. The error in reconstructing the map was of 4.05 dB, which is remarkably low if be compared to 10.77dB of standard deviation experienced in the current shadow fading map realization. An inspection of Fig. 3.6, where the error in estimating the channel gain is reported, reveals that a substantial contribution in the experienced estimation error is due to grid points close to the edge of $\mathcal{A}$ (points that, however, might not be of relevant interest), which is essentially due to a lack of measurements on that portion of area (see, e.g., the upper border).

Wrapping up, the shadow fading effect is well captured in the estimated channel gain map, confirming that the KKF machinery can effectively predict the values of the shadow fading and, hence, avoid the oversimplified disc-shaped description of the propagation environment, as depicted in Fig. 3.7, entailed by a simple path loss-only model.

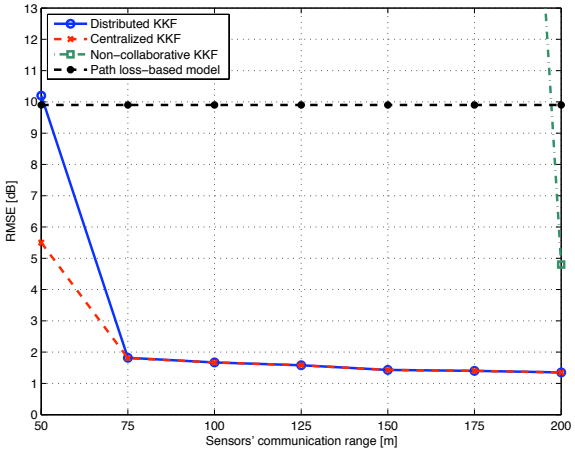

(a) $N_r = 20$.

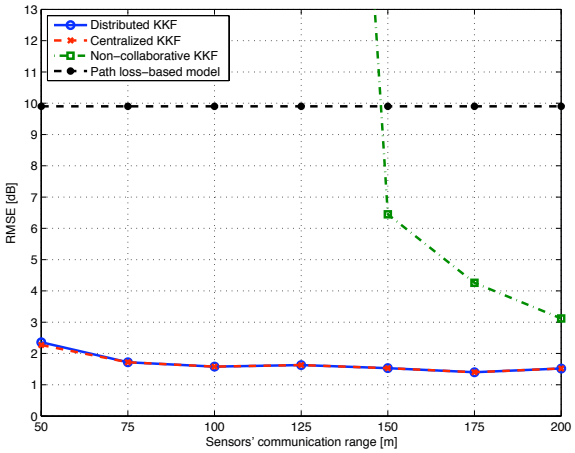

(b) $N_r = 40$.

Figure 3.3: CG map estimation RMSEs.

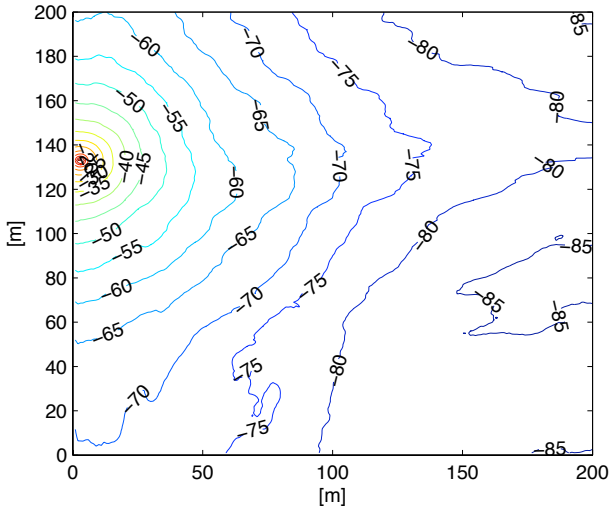

Figure 3.4: Global CG map estimation, snapshot, true CG map.

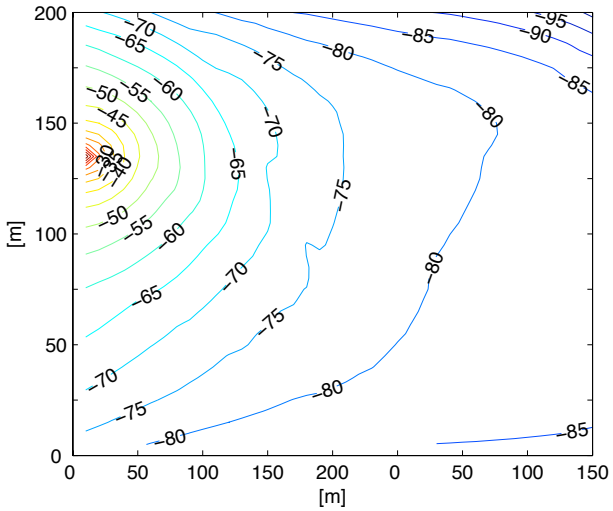

Figure 3.5: Global CG map estimation, snapshot, estimated CG map.

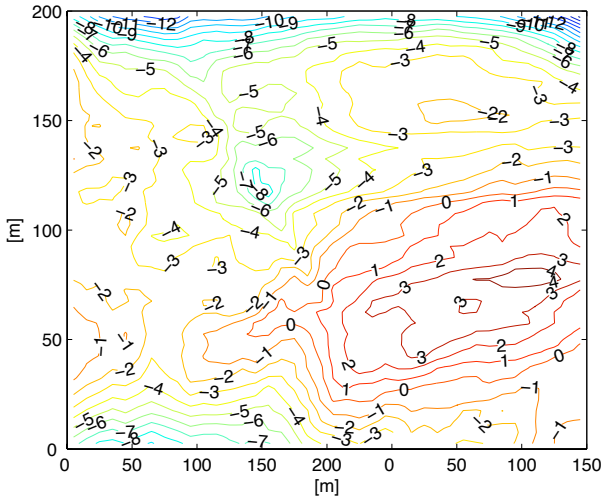

Figure 3.6: Global CG map estimation, snapshot, estimation error.

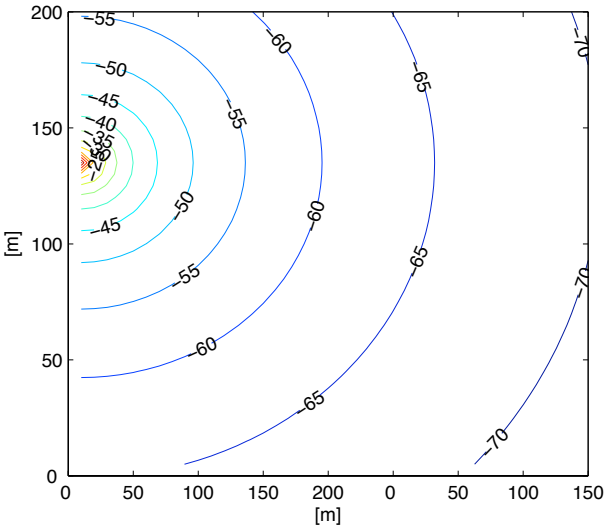

Figure 3.7: Global CG map estimation, snapshot, path loss model.

3.6 Appendix: Proof of the propositions

3.6.1 Proof of proposition 3.3.1

Recall that the cross-covariance between $\tilde{S}_{\mathbf{x}\to\mathbf{y}}(t)$ and $\tilde{S}_{\mathbf{x_i}\to\mathbf{x}_j}(t)$ for two arbitrary (and possibly disjoint, i.e., $\mathbf{x}\neq\mathbf{x}_i,\mathbf{x}_j$ and $\mathbf{y}\neq\mathbf{x}_i,\mathbf{x}_j$) links $\mathbf{x}\to\mathbf{y}$ and $\mathbf{x}_i\to\mathbf{x}_j$ follows (3.23). Also, recall that the $M\times t$ matrix $\check{\mathbf{S}}_{1:t}$ collects the measurements gathered by all the nodes up to the current time instant t. Define the $(Mt\times 1)$ vector $\check{\mathbf{S}}_{1:t}:=\text{vec}(\check{\mathbf{S}}_{1:t})$. It can be verified from the modeling assumptions that $\check{\mathbf{S}}_{1:t}$ and $S_{\mathbf{x}\to\mathbf{y}}(t)=\boldsymbol{\phi}_{\mathbf{x}\to\mathbf{y}}^T\boldsymbol{\alpha}(t)+\tilde{S}_{\mathbf{x}\to\mathbf{y}}(t)$ are jointly Gaussian. Thus, conditioned on $\check{\mathbf{S}}_{1:t}$, the process $S_{\mathbf{x}\to\mathbf{y}}(t)$ is Gaussian distributed.

Derivation of the conditional mean. To derive (3.32), note first that

$$\mathbb{E}\{S_{\mathbf{x}\to\mathbf{y}}(t)|\check{\mathbf{S}}_{1:t}\}=\mathbb{E}\left\{\mathbb{E}\left\{S_{\mathbf{x}\to\mathbf{y}}(t)\big|\check{\mathbf{S}}_{1:t},\boldsymbol{\alpha}(t)\right\}\Big|\check{\mathbf{S}}_{1:t}\right\} \tag{3.65}$$

where the outer expectation is with respect to $\boldsymbol{\alpha}(t)|\check{\mathbf{S}}_{1:t}$.

Define the $(M\times 1)$ vector $\mathbf{c}_{\tilde{S}}(\mathbf{x},\mathbf{y})=\mathbb{E}\{\tilde{\mathbf{S}}(t)\tilde{S}_{\mathbf{x}\to\mathbf{y}}(t)\}$, which entries are computed according to (3.23). To compute the inner expectation recall that, by modeling assumption, one has that

$$\mathbb{E}\{\bar{S}_{\mathbf{x}\to\mathbf{y}}(t)S_{\mathbf{x}\to\mathbf{y}}(t)\}=0 \tag{3.66}$$

$$\mathbb{E}\{\tilde{S}_{\mathbf{x}\to\mathbf{y}}(t)\tilde{S}_{\mathbf{x}_i\to\mathbf{x}_j}(\tau)\}=0,\quad \text{if } \tau\neq t \tag{3.67}$$

$$\mathbb{E}\{\tilde{S}_{\mathbf{x}\to\mathbf{y}}(t)\epsilon_{\mathbf{x}_i\to\mathbf{x}_j}(\tau)\}=0,\quad \text{forall}\,\tau,t,\mathbf{x},\mathbf{y},\mathbf{x}_i,\mathbf{x}_i. \tag{3.68}$$

Rewrite then the inner expectation in (3.65) as $\mathbb{E}\{\bar{S}_{\mathbf{x}\to\mathbf{y}}(t)\big|\check{\mathbf{S}}_{1:t},\boldsymbol{\alpha}(t)\}+\mathbb{E}\{\tilde{S}_{\mathbf{x}\to\mathbf{y}}(t)\big|\check{\mathbf{S}}_{1:t},\boldsymbol{\alpha}(t)\}$, where the first term reads $\mathbb{E}\{\bar{S}_{\mathbf{x}\to\mathbf{y}}(t)|\check{\mathbf{S}}_{1:t},\boldsymbol{\alpha}(t)\}=\boldsymbol{\phi}_{\mathbf{x}\to\mathbf{y}}^T\boldsymbol{\alpha}(t)$. Then, it remains to compute $\mathbb{E}\{\tilde{S}_{\mathbf{x}\to\mathbf{y}}(t)|\check{\mathbf{S}}_{1:t},\boldsymbol{\alpha}(t)\}$. To do so, from [58, Theorem 10.2] it follows that

$$\begin{aligned}\mathbb{E}\{\tilde{S}_{\mathbf{x}\to\mathbf{x}_r}(t)|\check{\mathbf{S}}_{1:t},\boldsymbol{\alpha}(t)\}&=\mathbb{E}\{\tilde{S}_{\mathbf{x}\to\mathbf{x}_r}(t)|\boldsymbol{\alpha}(t)\}\\&-\text{cov}\left\{\tilde{S}_{\mathbf{x}\to\mathbf{x}_r}(t)|\boldsymbol{\alpha}(t),\check{\mathbf{S}}_{1:t}|\boldsymbol{\alpha}(t)\right\}^T\left(\text{var}\left\{\check{\mathbf{S}}_{1:t}|\boldsymbol{\alpha}(t)\right\}\right)^{-1}\left(\check{\mathbf{S}}_{1:t}-\mathbb{E}\{\check{\mathbf{S}}_{1:t}\}\right)\end{aligned} \tag{3.69}$$

where $\mathbb{E}\{\tilde{S}_{\mathbf{x}\to\mathbf{x}_r}(t)|\boldsymbol{\alpha}(t)\}=0$. From the modeling assumptions (3.67)–(3.67) one can show that $\text{cov}\{\tilde{S}_{\mathbf{x}\to\mathbf{x}_r}(t)|\boldsymbol{\alpha}(t),\check{\mathbf{S}}_{1:t}|\boldsymbol{\alpha}(t)\}=[\mathbf{c}_{\tilde{S}}^T(\mathbf{x},\mathbf{y}),\mathbf{0}_{1\times(M-1)t}]^T$

and $\text{var}\{\check{\mathbf{S}}_{1:t}|\boldsymbol{\alpha}(t)\}$ is block-diagonal with copies of the $M \times M$ matrix $\boldsymbol{\Sigma}$ on its main diagonal. Then,

$$\mathbb{E}\{\tilde{S}_{\mathbf{x}\to\mathbf{x}_r}(t)|\check{\mathbf{S}}_{1:t}, \boldsymbol{\alpha}(t)\} = \mathbf{c}_{\tilde{S}}^T(\mathbf{x},\mathbf{y})\boldsymbol{\Sigma}^{-1}[\check{\mathbf{S}}(t) - \boldsymbol{\Phi}\boldsymbol{\alpha}(t)] \tag{3.70}$$

and the inner expectation is evaluated as

$$\mathbb{E}\{S_{\mathbf{x}\to\mathbf{x}_r}(t)|\check{\mathbf{S}}_{1:t}, \boldsymbol{\alpha}(t)\} = \boldsymbol{\phi}_{\mathbf{x}\to\mathbf{x}_r}^T\boldsymbol{\alpha}(t) + \mathbf{c}_{\tilde{S}}^T(\mathbf{x},\mathbf{y})\boldsymbol{\Sigma}^{-1}[\check{\mathbf{S}}(t) - \boldsymbol{\Phi}\boldsymbol{\alpha}(t)]\,. \tag{3.71}$$

Plugging (3.71) into (3.65), and using the definition $\hat{\boldsymbol{\alpha}}(t|t) := \mathbb{E}\{\boldsymbol{\alpha}(t)|\check{\mathbf{S}}_{1:t}\}$, we obtain

$$\mathbb{E}\{S_{\mathbf{x}\to\mathbf{y}}(t)|\check{\mathbf{S}}_{1:t}\} = \boldsymbol{\phi}_{\mathbf{x}\to\mathbf{y}}^T\hat{\boldsymbol{\alpha}}(t|t) + \mathbf{c}_{\tilde{S}}^T(\mathbf{x},\mathbf{y})\boldsymbol{\Sigma}^{-1}\left[\check{\mathbf{S}}(t) - \boldsymbol{\Phi}\hat{\boldsymbol{\alpha}}(t|t)\right]\,. \tag{3.72}$$

Derivation of the conditional variance. To verify (3.33) in Proposition 3.3.1, recall first the variance decomposition formula

$$\begin{aligned}\text{var}\{S_{\mathbf{x}\to\mathbf{y}}(t)\big|\check{\mathbf{S}}_{1:t}\} = \mathbb{E}\left\{\text{var}\left\{S_{\mathbf{x}\to\mathbf{y}}(t)\big|\check{\mathbf{S}}_{1:t}, \boldsymbol{\alpha}(t)\right\}\big|\check{\mathbf{S}}_{1:t}\right\} \\ + \text{var}\left\{\mathbb{E}\left\{S_{\mathbf{x}\to\mathbf{y}}(t)\big|\check{\mathbf{S}}_{1:t}, \boldsymbol{\alpha}(t)\right\}\big|\check{\mathbf{S}}_{1:t}\right\}.\end{aligned} \tag{3.73}$$

The first term on the right hand side of (3.73) can be re-written as

$$\begin{aligned}&\mathbb{E}\left\{\text{var}\left\{S_{\mathbf{x}\to\mathbf{y}}(t)\big|\check{\mathbf{S}}_{1:t}, \boldsymbol{\alpha}(t)\right\}\big|\check{\mathbf{S}}_{1:t}\right\} \\ &\quad= \mathbb{E}\left\{\text{var}\left\{\boldsymbol{\phi}_{\mathbf{x}\to\mathbf{y}}^T\boldsymbol{\alpha}(t) + \tilde{S}_{\mathbf{x}\to\mathbf{y}}(t)\big|\check{\mathbf{S}}_{1:t}, \boldsymbol{\alpha}(t)\right\}\big|\check{\mathbf{S}}_{1:t}\right\} &(3.74)\\ &\quad= \mathbb{E}\left\{\text{var}\left\{\tilde{S}_{\mathbf{x}\to\mathbf{y}}(t)\big|\check{\mathbf{S}}_{1:t}, \boldsymbol{\alpha}(t)\right\}\big|\check{\mathbf{S}}_{1:t}\right\} &(3.75)\\ &\quad= \mathbb{E}\left\{\sigma_{\tilde{S}}^2 - \mathbf{c}_{\tilde{S}}^T(\mathbf{x},\mathbf{y})\boldsymbol{\Sigma}^{-1}\mathbf{c}_{\tilde{S}}(\mathbf{x},\mathbf{y})\big|\check{\mathbf{S}}_{1:t}\right\} &(3.76)\\ &\quad= \sigma_{\tilde{S}}^2 - \mathbf{c}_{\tilde{S}}^T(\mathbf{x},\mathbf{y})\boldsymbol{\Sigma}^{-1}\mathbf{c}_{\tilde{S}}(\mathbf{x},\mathbf{y}) &(3.77)\end{aligned}$$

where (3.76) follows from [58, Theorem 10.2], using the fact that $\tilde{S}_{\mathbf{x}\to\mathbf{y}}(t)$ is jointly Gaussian with $\check{\mathbf{S}}_{1:t}$, temporally white and uncorrelated with $\boldsymbol{\alpha}(t)$. The second term on the right hand side of (3.73) is found to be

$$\begin{aligned}&\text{var}\left\{\mathbb{E}\left\{S_{\mathbf{x}\to\mathbf{y}}(t)\big|\check{\mathbf{S}}_{1:t}, \boldsymbol{\alpha}(t)\right\}\big|\check{\mathbf{S}}_{1:t}\right\} &(3.78)\\ &= \text{var}\left\{\left[\boldsymbol{\phi}_{\mathbf{x}\to\mathbf{y}}^T - \mathbf{c}_{\tilde{S}}^T(\mathbf{x},\mathbf{y})\boldsymbol{\Sigma}^{-1}\boldsymbol{\Phi}\right]\boldsymbol{\alpha}(t) + \mathbf{c}_{\tilde{S}}^T(\mathbf{x},\mathbf{y})\boldsymbol{\Sigma}^{-1}\check{\mathbf{S}}(t)\big|\check{\mathbf{S}}_{1:t}\right\} &(3.79)\\ &= \left[\boldsymbol{\phi}_{\mathbf{x}\to\mathbf{y}}^T - \mathbf{c}_{\tilde{S}}^T(\mathbf{x},\mathbf{y})\boldsymbol{\Sigma}^{-1}\boldsymbol{\Phi}\right]\mathbf{P}(t|t)\left[\boldsymbol{\phi}_{\mathbf{x}\to\mathbf{y}} - \boldsymbol{\Phi}^T\boldsymbol{\Sigma}^{-1}\mathbf{c}_{\tilde{S}}(\mathbf{x},\mathbf{y})\right]^T. &(3.80)\end{aligned}$$

Then, plugging (3.77) and (3.80) into (3.73) yields (3.33), and completes the proof of the proposition.

3.6.2 Derivation of the ADMoM-based consensus algorithm

The steps of the iterative algorithm (3.56)–(3.57) will be meticulously derived and the proof of proposition 3.4.1 will be provided. The derivation of (3.63)–(3.64) as well as the proof of proposition 3.4.2 follow a similar procedure.

The solution $\{\boldsymbol{\chi}_r(t)\}_{r=1}^{N_r}$ to the constrained optimization problem (3.54)–(3.55) will coincide with the solution $\boldsymbol{\chi}(t)$ of (3.51) when the wireless network is connected. Thus, it suffices to show that the iterates (3.56)-(3.57) yield the sequences of $\{\boldsymbol{\chi}_r^{(j)}(t)\}_{r=1}^{N_r}\}$, $j = 0, 1, \ldots$, that converge to the optimum solution of (3.54)–(3.55). We will establish this by showing that iterates (3.56)-(3.57) corresponds to the steps involved by the provably convergent ADMoM.

Denote as $\mathbf{A}$ the $N_r \times N_r$ adjacency matrix that carries the information on the connectivity of the CR network. The (i, j)-th entry of $\mathbf{A}$ is set to one if $j \in \mathcal{N}_i$ and it is zero otherwise. It holds that $\mathbf{A} = \mathbf{A}^T$. Define the $(\sum_{r=1}^{N_r} |\mathcal{N}_r|)K \times N_r K$ matrix $\mathbf{B} := [\mathbf{B}_1^T, \ldots, \mathbf{B}_{N_r}^T]^T$, where $\mathbf{B}_r = [\mathbf{b}_{r_1}^T, \ldots, \mathbf{b}_{r_{|\mathcal{N}_r|}}^T]^T \otimes \mathbf{I}_K$ and $\mathbf{b}_{r,j}$ is a $(N_r \times 1)$ vector with entry r_j set to one and zero elsewhere, $j = 1, \ldots, |\mathcal{N}_r|$; $r_1 > r_2 > \ldots > r_{|\mathcal{N}_r|}$ are the indexes of the non-zero entries on the r-th column of $\mathbf{A}$. Moreover, define

$$\mathcal{J}_r(\boldsymbol{\chi}_r) := \|\boldsymbol{\chi}_r - \check{\mathbf{y}}_r(t)\|_2^2 = \boldsymbol{\chi}_r^T \boldsymbol{\chi}_r - 2\boldsymbol{\chi}_r^T \mathbf{y}_r(t) + \mathbf{y}_r^T(t)\mathbf{y}_r(t)\,. \tag{3.81}$$

with, for notation simplicity, $\mathbf{y}_r := N_r \mathbf{H}_r \mathbf{y}_r$, $r = 1, \ldots, N_r$.

Problem (3.54)–(3.55) can be re-formulated as

$$\begin{aligned} \{\boldsymbol{\chi}_r\}_{r=1}^{N_r} = &\min_{\boldsymbol{\chi}} \mathcal{F}_1(\boldsymbol{\chi}) + \mathcal{F}_2(\mathbf{q}) \\ &\text{subject to } \mathbf{q} = \mathbf{B}\boldsymbol{\chi} \end{aligned} \tag{3.82}$$

where $\boldsymbol{\chi} := [\boldsymbol{\chi}_1^T, \ldots, \boldsymbol{\chi}_{N_r}^T]^T$, $\mathcal{F}_1(\boldsymbol{\chi}) := \sum_{r=1}^{N_r} \mathcal{J}_r(\boldsymbol{\chi}_r)$ and $\mathcal{F}_2(\mathbf{B}\boldsymbol{\chi}) = \mathbf{0}$. Note that (3.82) is in the same form of the optimization problem in [57, p. 255, Eq. (4.76)] and, thus, the ADMoM can be applied to iteratively find its optimum solution.

To find the steps involved by the ADMoM, we conveniently rewrite (3.82)

in the following form:

$$\begin{aligned} &\min_{\substack{\{\boldsymbol{\chi}_r\},\{\mathbf{q}_{r,\varrho}\} \\ \varrho\in\mathcal{N}_r,\ r=1,2,\ldots,N_r}} \sum_{r=1}^{N_r} \mathcal{J}_r(\boldsymbol{\chi}_r) \\ \text{subject to } &\boldsymbol{\chi}_r = \mathbf{q}_{r,\varrho} \quad \forall \varrho \in \mathcal{N}_r,\ r = 1,2,\ldots,N_r \\ &\mathbf{q}_{r,\varrho} = \mathbf{q}_{\varrho,r} \quad \forall \varrho \in \mathcal{N}_r,\ r = 1,2,\ldots,N_r \end{aligned} \tag{3.83}$$

where $\{\mathbf{q}_{r,\varrho}\}$ are auxiliary optimization $(K \times 1)$ dummy vector variables associated to the links $r \to \varrho$ (collected in $\mathbf{q}$). Consider the augmented (partial) Lagrangian function given by

$$\begin{aligned} \mathcal{L}(\{\boldsymbol{\chi}_r\},\{\mathbf{q}_{r,\varrho}\},\{\boldsymbol{\xi}_{r,\varrho}\}) = &\sum_{r=1}^{N_r} \mathcal{J}_r(\boldsymbol{\chi}_r) \\ &+ \sum_{r=1}^{N_r} \sum_{\varrho\in\mathcal{N}_r} \boldsymbol{\xi}_{r,\varrho}^T(\boldsymbol{\chi}_r - \mathbf{q}_{r,\varrho}) \\ &+ c\sum_{r=1}^{N_r} \sum_{\varrho\in\mathcal{N}_r} \|\boldsymbol{\chi}_r - \mathbf{q}_{r,\varrho}\|_2^2 \end{aligned} \tag{3.84}$$

where $\{\boldsymbol{\xi}_{r,\varrho}\}$ are the Lagrange multipliers, and c is a positive arbitrary constant. The curly brackets $\{\cdot\} = \{\cdot\}_{r=1,\varrho\in\mathcal{N}_r}^{N_r}$ indicates the set of all variables included. With $j = 0,1,\ldots$ denoting the iteration index, the ADMoM procedure updates the primal variables $\{\boldsymbol{\chi}_r\},\{\mathbf{q}_{r,\varrho}\}$ and the dual variables $\{\boldsymbol{\xi}_{r,\varrho}\}$, alternately, as

$$\{\boldsymbol{\chi}_r^{(j+1)}\} = \arg\min_{\{\boldsymbol{\chi}_r\}} \mathcal{L}(\{\boldsymbol{\chi}_r\},\{\mathbf{q}_{r,\varrho}^{(j)}\},\{\boldsymbol{\xi}_{r,\varrho}^{(j)}\}) \tag{3.85}$$

$$\{\mathbf{q}_{r,\varrho}^{(j+1)}\} = \arg \min_{\substack{\mathbf{q}_{r,\varrho}=\mathbf{q}_{\varrho,r}, \\ \varrho\in\mathcal{N}_r,\ r=1,2,\ldots,N_r}} \mathcal{L}(\{\boldsymbol{\chi}_r^{(j+1)}\},\{\mathbf{q}_{r,\varrho}\},\{\boldsymbol{\xi}_{r,\varrho}^{(j)}\}) \tag{3.86}$$

$$\boldsymbol{\xi}_{r,\varrho}^{(j+1)} = \boldsymbol{\xi}_{r,\varrho}^{(j)} + 2c\left(\boldsymbol{\chi}_r^{(j+1)} - \mathbf{q}_{r,\varrho}^{(j+1)}\right), \quad \varrho \in \mathcal{N}_r,\ r = 1,2,\ldots,N_r. \tag{3.87}$$

Since (3.54)–(3.55) is convex and it can be shown that matrix $\mathbf{B}^T\mathbf{B}$ is invertible, Proposition 4.2 in [57] implies that the sequence $\boldsymbol{\chi}_r^{(j)}$, $j = 1,2,\ldots$, generated by (4.43)–(4.45) converges to the optimal solution $\boldsymbol{\chi}_r$ of (3.83) for each r (equivalently, converges to the optimal solution of (3.82)) for an arbitrary initial $\boldsymbol{\chi}_r^{(0)}$ and any positive constant c.

It is now shown that the iterates (3.56)–(3.57) can be derived from (4.43)–(4.45). First, it is noted that (4.44) can be re-written as

$$\begin{aligned}
&\{\mathbf{q}_{r,\varrho}^{(j+1)}\} \\
&= \arg \min_{\substack{\mathbf{q}_{r,\varrho}=\mathbf{q}_{\varrho,r}, \\ \varrho\in\mathcal{N}_r,\ r=1,2,\ldots,N_r}} -\sum_{r=1}^{N_r}\sum_{\varrho\in\mathcal{N}_r} \boldsymbol{\xi}_{r,\varrho}^{(j)T}\mathbf{q}_{r,\varrho} + c\sum_{r=1}^{N_r}\sum_{\varrho\in\mathcal{N}_r} \|\boldsymbol{\chi}_r^{(j+1)} - \mathbf{q}_{r,\varrho}\|_2^2
\end{aligned} \tag{3.88}$$

$$\begin{aligned}
&= \arg \min_{\{\mathbf{q}_{r,\varrho}\}} \sum_{\{(r,\varrho)|\varrho\in\mathcal{N}_r, r>\varrho\}} \Big\{ -(\boldsymbol{\xi}_{r,\varrho}^{(j)} + \boldsymbol{\xi}_{\varrho,r}^{(j)})^T\mathbf{q}_{r,\varrho} \\
&\qquad\qquad + c\left[\|\boldsymbol{\chi}_r^{(j+1)} - \mathbf{q}_{r,\varrho}\|_2^2 + \|\boldsymbol{\chi}_\varrho^{(j+1)} - \mathbf{q}_{r,\varrho}\|_2^2\right]\Big\}
\end{aligned} \tag{3.89}$$

where in the last step the conditions $\{\mathbf{q}_{r,\varrho} = \mathbf{q}_{\varrho,r}\}$ and the assumption that the links are bi-directional are used. Note that (4.47) is quadratic and unconstrained in the set of variables $\{\mathbf{q}_{r,\varrho}^{(j+1)}\}$; furthermore, it decouples in sub-problems in one variable that can be solved in close form. In particular, $\mathbf{q}_{r,\varrho}^{(j+1)}$ is given by

$$\mathbf{q}_{r,\varrho}^{(j+1)} = \frac{1}{2}\left(\boldsymbol{\chi}_r^{(j+1)} + \boldsymbol{\chi}_\varrho^{(j+1)}\right) + \frac{1}{4c}\left(\boldsymbol{\xi}_{r,\varrho}^{(j)} + \boldsymbol{\xi}_{\varrho,r}^{(j)}\right), \quad \varrho\in\mathcal{N}_r,\ r=1,2,\ldots,N_r. \tag{3.90}$$

By substituting (4.48) into (4.45), one obtains

$$\boldsymbol{\xi}_{r,\varrho}^{(j+1)} = c\left(\boldsymbol{\chi}_r^{(j+1)} - \boldsymbol{\chi}_\varrho^{(j+1)}\right) + \frac{1}{2}\left(\boldsymbol{\xi}_{r,\varrho}^{(j)} - \boldsymbol{\xi}_{\varrho,r}^{(j)}\right), \quad \varrho\in\mathcal{N}_r,\ r=1,2,\ldots,N_r. \tag{3.91}$$

Thus, it can be verified by inspection that

$$\boldsymbol{\xi}_{r,\varrho}^{(j)} + \boldsymbol{\xi}_{\varrho,r}^{(j)} = 0, \quad \varrho\in\mathcal{N}_r,\ r=1,2,\ldots,N_r. \tag{3.92}$$

From (4.50) and (4.48)–(4.49), it follows readily that

$$\mathbf{q}_{r,\varrho}^{(j+1)} = \frac{1}{2}\left(\boldsymbol{\chi}_r^{(j+1)} + \boldsymbol{\chi}_\varrho^{(j+1)}\right), \quad \varrho\in\mathcal{N}_r,\ r=1,2,\ldots,N_r \tag{3.93}$$

$$\boldsymbol{\xi}_{r,\varrho}^{(j+1)} = \boldsymbol{\xi}_{r,\varrho}^{(j)} + c\left(\boldsymbol{\chi}_r^{(j+1)} - \boldsymbol{\chi}_\varrho^{(j+1)}\right), \quad \varrho\in\mathcal{N}_r,\ r=1,2,\ldots,N_r. \tag{3.94}$$

Consider now equation (4.43). It can be re-written as

$$\{\boldsymbol{\chi}_r^{(j+1)}\} = \arg\min_{\{\boldsymbol{\chi}_r\}} \sum_{r=1}^{N_r} \left[\mathcal{J}_r(\boldsymbol{\chi}_r) + \sum_{\varrho\in\mathcal{N}_r} \boldsymbol{\xi}_{r,\varrho}^{(j)T}\boldsymbol{\chi}_r + c\sum_{\varrho\in\mathcal{N}_r} \|\boldsymbol{\chi}_r - \mathbf{q}_{r,\varrho}^{(j)}\|_2^2 \right] \tag{3.95}$$

$$= \arg\min_{\{\boldsymbol{\chi}_r\}} \sum_{r=1}^{N_r} \Big[(1+c|\mathcal{N}_r|)^{-1}\boldsymbol{\chi}_r^T\boldsymbol{\chi}_r + \boldsymbol{\chi}_r^T \left(-2\check{\mathbf{y}}_r(t) + \sum_{\varrho\in\mathcal{N}_r} \boldsymbol{\xi}_{r,\varrho}^{(j)} - 2c\sum_{\varrho\in\mathcal{N}_r} \mathbf{q}_{r,\varrho}^{(j)} \right) \Big] . \tag{3.96}$$

The quadratic unconstrained problem (3.96) can be decoupled for each variable $\boldsymbol{\chi}_r$ into N_r subproblems. Clearly, $\boldsymbol{\chi}_r^{(j+1)}$ can be obtained in closed-form as

$$\boldsymbol{\chi}_r^{(j+1)} = (1+c|\mathcal{N}_r|)^{-1} \left[\check{\mathbf{y}}_r(t) - \frac{1}{2}\sum_{\varrho\in\mathcal{N}_r} \boldsymbol{\xi}_{r,\varrho}^{(j)} + c\sum_{\varrho\in\mathcal{N}_r} \mathbf{q}_{r,\varrho}^{(j)} \right] \tag{3.97}$$

Upon defining $\boldsymbol{\zeta}_r^{(j)} := \sum_{\varrho\in\mathcal{N}_r} \boldsymbol{\xi}_{r,\varrho}^{(j)}$, and substituting (4.51) to (4.55), (3.57) is obtained. Finally, (3.56) follows from the definition of $\boldsymbol{\zeta}_r^{(j)}$ and (4.52).

Chapter 4

Sparsity-aware Cooperative Spectrum Sensing

Tracking the primary system activity is the first essential step toward a dynamical reuse of the available licensed spectrum. Based on a parsimonious model accounting for PU mutual interference concerns, and motivated by recent advances in sparse linear regression, a sparsity-cognizant state tracker is developed in this chapter in both centralized and distributed formats. The PU transmission power estimation and PU localization capabilities offered by the proposed scheme lead to the ability in estimating the actual power spectral density (PSD) map of the primary system. Thus, detection of the so called spectrum spatial holes is efficiently attainable, enhancing the spatial re-use of the primary frequency bands. In this context, the channel gain map estimate provides an invaluable means to overcome a disc-shaped over-simplification of the per-user coverage region, portraying the effect of propagation phenomena more accurately.

4.1 Preliminaries

4.1.1 Spectrum sensing

Due to a lack of explicit cooperation between primary system and CRs [59], spectrum sensing algorithms are essential for spectrum opportunities identification in an autonomous and dynamical manner. In its primal, although

naïve, implementation, a sensing algorithm entails a single CR to listen to the spectrum in order to reveal the presence of ongoing PU transmissions or, equivalently, the primary channel idle time intervals.

Prior knowledge of the PU signal features might not be available and, thus, CR system needs to resort to less efficient detection techniques. Taking into consideration also transceiver complexity concerns, the non-coherent energy detector [60] has been vastly employed as a building block for spectrum sensing algorithms. See, e.g., [61], and [62], where a bank of energy detectors was used to sense a large swath of bandwidth. Also, see [63], where a sequential sensing algorithm was developed for OFDM-based CR systems. Conversely, if prior information on the signal waveform or statistical properties of the PU signals is available, alternative techniques based on coherent matched-filter detection [61] or feature detection [64] can be devised.

At the expense of increased communication overhead among CRs, *cooperative sensing* schemes can achieve significantly improved performance relative to single-CR sensing [62], [65], [66]. Conceivably, through fusion of local measurements, cooperative sensing can collect the spatial diversity provided by different propagation distances and fading experienced by the PU-to-CR channels. Thus, the hurdle represented by the fading-induced "hidden terminal" problem, which affects the performance of single-CR sensing, can be effectively overcome [67].

In this cooperative sensing context, a weighted sum of the power measurements was used as a test statistic at the fusion center (FC) in [68] in order to maximize the probability of detecting available primary bands. However, PU-to-CR channel gains were assumed to be mutually uncorrelated, and thus spatial correlation of observations across CR nodes was not accounted for. In [67], the sensing decisions made by individual CRs were combined at the FC using a linear-quadratic fusion rule, which takes into account correlated observations. However, the signal-to-noise-ratios (SNRs) of all channels were assumed to have identical means, which may not be realistic.

Recently, the sensing vision has advocated the utilization of the spatial dimension besides the temporal and frequency ones. Thus, interest has grown in *spatio-temporal* spectrum re-use techniques, where CR transmis-

sions are permitted as long as the SINR requirements of the PU receivers are satisfied thanks to attenuation in the propagation paths [15], [32]. It is thus clear that primary and secondary devices can coexist in the same time instant and deployment area provided that any ongoing PU transmission is protected, i.e., spectrum holes are filled in time and space in an underlay fashion.

Toward this direction, initial efforts have been devoted to construct PSD maps, as explained in the previous chapter. PSD maps portray the ambient RF power distribution in space, time, and frequency and provide vivid description of which region in the area of interest is "crowded" in terms of RF interference caused by PUs. Thus, areas that must be avoided by the CR transceivers. To reconstruct such interference atlas starting from raw power measurements, a spatial interpolation technique called Kriging [69] was employed by [33] and [70]; however, time-varying PU activities are not accounted for, being maps obtained in a batch setup. In [40], a smooth PSD map was computed using the method of splines; compared to [33] and [70], [40] has the well-appreciate merit of accounting for shadowing propagation effects. However, these works cannot cope with time-varying channel gains.

In this chapter, a cooperative CR sensing scheme is developed, in which *PU positions* and *transmit powers* are *tracked* by exploiting raw power measurements obtained via energy detection in the area where the CR network is deployed.

First, a parsimonious system model accounting for the thin presence of active PU transmitters in the same area, which happens due to well-known mutual interference concerns, is stated. The parsimony in modeling the spatial distribution of the simultaneously active PUs naturally leads to the formulation of a sparse regression problem, which is to be collaboratively solved by the CRs in order to accomplish to the sensing task. Motivated by recent advances in compressive sampling [71], this underlying sparsity was exploited to estimate transmission powers and the positions of an unknown number of active PUs in [39]. Here, this approach is considerably broadened in order to track time-varying PU activities; also, the CG maps are pragmatically incorporated to enhance the performance of the algorithm.

For completeness, a high-level introduction to sparse regression is briefly reported in 4.1.2 along with the main machinery that will be employed in this chapter to devise the sparsity-cognizant PU state tracker.

Motivated by scalability and robustness concerns, a distributed version of the PU state tracker is also developed. Based on the ADMoM, the distributed algorithm is provably convergent to the solution of its centralized counterpart and entails only local message-passing among neighboring nodes in the CR network.

PSD maps cannot be used by the CR transmitters to prevent disruption to the existing PU links in a succeeding power allocation phase. In fact, in addition to coping with time-varying environments, the latter constitutes the major complementary information provided by CG maps that is not available with PSD maps. To allow aggressive opportunistic reuse of the spectrum resources in a non-intrusive manner, CG cartography is exploited to reconstruct the PSD map of the primary system and the interference map of the CRs; from the former, which can be obtained (and tracked) using the estimated locations and transmission powers of the PUs, the PU coverage area can be extracted. Remarkably, CG cartography represents a bright means for sidestepping the time-invariant disc-shaped simplification of coverage and interference regions that would be obtained by relying on a path loss-only propagation model.

Coverage area and (potential) interference map can then be used to compute the maximum interference-free transmit-power (MIFTP) [32] that a CR transmitter can afford; i.e., the maximum value of the transmission power such that the interference constraint that protects any PU receiver is observed.

Before proceeding with the problem formulation, sparse linear regression problems along with the techniques for their solution used in the ensuing sections are briefly introduced.

4.1.2 Sparse linear regression

Sparse linear regression is a topic of intense research in the last decade, motivated by the sparsity inherent to a plethora of natural as well as man-made

signals and systems. Just to make few examples, exploiting the sparsity of the underlying model has vital importance in applications as diverse as image compression [72], signal decomposition using overcomplete bases [73], and, entering in the wireless communications context, estimation of wireless multipath channels [74].

Then, consider the classical setup for linear regression comprising a real-valued $p \times 1$ input vector $\mathbf{h} := [h_1, \ldots, h_p]^T$, a scalar response $y \in \mathbb{R}$, and a linear approximation to the regression function $\mathbb{E}[y|\mathbf{h}]$, namely, $f(\mathbf{h}) = \mathbf{h}^T\boldsymbol{\beta}$, with $\boldsymbol{\beta} := [\beta_1, \ldots, \beta_p]^T$ the vector of model coefficients. Also, consider a training data set $\{y_n, \mathbf{h}_n\}_{n=1}^N$, where n is the sampling index. The vector $\boldsymbol{\beta}$ is sparse if condition $\|\boldsymbol{\beta})\|_0 \ll p$ holds, where $\|\boldsymbol{\beta}\|_0 := |\text{supp}(\boldsymbol{\beta})|$ is the ℓ_0-(pseudo-)norm of vector $\boldsymbol{\beta}$. Then, given the training data set, the model parameter vector $\boldsymbol{\beta}$ is to be estimated according to a given criterion.

The most popular criterion for estimating $\boldsymbol{\beta}$ is the least-squares (LS) which however fails to provide a parsimonious model estimate where only the prominent predictor variables must be selected and, furthermore, often times yields unsatisfactory prediction accuracy. The *least-absolute shrinkage and selection operator* (Lasso), which combines the features of subset selection and ridge regression, was proposed to overcome the aforementioned limitations of the LS [71]. Note that subset selection and ridge regression address the unawareness of a sparse model parameter vector and the unsatisfactory prediction accuracy of the LS separately. See, also, [73], where the term *basis pursuit denoising* was coined.

Define the $N \times 1$ observation vector $\mathbf{y} := [y_1, \ldots, y_N]^T$ and the $N \times p$ (input) regression matrix $\mathbf{H} := [\mathbf{h}_1, \ldots, \mathbf{h}_N]^T$. Then, the Lasso estimator is the minimizer of the following non-smooth convex optimization problem:

$$\hat{\boldsymbol{\beta}} = \arg\min_{\boldsymbol{\beta}} \frac{1}{2}\|\mathbf{y} - \mathbf{H}\boldsymbol{\beta}\|_2^2 + \lambda\|\boldsymbol{\beta}\|_1 \tag{4.1}$$

where $\|\boldsymbol{\beta}\|_1 := \sum_{i=1}^p |\beta_i|$ is the ℓ_1-norm of the vector $\boldsymbol{\beta}$, and $\lambda > 0$ is a tuning parameter that controls the sparsity of the solution. Here, the ℓ_1-norm, which is a regularization term that augments the LS cost, places itself as a cornerstone for lassoing the non-zero support of $\boldsymbol{\beta}$. The parameter λ is typically chosen via model selection techniques such as cross-validation;

see, e.g., [75]. Note that the Lasso has well-documented merits in sparse problems also in case of under-determined linear systems, i.e., when $N < p$.

In linear regression problems, the training set $\{y_n, \mathbf{h}_n\}_{n=1}^N$ is conventionally assumed to be fully available at a central processor unit, so that $\hat{\boldsymbol{\beta}}$ can be obtained by solving (4.1) in a *batch* form. A typical approach for obtaining $\hat{\boldsymbol{\beta}}$ in (4.1) is to use a cyclic coordinate descent (CCD) algorithm [76], which entails cyclic iterative minimization of in the cost in (4.1) with respect to one entry of $\boldsymbol{\beta}$ per iteration cycle. Denote as $J^{\text{Lasso}}(\boldsymbol{\beta})$ the cost in (4.1); also, denote as $\boldsymbol{\beta}^{(j)}(N)$ the solution at time N (after acquisition of the entire training set) at iteration j. Then, the CCD entails an update of the i-th entry of $\boldsymbol{\beta}$ at iteration j by solving the following problem

$$\hat{\beta}_i^{(j)}(N) = \arg\min_{\beta} J^{\text{Lasso}}([\hat{\beta}_1^{(j)}(N), \ldots, \hat{\beta}_{i-1}^{(j)}(N), \beta, \hat{\beta}_{i+1}^{(j-1)}(N), \ldots, \hat{\beta}_p^{(j-1)}(N)]) \tag{4.2}$$

for $i = 1, \ldots, P$. Basically, at the j-th cycle of the CCD algorithm each coordinate β_i, $i = 1, \ldots, p$, is optimized by keeping fixed the pre-cursor coordinates indexed by $i' < i$ to their values obtained at the j-th cycle, and the post-cursor coordinates $i'' > i$ to their values at the $(j-1)$-st cycle.

Note that the cost in (4.13) is convex, but non-differentiable. However, in view of the results of [77], convergence of the CCD algorithm for Lasso problems can be readily established. Also, comparative studies show numerical stability of the algorithm and verify that CCD requires a computational effort that is similar to the state-of-the-art batch Lasso solvers [76], [78].

4.1.3 Online Lasso

Knowledge of the whole set $\{y_n, \mathbf{h}_n\}_{n=1}^N$ is typically assumed in linear regression problems and, hence, (4.1) can be solved in a batch form. However, in many practical applications, (possibly noisy) observations may be collected sequentially in time. In this case, solving (4.1) in a batch fashion would incur computational burden and memory requirements that grow as time goes by. Also, the support of the sparse vector $\boldsymbol{\beta}$ may vary with time along with the values of its nonzero entries.

To overcome these issues, a time-wighted (TW) Lasso was devised in [79],

which ensures recursive estimation and tracking of possibly time-varying sparse signals based on sequentially gathered observations. Specifically, upon denoting as $\mu_{N,n} \in (0,1]$ a possibly time-varying forgetting factor, the TW-Lasso is the minimizer of the following convex problem:

$$\hat{\boldsymbol{\beta}}(N) = \arg\min_{\boldsymbol{\beta}} \frac{1}{2} \sum_{n=1}^{N} \mu_{N,n} \left(y_n - \mathbf{h}_n^T \boldsymbol{\beta}\right)^2 + \lambda_N \|\boldsymbol{\beta}\|_1 \tag{4.3}$$

where the sparsity-encouraging parameter λ_N is also allowed to vary with the time index N. For future use, denote as $J_N^{\mathrm{TWL}}(\boldsymbol{\beta})$ the cost function in (4.3), where the sub-script N stresses the time variability of the cost function. The TW-Lasso (4.3) offers adaptability and tracking capability but, still, it requires to solve a convex program as a new datum is acquired, being the solution of (4.3) not available in closed form.

To cope with the possibly high computational burden demanded by (4.3) and to address the need for a real-time signal processing capability, [79] introduced the online coordinate descent (OCD) algorithm, an adaptive counterpart of the batch CCD Lasso where a new observation is incorporated at each iteration of the algorithm. In other words, the iteration index j in the CCD is replaced by the time index N in OCD.

For notational convenience, let us express the time index as $N = kp + i$, with $i \in \{1, \ldots, N\}$ indexing the entry of $\hat{\boldsymbol{\beta}}(N)$ updated at time N, and $k = \lceil \frac{N}{p} \rceil - 1$ representing the number of times that the i-th entry $\hat{\beta}_i(N)$ of $\hat{\boldsymbol{\beta}}(N)$ has been updated. Then, the online coordinate descent update can be expressed as

$$\begin{aligned}\hat{\beta}_i^{\mathrm{OCD}}(N) = \arg\min_{\beta} J_N^{\mathrm{TWL}}([\hat{\beta}_1^{\mathrm{OCD}}(N-1), \ldots, \hat{\beta}_{i-1}^{\mathrm{OCD}}(N-1), \beta, \\ \hat{\beta}_{i+1}^{\mathrm{OCD}}(N-1), \ldots, \hat{\beta}_p^{\mathrm{OCD}}(N-1)]) \,.\end{aligned} \tag{4.4}$$

Note that, in the update (4.4) of entry $\hat{\beta}_i^{\mathrm{OCD}}(N)$ at time N, the coordinates $\{\hat{\beta}_{i'}^{\mathrm{OCD}}(N-1)\}_{i'=1}^{i-1}$ have been updated $k+1$ times, whereas entries $\{\hat{\beta}_{i'}^{\mathrm{OCD}}(N-1)\}_{i'=i+1}^{p}$ have been updated k times.

Next, upon defining the following quantities

$$\mathbf{R}(N) := \sum_{n=1}^{N} \mu_{N,n} \mathbf{h}_n \mathbf{h}_n^T = \mu_{N,N} \mathbf{R}(N-1) + \mathbf{h}_N \mathbf{h}_N^T \tag{4.5}$$

$$\mathbf{r}(N) := \sum_{n=1}^{N} \mu_{N,n} y_n \mathbf{h}_n^T = \mu_{N,N} \mathbf{r}(N-1) + y_N \mathbf{h}_N^T \tag{4.6}$$

which can be computed recursively, and neglecting constant terms, $J_N^{\mathrm{TWL}}(\beta_i)$ can be re-written as

$$J_N^{\mathrm{TWL}}(\beta_i) = \frac{1}{2} R_{i,i}(N) \beta_i^2 - \tilde{r}_i(N) \beta_i + \lambda_N |\beta_i| \tag{4.7}$$

where $R_{i,j}(N)$ and $r_i(N)$ denote the (i,j)-th entry of $\mathbf{R}(N)$, and the i-th entry of $\mathbf{r}(N)$, respectively, and

$$\tilde{r}_i(N) := r_i(N) - \sum_{j=1, j\neq i}^{p} R_{i,j}(N) \hat{\beta}_j^{\mathrm{OCD}}(N-1). \tag{4.8}$$

Then, since (4.4) is a scalar optimization problem, the solution $\hat{\beta}_i^{\mathrm{OCD}}(N)$ is obtained in closed form as [79]

$$\hat{\beta}_i^{\mathrm{OCD}}(N) = \frac{\mathrm{sgn}(\tilde{r}_i(N))}{R_{i,i}(N)} [\tilde{r}_i(N) - \lambda_N]_+ \tag{4.9}$$

where $[a]_+ := \max\{a, 0\}$ enforces convergence to a sparse solution and $\mathrm{sgn}(\cdot)$ is the sign function.

The OCD Lasso will be considered in the ensuing sections as a building block for the proposed spectrum sensing algorithm, upon adapting it to the problem at hand.

4.2 Problem Formulation

Consider again a set of N_r CRs located in $\mathcal{A}$ and assume, as in the previous chapter, that their locations $\{\mathbf{x}_r \in \mathcal{A}\}_{r=1}^{N_r}$ are known to one another. The CRs *cooperate* in order to monitor the activity of an incumbent PU system. In lieu of prior information on the PU signal characteristics, and motivated by low-complexity considerations, assume that the CRs employ non-coherent energy detectors to detect the presence of PU signals [60], [61]. Suppose

that N_p PU transmitters (sources) are located at $\mathcal{S}_p := \{\mathbf{x}_p \in \mathcal{A}\}_{p=1}^{N_p}$. Neither the *number* of PU transmitters nor their *positions* are known to the CRs.

Recall that $g_{\mathbf{x}\to\mathbf{x}_r}(t)$ denotes the averaged channel gain[1] (with the small-scale fading averaged out) from an arbitrary position $\mathbf{x} \in \mathcal{A}$ to CR r at time t. Assuming that the PU signals are statistically independent, the *receive-power* in the band of interest measured by CR r at time t is given by

$$\pi_r(t) = \sum_{p=1}^{N_p} g_{\mathbf{x_p}\to\mathbf{x_r}}(t)p_p(t) + z_r(t), \qquad r = 1, 2, \ldots, N_r \tag{4.10}$$

where $p_p(t)$ is the *transmit-power* of the PU located at $\mathbf{x}_p$ at time t, and $z_r(t)$ the receiver noise at CR r at time t with mean zero and variance[2] σ_z^2.

Consider a set of N_s *candidate* PU source locations $\mathcal{S} := \{\mathbf{x}_s \in \mathcal{A}\}_{s=1}^{N_s}$. Without prior knowledge of the potential PU positions, $\mathcal{S}$ can be formed simply by discretizing the area $\mathcal{A}$ into a set of equidistant grid points. Assume that $\mathcal{S}_p \subset \mathcal{S}$, as the grid can be designed sufficiently dense to incorporate the actual locations of the PUs. Let $\mathbf{p}(t) := [p_1(t) \ \ldots \ p_{N_s}(t)]^T$, $p_s \in \mathbb{R}^+$ for all s, where $p_s(t) > 0$ implies presence of an active PU transmitter at location $\mathbf{x}_s$ at time t, while $p_s(t) = 0$ the absence of the same. With $\mathbf{g}_r(t) := [g_{\mathbf{x_1}\to\mathbf{x_r}}(t) \ \ldots \ g_{\mathbf{x_{Ns}}\to\mathbf{x_r}}(t)]^T$, the power measurement equation (4.10) can be compactly re-written as

$$\pi_r(t) = \mathbf{g}_r^T(t)\mathbf{p}(t) + z_r(t), \qquad r = 1, 2, \ldots, N_r. \tag{4.11}$$

Since the number of active transmitters over the same spectral band in a given geographical area is limited due to mutual interference concerns [80], the number of non-zero entries of $\mathbf{p}(t)$ at a given time t is far smaller than N_s for large N_s, i.e., for sufficiently dense grid points. Thus, the vector $\mathbf{p}(t)$ is *sparse*, i.e., $N_s \gg N_p$ holds.

Motivated by the recent advances in sparse linear regression, as briefly discussed in sections 4.1.2 and 4.1.3, the spectrum sensing problem has been

[1] Henceforth, the analysis applies on a per frequency f basis; but f is dropped for notational brevity.

[2] When all the PUs are silent, i.e., $p_p(t) = 0$ for all $p = 1, \ldots, N_p$, $z_r(t)$ is restricted to take only non-negarive values, being an error component affecting a power.

formulated as a sparse regression problem with an ℓ_1-norm-based regularization term in [39]. This formulation is considerably broadened here in order to account for not only for time-varying PU activities but also for spatio-temporal shadow fading propagation effects via the use of the CG maps. In order to track the time-varying PU activities, the following time-weighted non-negative Lasso formulation is considered:

$$\hat{\mathbf{p}}(t) = \arg\min_{\mathbf{p}\succeq\mathbf{0}} \left[\frac{1}{2} \sum_{\tau=1}^{t} \mu^{t-\tau} \sum_{r=1}^{N_r} \left(\pi_r(\tau) - \mathbf{g}_r^T(\tau)\mathbf{p} \right)^2 + \lambda_t \|\mathbf{p}\|_1 \right] \tag{4.12}$$

where $\mu \in (0, 1]$ denotes the forgetting factor and $\lambda_t > 0$ is the sparsity-encouraging parameter. Note that for $\lambda_t = 0$, (4.12) boils down to the cost function of the recursive LS (RLS) [79].

Albeit non-differentiable, problem (4.12) is convex; thus, it can be solved efficiently using standard quadratic programming iterations. However, solving it in a batch fashion would incur considerable overhead in terms of computational complexity and memory requirement. Thus, *adaptive online* algorithms are developed in the ensuing section, both in *centralized* and *distributed* formats.

4.3 Online PU State Tracker

4.3.1 Centralized algorithm for state tracking

In a centralized setup, the power measurements and the CG estimates from all cooperating CRs are collected at a central unit, also known as fusion center (FC). The central processing unit may be be either one of the CR nodes, or a separate control node.

To track PU activities centrally at the FC, one can employ the adaptive OCD-Lasso explained in section 4.1.3. Recall that OCD performs cyclic iterative minimization of the TW-Lasso cost, with respect to one entry of $\mathbf{p}$ per iteration. Here, OCD-Lasso is employed upon properly adapting it to the vector observation case, and by imposing the non-negativity constraints on the PU transmission powers.

For the sake of notation commodity, express the time index as $t = iN_s + n$, with $n \in \{1, \ldots, N_s\}$ corresponding to the entry of $\hat{\mathbf{p}}(t)$ updated at time t,

and $i = \lceil \frac{t}{N_s} \rceil - 1$ representing the number of times that the n-th entry $\hat{p}_n(t)$ of $\hat{\mathbf{p}}(t)$ has been updated. With $J_t(\mathbf{p})$ denoting the objective function of the optimization problem in (4.12), the cyclic coordinate descent update can be expressed as

$$\hat{p}_n(t) = \arg\min_{\hat{p}_n \geq 0} J_t([\hat{p}_1(t-1), \ldots, \hat{p}_{n-1}(t-1), \hat{p}_n, \hat{p}_{n+1}(t-1), \ldots, \hat{p}_{N_s}(t-1)]) \tag{4.13}$$

$$\hat{p}_j(t) = \hat{p}_j(t-1) \qquad \forall j \neq n. \tag{4.14}$$

Now define

$$\mathbf{R}(t) := \sum_{\tau=1}^{t} \mu^{t-\tau} \sum_{r=1}^{N_r} \mathbf{g}_r(\tau)\mathbf{g}_r^T(\tau) \tag{4.15}$$

$$\mathbf{r}(t) := \sum_{\tau=1}^{t} \mu^{t-\tau} \sum_{r=1}^{N_r} \pi_r(\tau)\mathbf{g}_r(\tau) \tag{4.16}$$

which can be recursively updated as

$$\mathbf{R}(t) = \mu\mathbf{R}(t-1) + \sum_{r=1}^{N_r} \mathbf{g}_r(t)\mathbf{g}_r^T(t) \tag{4.17}$$

$$\mathbf{r}(t) = \mu\mathbf{r}(t-1) + \sum_{r=1}^{N_r} \pi_r(t)\mathbf{g}_r(t). \tag{4.18}$$

Then, the update in (4.13) is equivalent to

$$\hat{p}_n(t) = \arg\min_{\hat{p}_n \geq 0} \frac{1}{2} R_{n,n}(t)\hat{p}_n^2 - \tilde{r}_n(t)\hat{p}_n + \lambda_t|\hat{p}_n| \tag{4.19}$$

where $R_{n,j}(t)$ and $r_n(t)$ denote the (n,j)-th entry of $\mathbf{R}(t)$, and the n-th entry of $\mathbf{r}(t)$, respectively, and

$$\tilde{r}_n(t) := r_n(t) - \sum_{j=1, j\neq n}^{N_s} R_{n,j}(t)\hat{p}_j(t-1). \tag{4.20}$$

Being a scalar optimization problem, the minimization problem (4.19) accepts a closed-form solution, namely:

$$\hat{p}_n(t) = \frac{[\tilde{r}_n(t) - \lambda_t]_+}{R_{n,n}(t)}\,. \tag{4.21}$$

Note that equation (4.21) amounts to a soft-thresholding operation that sets to zero inactive entries. It is thus clear that possible changes in the support of $\mathbf{p}$ as time goes by can be caught.

4.3.2 Distributed algorithm for state tracking

In certain cases, a distributed algorithm may be more desirable than a centralized implementation, due to scalability and robustness issues. A distributed algorithm does not require all the measurements to be collected at a single processor, but rather performs consensus-based in-network processing, which requires only local message-passing among single-hop neighboring nodes in the CR network.

Recall from the previous chapter that $\mathcal{N}_r \subset \{1, \ldots, r-1, r+1, \ldots, N_r\}$ denotes the set of one-hop neighbors of CR r. Also, assumed that the links in the CR network are bi-directional; i.e., $\varrho \in \mathcal{N}_r$ implies $r \in \mathcal{N}_\varrho$. Following the approach pursued in section 3.4, define local copies $\mathbf{p}_r(t) := [p_{r,1}(t), \ldots, p_{r,N_s}(t)]^T$, $r = 1, \ldots, N_r$, of the global vector $\mathbf{p}(t)$ and solve a constrained optimization problem where local copies in the one-hop neighborhood are enforced to be coherent; i.e., constant. Under the assumption that the network is connected, i.e., that there are paths from any node in the network to any other nodes, the localized problem is equivalent to the original centralized problem.

Specifically, consider the coordinate descent update at time t for the n-th coordinate of $\hat{\mathbf{p}}(t)$ given in (4.13). Define the per CR (i.e., local) cost function $\mathcal{J}_{r,t}(\mathbf{p}_r)$ as [cf. (4.12)]

$$\mathcal{J}_{r,t}(\mathbf{p}_r) := \frac{1}{2}\sum_{\tau=1}^{t} \mu^{t-\tau} \left(\pi_r(\tau) - \mathbf{g}_r^T(\tau)\mathbf{p}_r\right)^2 + \frac{\lambda_t}{N_r}||\mathbf{p}_r||_1. \tag{4.22}$$

Then, the following formulation, which is equivalent to (4.13), is amenable to distributed implementation:

$$\begin{aligned}\{\hat{p}_{r,n}(t)\}_{r=1}^{N_r} = \arg \min_{\substack{\hat{p}_{r,n}\geq 0,\\ r=1,\ldots,N_r}} \sum_{r=1}^{N_r} \mathcal{J}_{r,t}([\hat{p}_{r,1}(t-1), \ldots, \\ \hat{p}_{r,n-1}(t-1), \hat{p}_{r,n}, \hat{p}_{r,n+1}(t-1), \ldots, \hat{p}_{r,N_s}(t-1)]^T) \\ \text{subject to } \hat{p}_{r,n} = \hat{p}_{\varrho,n}, \quad \forall \varrho \in \mathcal{N}_r, \quad r = 1, 2, \ldots, N_r. \end{aligned} \tag{4.23}$$

Using the ADMoM, a solver of (4.23) will be devised next, which converges to to the solution of (4.13)–(4.14) using only local message-passing. To this end, and similar to the centralized algorithm, define the following

quantities

$$\mathbf{R}_r(t) := \sum_{\tau=1}^{t} \mu^{t-\tau} \mathbf{g}_r(\tau)\mathbf{g}_r^T(\tau) = \mu \mathbf{R}_r(t-1) + \mathbf{g}_r(t)\mathbf{g}_r^T(t) \tag{4.24}$$

$$\mathbf{r}_r(t) := \sum_{\tau=1}^{t} \mu^{t-\tau} \pi_r(\tau)\mathbf{g}_r(\tau) = \mu \mathbf{r}_r(t-1) + \pi_r(\tau)\mathbf{g}_r(t) \tag{4.25}$$

$$\tilde{r}_{r,n}(t) := r_{r,n}(t) - \sum_{\substack{n'=1 \\ n' \neq n}}^{N_s} R_{r,n,n'}(t)\hat{p}_{r,n'}(t-1) \tag{4.26}$$

where $R_{r,n,n'}(t)$ and $r_{r,n}(t)$ denote the (n,n')-th element of $\mathbf{R}_r(t)$ and the n-th entry of $\mathbf{r}_r(t)$, respectively. Note that the computation of $\mathbf{R}_r(t)$, $\mathbf{r}_r(t)$ and $\tilde{r}_{r,n}$ is performed locally, and does not require any message passing between nodes. Then, at time t, each CR r performs the following updates iteratively:

$$\hat{p}_{r,n}^{(j+1)}(t) = \frac{\left[\tilde{r}_{r,n}(t) - \frac{\lambda_t}{N_r} - \zeta_r^{(j)} + c\left(|\mathcal{N}_r|\hat{p}_{r,n}^{(j)}(t) + \sum_{\varrho\in\mathcal{N}_r} \hat{p}_{\varrho,n}^{(j)}(t)\right)\right]_+}{R_{r,n,n}(t) + 2c|\mathcal{N}_r|} \tag{4.27}$$

$$\zeta_r^{(j+1)} = \zeta_r^{(j)} + c\left(|\mathcal{N}_r|\hat{p}_{r,n}^{(j+1)}(t) - \sum_{\varrho\in\mathcal{N}_r} \hat{p}_{\varrho,n}^{(j+1)}(t)\right) \tag{4.28}$$

where j is the iteration index, $c > 0$ is a given constant, and $|\mathcal{N}_r|$ denotes the cardinality of the set $\mathcal{N}_r$. To compute $\hat{p}_{r,n}^{(j+1)}(t)$, CR r must collect from its one-hop neighbors, the power estimates $\hat{p}_{\varrho,n}^{(j)}(t)$, $\varrho \in \mathcal{N}_r$, of the previous iteration. These messages are exchanged over a dedicated control channel.

The following proposition states the convergence property of the distributed algorithm.

Proposition 4.3.1. *By performing the updates in* (4.27) *and* (4.28) *at each CR* $r \in \{1, 2, \ldots, N_r\}$ *per iteration* $j = 0, 1, \ldots$, *the local copies* $\hat{p}_{r,n}^{(j)}(t)$ *for all* $r \in \{1, 2, \ldots, N_r\}$ *converge and coincide with* $\hat{p}_n(t)$ *of* (4.13) *as* $j \to \infty$, *for any positive* c *and any initialization for* $\{\hat{p}_{r,n}^{(0)}(t)\}$, *provided that the network is connected, and the links in the network are bi-directional.*

Proof: See section 4.5. □

The overall centralized and distributed spectrum sensing algorithms are schematized in Table 4.1.

0: Initialize $t = 0$.

1: Acquire measurements $\{\pi_r(t)\}$ at CR $r \in \{1, \ldots, N_r\}$.

2: **[Centralized Algorithm]**

Collect the measurements $\{\pi_r(t)\}_{r=1}^{N_r}$ at an FC.

Update $\mathbf{R}(t)$ and $\mathbf{r}(t)$ by (4.15) and (4.16).

Compute $\hat{p}_n(t)$ by (4.21).

2': **[Distributed Algorithm]**

Set $\hat{p}_{r,n}^{(0)}(t) = \hat{p}_{r,n}(t)$ for all r.

Update $\mathbf{R}_r(t)$ and $\mathbf{r}_r(t)$ by (4.24) and (4.25), for all r.

For $j = 0, 1, \ldots, N_I - 1$

For each CR $r \in \{1, 2, \ldots, N_r\}$

Collect from the neighbors $\hat{p}_{\varrho,n}^{(j)}(t)$, $\varrho \in \mathcal{N}_r$.

Compute $\hat{p}_{r,n}^{(j+1)}(t)$ from (4.27).

Next r

Next j

Set $\hat{p}_{r,n}(t) = \hat{p}_{r,n}^{(N_I)}(t)$ for all r.

3: Increment t and go to Step 1.

Table 4.1: Summary of the spectrum sensing algorithms.

4.3.3 Incorporating CG atlases

The proposed sensing algorithms entails utilization of the CG maps in the updates (4.15)–(4.16) and (4.24)–(4.25) of the centralized and distributed algorithms, respectively. Then, the estimates $\{\hat{\mathbf{g}}_r(t)\}$ of the CG vectors $\{\mathbf{g}_r(t)\}$ replace the ideal quantities in the aforementioned recursions.

CG atlases can be effectively employed in order to avoid the utilization of a crude path loss-only propagation model and, thus, enhance tracking and localization accuracy of the sensing algorithm. Note that, in a challenging scenario such as the hierarchical spectrum access, the training signals required for CG update purposes have to respect the PU-CR hierarchy. Hence, CG measurements can be acquired only when the PUs are silent; some measurements can be acquired if no PU activity is present in a sub-region of $\mathcal{A}$, as it will be shown in chapter 5.

CG map update without current measurements being available was addressed in section 3.3.3; it was shown that the KKF-based model safely falls back to the path loss-only model [cf. (3.6)] if measurements can not be acquired for a prolonged period of time. However, it should be noted that in the usual deployment scenarios for CRs, the probability of PU presence is very low. Moreover, shadowing typically varies very slowly compared to the coherence time of the PU activities. These considerations indicate that a prolonged outage of measurements should be a rare event.

4.3.4 Numerical results

Numerical tests are now performed to verify the performance of the proposed sensing algorithms. Also, the profit in terms of power estimation and localization offered by the algorithms when CG maps are employed will be emphasized.

The CR network of $N_r = 20$ nodes used in the previous chapter is considered again. Here, the CRs' communication range is set to 150m, leading to the connected network shown in Fig. 4.1. Also, the detection range, which is used for the CG measurements, is set to 200m. Two PUs are involved at positions marked by the triangles in Fig. 4.1, with the time-varying activities depicted in Fig. 4.2. The square dots represent $N_s = 36$ grid points. It

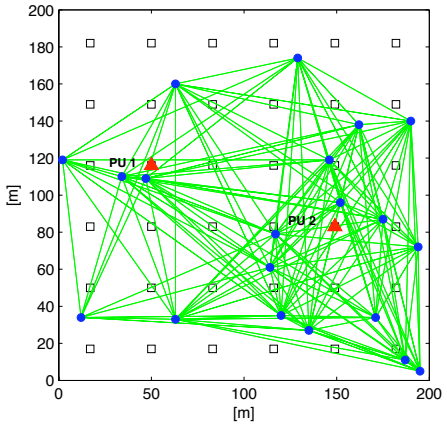

Figure 4.1: PU state tracking. Simulation scenario.

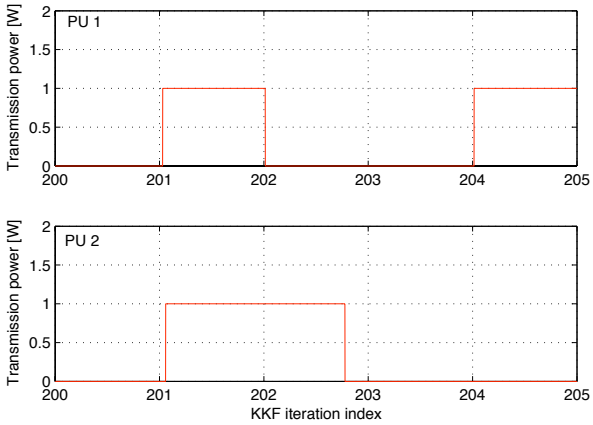

Figure 4.2: PU state tracking. PU activity patterns.

is assumed that the PUs transmit at a constant power of 1W when active.

The path loss parameters were set to $\{G_{0,\mathbf{x}_j \to \mathbf{x}_r} = 0\}$ dB and $\eta = 3$. The measurement noise variance σ_ϵ^2 was set to 10, and $K = 15$ orthonormal Legendre polynomials were used for the basis expansion. To generate the space-time shadow fading field for each CR, the model in chapter 3 was adopted and the same simulation parameters were used. The generated shadow fading has standard deviation $\sigma_S = 10$ dB, coherence distance of approximately 70m, and coherence time corresponding to 9.9 KKF iterations.

The CG map and the PU state tracking are performed in two different time scales, since the shadow fading evolves very slowly with the coherence

time on the order of seconds to minutes [22], while agility is desired in detecting the changes in spectrum occupancy. In the experiments, $40N_s$ OCD-Lasso iterations were performed between consecutive map updates; i.e., the Lasso iteration index $t^{\text{Lasso}} = 40N_s t$, where t is the KKF iteration index. However, if the spectrum is sensed to be occupied, the training signals cannot be transmitted; in this case, the map was updated open-loop, as described in Section 3.3.3.

Remark 4.3.2. Actual design of the PU detection strategies goes beyond the scope this work, and all the numerical tests assume that the detection is practically error-free. There are a couple of justifications for such an idealization. In CR systems, the miss detection, which is the event of not identifying active PU transmissions, must be strictly regulated to protect the licensed PU systems. In other words, no matter which detector is selected, it has to be designed to yield very low probability of miss detection. Therefore, the implication of miss detection to the map tracking performance would be negligible. On the other hand, false alarms, which are the cases where the detector erroneously reports the presence of active PUs, may affect the map tracking performance through missed measurements. However, as was discussed in section 3.3.3, the performance degradation is lower-bounded by the schemes based on the path-loss-only map. In fact, the PU tracking performance is hardly affected even if the path loss-only map is used, when there are no active PUs. □

To track the PU state centrally at the FC, the forgetting factor $\mu = 0.9$ was used, and weighting factor λ_t for the ℓ_1-penalty term was set as suggested in [79] to

$$\lambda_{t^{\text{Lasso}}} = \sigma_z \sqrt{2 \cdot (\log_{10} N_s) \sum_{\tau=1}^{t^{\text{Lasso}}} \mu^{2(t^{\text{Lasso}}-\tau)}} \tag{4.29}$$

where t^{Lasso} is the iteration index for the OCD-Lasso algorithm, and $\sigma_z^2 = 10^{-10}$ was used.

In Fig. 4.3, the average performance of the centralized algorithm is considered. Specifically, the mean-squared error (MSE), i.e., $\mathbb{E}\{\|\mathbf{p}(t) - \hat{\mathbf{p}}(t)\|_2^2\}$, is plotted in Fig. 4.3 and it was computed by averaging over 20 independent

shadow fading realizations. The trajectories of the PU state estimate MSE are shown for four different cases:

i) perfect knowledge of the grid-to-CR CGs, i.e., $\hat{G}_{\mathbf{x}_j \to \mathbf{x}_r}(t) = G_{\mathbf{x}_j \to \mathbf{x}_r}(t)$, $\forall \mathbf{x}_j \in \mathcal{S}$, $\forall\, r, t$;

ii) by resorting to the path loss-only model, which sets $\hat{S}_{\mathbf{x}_j \to \mathbf{x}_r}(t) = 0$, $\forall \mathbf{x}_j \in \mathcal{S}$, $\forall\, r, t$;

iii) using the CG maps estimated via KKF;

iv) employing the plain recursive least-squares (RLS) and the estimated CG maps.

With the latter trajectory, which is obtained by setting $\lambda_t = 0$, the merits of the sparsity-exploiting technique can be stressed.

The plain RLS, which does not exploit sparsity of the estimand is seen to yield much higher MSE in the whole considered sensing interval. Note that, compared to the sparsity-aware algorithm proposed here, the error of the plain RLS is more pronounced when both PUs are silent. In this case, the RLS algorithm essentially reports the presence of low-power PUs, which may cause false alarm events. Turning the attention to the proposed algorithm, it is noticed that by exploiting the estimated CG maps, the estimation performance of the PU power levels is significantly improved with respect to a crude path loss-only model. This in turn may have vital importance when it comes to consider spatial reuse techniques, which performance may be significantly compromised when CRs fail to accurately estimate the PU power levels and locations.

Fig. 4.3(b) plots the mean spurious power (MSP), which is the MSE evaluated only at those grid points where PUs are absent. The MSP, which should ideally be zero, is an index that assesses the accuracy in localizing the active PUs of the proposed centralized algorithm. Again, the KKF-based method exhibits superior performance with respect to the path loss-based method, which yields large spurious power, thus indicating that the positions of the RF emitters are not correctly identified.

Fig. 4.4(a) depicts the trajectories for the MSE when the distributed algorithm is employed. The parameter $c = 0.1$ was used and the number

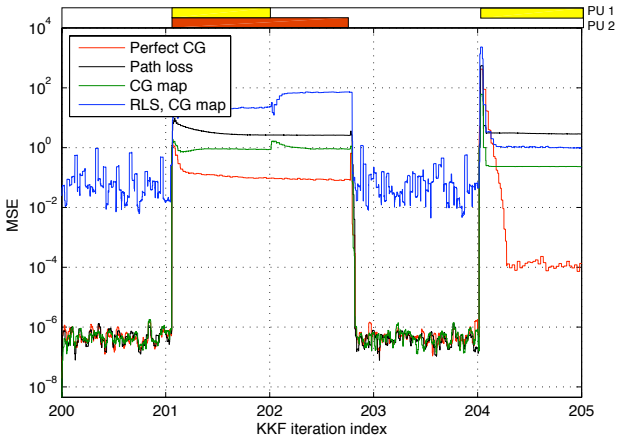

(a)

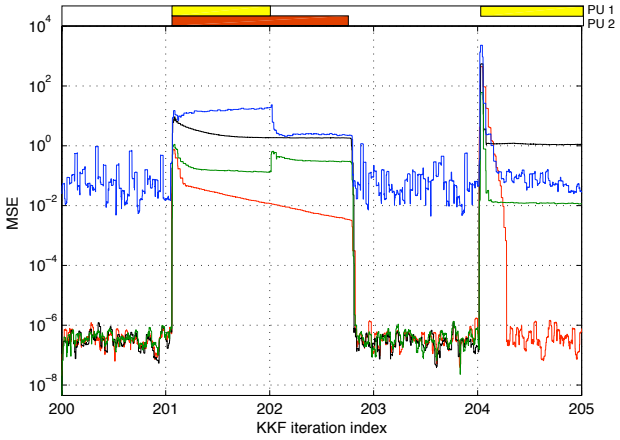

(b)

Figure 4.3: Average performance of the centralized algorithm and the plain RLS algorithm. (a) MSE evaluated over all grid points. (b) MSP evaluated at the grid points where the PU activity is absent.

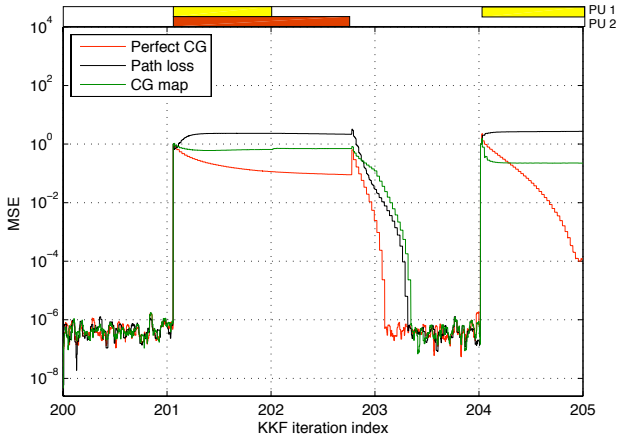

(a)

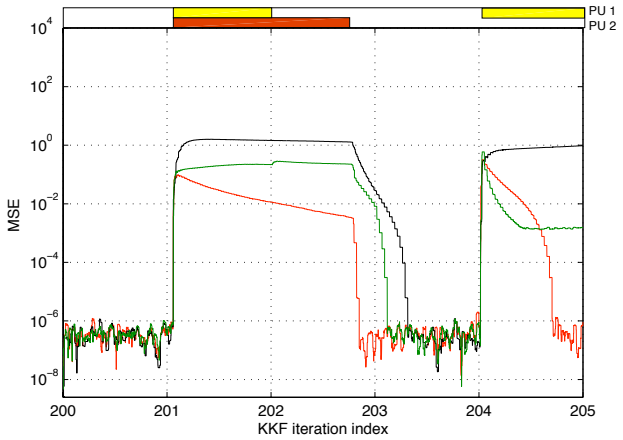

(b)

Figure 4.4: Average performance of the distributed algorithm. (a) MSE evaluated over all grid points. (b) MSP evaluated at the grid points where the PU activity is absent.

of iterations to reach consensus on the power estimates was set to $N_I = 50$. Comparing Fig. 4.4(a) with Fig. 4.3(a), it is clear that the distributed algorithm achieves tracking performance very close to that of its centralized counterpart, even if the number of iterations to reach consensus was kept substantially small to address practical complexity concerns.

Fig. 4.4(a) shows the MSE curves for the distributed algorithm when: i) the channel is perfectly known; ii) the path loss-only model is adopted; and iii) the KKF-based CG map estimates are utilized. The MSE is seen to be a bit larger than that of the centralized case when all the PUs are silent. This is because the number of consensus iterations N_I is sometimes insufficient to bring the local estimates to convergence. In other words, there is a trade-off between message-passing overhead and tracking performance in the distributed algorithm. In Fig. 4.4(b), the trajectories corresponding to the MSP are reported. In this case, it is observed that after $t = 203$, there is difference in the convergence speed of the three cases. For example, it is seen that it takes longer for the path loss-based scheme than for the KKF-based scheme for the same number of iterations N_I.

4.4 System coverage and interference maps

In this section, the usefulness of the CG map information is demonstrated when it comes to study resource allocation techniques for CR networks. In order to make opportunistic spatial reuse of the spectrum, the unused spectral resources, or spectrum holes in the space domain [15] have to be detected. In this context, the PSD maps provide vivid description of which region in the area of interest is crowded in terms of RF interference, and must hence be avoided by the CR transceivers. In other words, the coverage region of the primary system can be extracted from the PSD map.

Once the PU coverage region is obtained, the CG atlases can be used even to compute the range of power levels that can be used by the CR transmitters to prevent disruption to the existing PU links. In addition to coping with time-varying environments, CG maps provide vital information about the CR-to-PU CGs, which is not available with PSD maps [33], [81], allowing PU protection under shadowing propagation effects.

4.4.1 Coverage map estimation

Once the information on the RF environment is acquired, the CR network can perform resource allocation to make the most use of the available transmission opportunities. Here, it is assumed that power control is employed so as to restrict the interference exposed to the PU links. For simplicity, suppose that a single PU transmitter has been detected to be active at location $\mathbf{x}_s$ at transmit-power level p_s. The exposition can be easily extended to the multi-PU case.

However, the positions of the PU *receivers* are assumed unknown. To reveal the potential locations where PU receivers could reside, consider estimating the coverage region [82, Ch. 3] of the PU system. To this end, let $\Pi(\mathbf{x})$ denote the averaged power in dB that is received at location $\mathbf{x} \in \mathcal{A}$ due to the PU transmission, which can be expressed as [cf. (3.7)]

$$\Pi(\mathbf{x}, t) = P_s + G_{0,\mathbf{x}_s \to \mathbf{x}} - 10\eta \log_{10} \|\mathbf{x}_s - \mathbf{x}\|_2 + S_{\mathbf{x}_s \to \mathbf{x}}(t) \tag{4.30}$$

where $P_s := 10 \log_{10} p_s$. Using a path loss-based model, $\Pi(\mathbf{x})$ can be modeled as Gaussian with mean $P_s + G_{0,\mathbf{x}_s \to \mathbf{x}} - 10\eta \log_{10} \|\mathbf{x}_s - \mathbf{x}\|_2$ and variance $\sigma^2_{S_{\mathbf{x}_s \to \mathbf{x}}}$; recall that $\sigma^2_{S_{\mathbf{x}_s \to \mathbf{x}}}$ is the variance of the shadow fading, a parameter that might be available from measurements campaigns and, usually, it does not change over the links [26].

Since a PU receiver can reliably decode the desired message only if the received power level exceeds a threshold $\Pi_{\min}$ (dB), one can compute the probability of coverage that a PU receiver at location $\mathbf{x}$ would experience as

$$\begin{aligned} P_{\text{cov}}(\mathbf{x}) :=& \Pr\{\Pi(\mathbf{x}) \geq \Pi_{\min}\} \\ =& Q\left(\frac{\Pi_{\min} - P_s - G_{0,\mathbf{x}_s \to \mathbf{x}} + 10\eta \log_{10} \|\mathbf{x}_s - \mathbf{x}\|_2}{\sigma_{S_{\mathbf{x}_s \to \mathbf{x}}}}\right) \end{aligned} \tag{4.31}$$

where $Q(\cdot)$ is the standard Gaussian tail function. Conversely, with the estimated CG map of the PU $\{G_{\mathbf{x}_s \to \mathbf{x}}(t)\}$, $\Pi(\mathbf{x}, t)$ can be modeled as Gaussian with mean $P_s + G_{0,\mathbf{x}_s \to \mathbf{x}} - 10\eta \log_{10} \|\mathbf{x}_s - \mathbf{x}\|_2 + \hat{S}_{\mathbf{x}_s \to \mathbf{x}}(t)$ and variance $\text{var}\{S_{\mathbf{x}_s \to \mathbf{x}}(t) | \check{\mathbf{S}}_{1:t}\}$, which is given by (3.33), with $\mathbf{x}$ and $\mathbf{y}$ replaced by $\mathbf{x}_s$ and $\mathbf{x}$, respectively. Thus, the probability of coverage that a PU receiver at

location $\mathbf{x}$ would experience becomes

$$P_{\text{cov}}(\mathbf{x},t) = Q\left(\frac{\Pi_{\min} - P_s - G_{0,\mathbf{x}_s\to\mathbf{x}} + 10\eta\log_{10}\|\mathbf{x}_s-\mathbf{x}\|_2 - \hat{S}_{\mathbf{x}_s\to\mathbf{x}}(t)}{\sqrt{\text{var}\{S_{\mathbf{x}_s\to\mathbf{x}}(t)|\breve{\mathbf{S}}_{1:t}\}}}\right) \tag{4.32}$$

and it is now allowed to vary with the time index t, being $\hat{S}_{\mathbf{x}_s\to\mathbf{x}}(t)$ and $\text{var}\{S_{\mathbf{x}_s\to\mathbf{x}}(t)|\breve{\mathbf{S}}_{1:t}\}$ time-varying quantities.

The PU coverage region can be defined as the set of locations in $\mathcal{A}$, for which the coverage probability is no smaller than a threshold ν_s; i.e.,

$$\mathcal{C}_s(t) := \{\mathbf{x}\in\mathcal{A}|P_{\text{cov}}(\mathbf{x},t)\geq\nu_s\}. \tag{4.33}$$

Note that, if the CG map is not used, $\mathcal{C}_s$ is a time-invariant disc centered at $\mathbf{x}_s$. The CG map estimate thus provides an invaluable means to overcome this over-simplification, and portray the coverage region more accurately. Also, the temporal evolution of the coverage region can be caught.

4.4.2 Maximum transmit power estimation

In order to maximize its own transmission rate, the CR transmitter needs to maximize the transmit-power, while adhering to the interference constraints. The CG map can provide valuable information in this set-up, allowing one to predict the MIFTP [32] that the CR transmitter can afford, based on the potential locations of the PU receivers.

To obtain the MIFTP for CR transmission, note first that the power received at position $\mathbf{x}$ due to a CR transmitter located at $\mathbf{x}_r$ employing transmit-power P_r (dB) can be characterized as a Gaussian random variable with mean $P_r + G_{0,\mathbf{x}_r\to\mathbf{x}} - 10\eta\log_{10}||\mathbf{x}_r-\mathbf{x}||_2$ and variance $\sigma^2_{S_{\mathbf{x}_r\to\mathbf{x}}}$ if a path loss-only model is employed. Thus, the probability that the CR interference at position $\mathbf{x}$ exceeds a prescribed threshold $I_{\max}$ is given by

$$P_{\text{int}}(\mathbf{x}) = Q\left(\frac{I_{\max} - P_r - G_{0,\mathbf{x}_r\to\mathbf{x}} + 10\eta\log_{10}||\mathbf{x}_r-\mathbf{x}||_2}{\sigma_{S_{\mathbf{x}_r\to\mathbf{x}}}}\right). \tag{4.34}$$

and it is a time-invariant quantity. By using the CG map of the CR, the power received at position $\mathbf{x}$ can be characterized as a Gaussian random variable with mean $P_r+G_{0,\mathbf{x}_r\to\mathbf{x}}-10\eta\log_{10}||\mathbf{x}_r-\mathbf{x}||_2+\hat{S}_{\mathbf{x}_r\to\mathbf{x}}(t)$ and variance

$\text{var}\{S_{\mathbf{x}_r\to\mathbf{x}}(t)|\breve{\mathbf{S}}_{1:t}\}$. The probability that the CR interference at position $\mathbf{x}$ exceeds a prescribed threshold $I_{\max}$ then becomes

$$P_{\text{int}}(\mathbf{x},t) = Q\left(\frac{I_{\max} - P_r - G_{0,\mathbf{x}_r\to\mathbf{x}} + 10\eta\log_{10}||\mathbf{x}_r-\mathbf{x}||_2 - \hat{S}_{\mathbf{x}_r\to\mathbf{x}}(t)}{\sqrt{\text{var}\{S_{\mathbf{x}_r\to\mathbf{x}}(t)|\breve{\mathbf{S}}_{1:t}\}}}\right). \tag{4.35}$$

Thus, the CR interference map can be defined as the set of locations in $\mathcal{A}$, for which the interference probability is no smaller than a threshold ν_r; i.e.,

$$\mathcal{I}_r(t) := \{\mathbf{x}\in\mathcal{A}|P_{\text{int}}(\mathbf{x},t)\geq\nu_r\}. \tag{4.36}$$

Again, the CG map estimate provides an invaluable means to overcome a disc-shaped time-invariant simplification of the interference region. The MIFTP can then be defined as the maximum value of P_r that yields a $P_{\text{int}}(\mathbf{x})$ no larger than a given outage threshold $\nu_r > 0$ for all potential receivers in the PU coverage region; that is,

$$P_r^*(t) := \max P_r \quad \text{subject to} \quad P_{\text{int}}(\mathbf{x},t)\leq\nu_r,\ \forall\mathbf{x}\in\mathcal{C}_s(t)\ . \tag{4.37}$$

Equivalently, $P_r^*(t)$ can be defined as the maximum value for P_r such that $\mathcal{C}_s(t)$ and $\mathcal{I}_r(t)$ do not overlap, i.e., $\mathcal{C}_s(t)\cap\mathcal{I}_r(t)=\emptyset$. Note that constraint $P_{\text{int}}(\mathbf{x},t)\leq\nu_r$ can be equivalently re-written as follows:

$$P_r + \hat{G}_{\mathbf{x}_r\to\mathbf{x}}(t) + Q^{-1}(\nu_r)\sqrt{\text{var}\{S_{\mathbf{x}_r\to\mathbf{x}}(t)|\breve{\mathbf{S}}_{1:t}\}} \leq I_{\max}\,. \tag{4.38}$$

Then, the MIFTP can be obtained by solving the following linear program (LP)

$$P_r^*(t) := \max_{P_r} P_r \tag{4.39}$$

$$\text{subject to } P_r + \hat{G}_{\mathbf{x}_r\to\mathbf{x}}(t) + Q^{-1}(\nu_r)\sqrt{\text{var}\{S_{\mathbf{x}_r\to\mathbf{x}}(t)|\breve{\mathbf{S}}_{1:t}\}} \leq I_{\max} \tag{4.40}$$

$$\forall\mathbf{x}\in\mathcal{C}_s(t)\,.$$

Note that, if CRs transmit in a TDMA fashion, $P_r^*(t)$ in (4.37) guarantees observation of the averaged interference temperature bounds at all the potential PU receivers. Conversely, if simultaneous CR transmissions are allowed, the per-CR maximum power $P_r^*(t)$ can be used so as to restrict the transmission power allocated to the CRs via power control techniques, as it will be shown in the ensuing chapter 5.

Remark 4.4.1. If the instantaneous interference caused to the PU system is a concern, then the estimate of the shadow fading along with the conditional variance carried out by the KKF can be used to compute mean and variance of the instantaneous dB-scale CGs $\{\dot{G}_{\mathbf{x}_s\to\mathbf{x}}\}$ and $\{\dot{G}_{\mathbf{x}_r\to\mathbf{x}}\}$, which can be approximates as Gaussian, as shown in section 3.2 and in the ensuing chapter 5. □

4.4.3 Numerical example

To illustrate the merits of the CG map in the CR resource allocation problem, consider again the CR network depicted in Fig. (4.1). Suppose that only PU 1 is transmitting at $P_s = 0$dBW, as happens for $t > 204$ in Fig. 4.2. A realization of the true received power map $\Pi(\mathbf{x})$ due to the PU transmission is depicted using the contour plot in Fig. 4.5(a). In Fig. 4.6(a) there is another contour plot of the true CG map $G_{\mathbf{x}_r\to\mathbf{x}}$ from the CR located at $\mathbf{x}_r = (192, 15)$, see Fig. 4.1. It is noted that the contours are not concentric circles, due to the shadowing effect. Thus, estimating the shadowing field is essential for efficient CR resource allocation. An estimated version of Fig. 4.5(a) using the distributed KKF is shown in Fig. 4.5(b). Likewise, the estimated CG map of the considered CR is depicted in Fig. 4.6. Number of consensus iterations and ADMoM-related constants were set as in chapter 3.

Based on the estimated CG map, the PU coverage region was estimated for $\Pi_{\min} = -60$dBW and $\nu_s = 0.4$, which is depicted by round dots in Fig. 4.7(a). Note that by setting $\nu_s < 0.5$ yields a conservative characterization of the PU coverage region. By setting $I_{\max} = -80$dB and $\nu_r = 0.01$, the MIFTP for the considered CR transmitter was found to be 7.2dBm with the use of the estimated CG maps. The estimated region in which the interference power due to the CR transmission is no less than $I_{\max}$ with probability at least ν_r is shown with square dots in Fig. 4.7(a). Note that although the estimated MIFTP is slightly conservative compared to the true MIFTP of 7.6dBm, it is vastly improved compared to the path loss-only map-based calculation that yields an MIFTP of only -18.5dBm.

The PU coverage region, as well as the interference region based on the path loss map is shown in Fig. 4.7(b). It can be seen that the PU

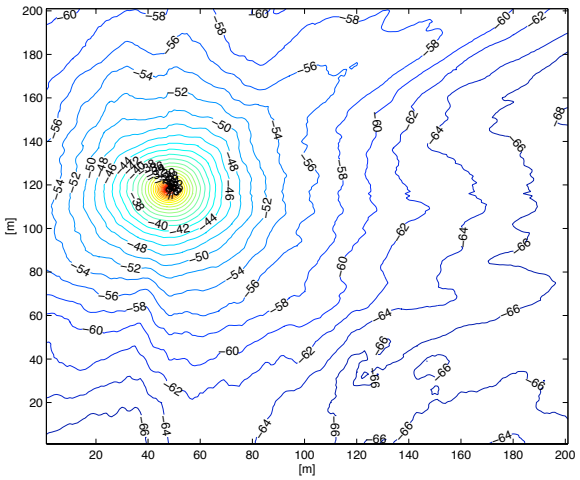

(a) True

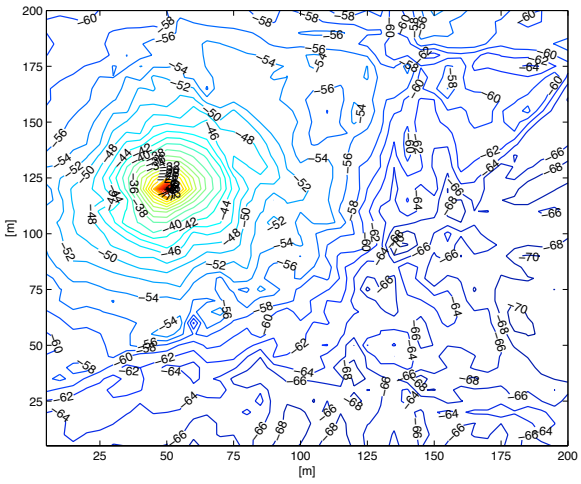

(b) Estimated

Figure 4.5: RF power map due to PU transmission

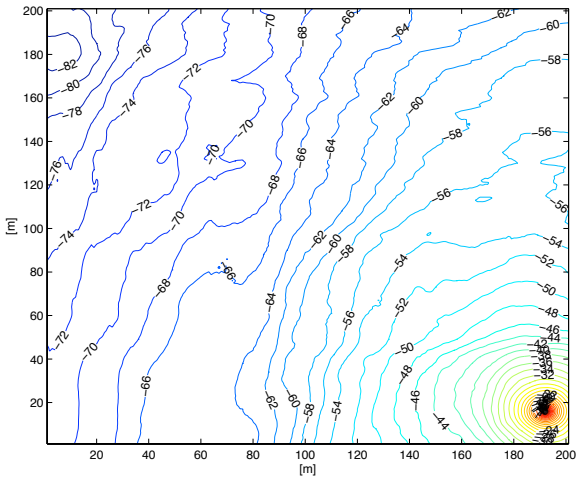

(a) True

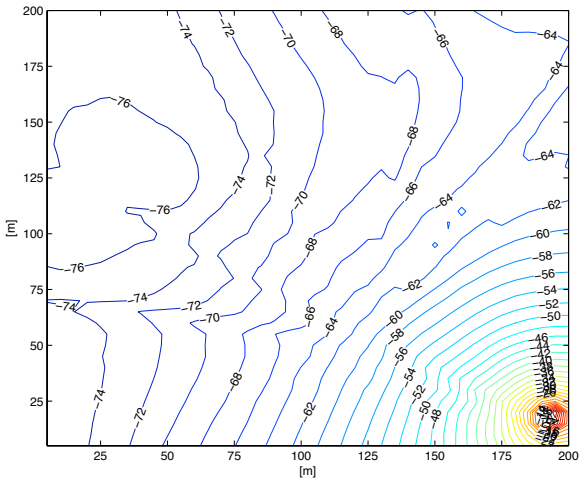

(b) Estimated

Figure 4.6: CG map for a CR transmitter.

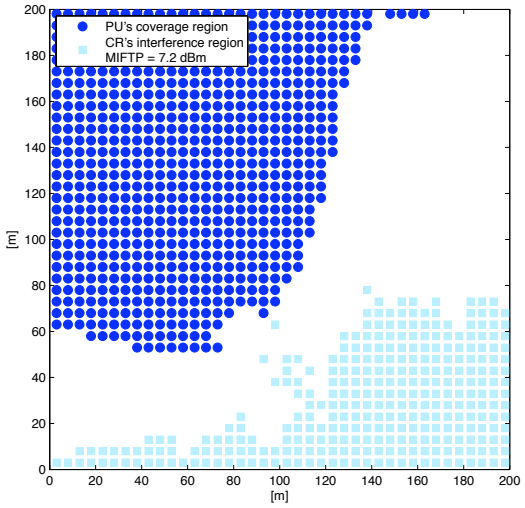

(a) KKF-based

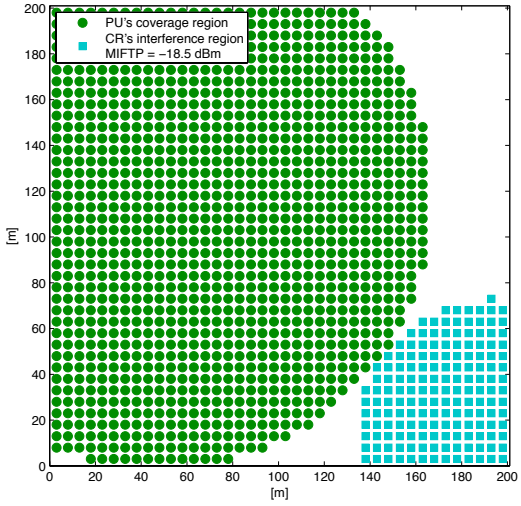

(b) Path loss-based

Figure 4.7: Estimated PU coverage and CR interference regions.

coverage region is grossly over-estimated, thus limiting the spatial reuse of the primary spectrum resources.

4.5 Appendix

The proof of (4.27)–(4.28) and proposition 4.3.1 follows steps that are similar to those in section 3.6.2. However, as a matter of completeness, and since the underlying optimization problem involves further challenges such as, e.g., non-negativity of the estimand, the complete proof will be reported next.

Then, consider the following equivalent re-formulation of (4.23):

$$\begin{aligned} \min_{\substack{\hat{p}_{r,n}\geq 0,\ q_{r,\varrho} \\ \varrho\in\mathcal{N}_r,\ r=1,2,\ldots,N_r}} & \sum_{r=1}^{N_r} \tilde{\mathcal{J}}_{r,t}(\hat{p}_{r,n}) \\ \text{subject to } \hat{p}_{r,n} = q_{r,\varrho} & \quad \forall \varrho \in \mathcal{N}_r,\ r = 1,2,\ldots,N_r \\ q_{r,\varrho} = q_{\varrho,r} & \quad \forall \varrho \in \mathcal{N}_r,\ r = 1,2,\ldots,N_r \end{aligned} \tag{4.41}$$

where $\tilde{\mathcal{J}}_{r,t}(\hat{p}_{r,n}) := \mathcal{J}_{r,t}([\hat{p}_{r,1}(t-1),\ldots,\hat{p}_{r,n-1}(t-1),\hat{p}_{r,n},\hat{p}_{r,n+1}(t-1),\ldots,\hat{p}_{r,N_s}(t-1)]^T)$, and $\{q_{r,\varrho}\}$ are auxiliary optimization variables. Problem (4.41) is in the form to which the alternating direction method of multipliers (ADMoM) can be applied [57, p. 253].

Specifically, consider the augmented (partial) Lagrangian given by

$$\begin{aligned} \mathcal{L}(\{\hat{p}_{r,n}\},\{q_{r,\varrho}\},\{\xi_{r,\varrho}\}) = & \sum_{r=1}^{N_r} \tilde{\mathcal{J}}_{r,t}(\hat{p}_{r,n}) \\ & + \sum_{r=1}^{N_r} \sum_{\varrho\in\mathcal{N}_r} \xi_{r,\varrho}(\hat{p}_{r,n} - q_{r,\varrho}) \\ & + c\sum_{r=1}^{N_r} \sum_{\varrho\in\mathcal{N}_r} (\hat{p}_{r,n} - q_{r,\varrho})^2 \end{aligned} \tag{4.42}$$

where $\{\xi_{r,\varrho}\}$ are the Lagrange multipliers, and c is a positive constant. The ADMoM procedure updates the primal variables $\{\hat{p}_{r,n}\},\{q_{r,\varrho}\}$ and the dual

variables $\{\xi_{r,\varrho}\}$, alternately, as

$$\{\hat{p}_{r,n}^{(j+1)}\} = \arg \min_{\{\hat{p}_{r,n}\geq 0\}} \mathcal{L}(\{\hat{p}_{r,n}\}, \{q_{r,\varrho}^{(j)}\}, \{\xi_{r,\varrho}^{(j)}\}) \tag{4.43}$$

$$\{q_{r,\varrho}^{(j+1)}\} = \arg \min_{\substack{q_{r,\varrho}=q_{\varrho,r},\\ \varrho\in\mathcal{N}_r,\ r=1,2,\ldots,N_r}} \mathcal{L}(\{\hat{p}_{r,n}^{(j+1)}\}, \{q_{r,\varrho}\}, \{\xi_{r,\varrho}^{(j)}\}) \tag{4.44}$$

$$\xi_{r,\varrho}^{(j+1)} = \xi_{r,\varrho}^{(j)} + 2c\left(\hat{p}_{r,n}^{(j+1)} - q_{r,\varrho}^{(j+1)}\right), \quad \varrho \in \mathcal{N}_r,\ r = 1, 2, \ldots, N_r. \tag{4.45}$$

Proposition 4.2 in [57] implies that the sequence $\hat{p}_{r,n}^{(j)}$, $j = 1, 2, \ldots$, generated by (4.43)–(4.45) converges to the optimal solution $\hat{p}_{r,n}(t)$ of (4.41), for each r, for an arbitrary initial $\hat{p}_{r,n}^{(0)}$ and any positive constant c.

It is now shown that the procedure (4.43)–(4.45) can be simplified to (4.27)–(4.28). First, it is noted that (4.44) can be re-written as

$$\{q_{r,\varrho}^{(j+1)}\} = \arg \min_{\substack{q_{r,\varrho}=q_{\varrho,r},\\ \varrho\in\mathcal{N}_r,\ r=1,2,\ldots,N_r}} -\sum_{r=1}^{N_r}\sum_{\varrho\in\mathcal{N}_r} \xi_{r,\varrho}^{(j)} q_{r,\varrho} + c\sum_{r=1}^{N_r}\sum_{\varrho\in\mathcal{N}_r} (\hat{p}_{r,n}^{(j+1)} - q_{r,\varrho})^2 \tag{4.46}$$

$$= \arg \min_{\{q_{r,\varrho}\}} \sum_{\{(r,\varrho)|\varrho\in\mathcal{N}_r, r>\varrho\}} \{-(\xi_{r,\varrho} + \xi_{\varrho,r})q_{r,\varrho} + c\left[(\hat{p}_{r,n}^{(j+1)} - q_{r,\varrho})^2 + (\hat{p}_{\varrho,n}^{(j+1)} - q_{r,\varrho})^2\right]\} \tag{4.47}$$

where in the last step the conditions $\{q_{r,\varrho} = q_{\varrho,r}\}$ and the assumption that the links are bi-directional are used. It is clear from (4.47) that $\{q_{r,\varrho}^{(j+1)}\}$ can be obtained as

$$q_{r,\varrho}^{(j+1)} = \frac{1}{2}\left(\hat{p}_{r,n}^{(j+1)} + \hat{p}_{\varrho,n}^{(j+1)}\right) + \frac{1}{4c}\left(\xi_{r,\varrho}^{(j)} + \xi_{\varrho,r}^{(j)}\right), \quad \varrho \in \mathcal{N}_r, r = 1, 2, \ldots, N_r. \tag{4.48}$$

By substituting (4.48) into (4.45), one obtains

$$\xi_{r,\varrho}^{(j+1)} = c\left(\hat{p}_{r,n}^{(j+1)} - \hat{p}_{\varrho,n}^{(j+1)}\right) + \frac{1}{2}\left(\xi_{r,\varrho}^{(j)} - \xi_{\varrho,r}^{(j)}\right), \quad \varrho \in \mathcal{N}_r,\ r = 1, 2, \ldots, N_r. \tag{4.49}$$

Thus, it can be verified that

$$\xi_{r,\varrho}^{(j)} + \xi_{\varrho,r}^{(j)} = 0, \quad \varrho \in \mathcal{N}_r,\ r = 1, 2, \ldots, N_r. \tag{4.50}$$

From (4.50) and (4.48)–(4.49), it follows readily that

$$q_{r,\varrho}^{(j+1)} = \frac{1}{2}\left(\hat{p}_{r,n}^{(j+1)} + \hat{p}_{\varrho,n}^{(j+1)}\right), \tag{4.51}$$

$$\xi_{r,\varrho}^{(j+1)} = \xi_{r,\varrho}^{(j)} + c\left(\hat{p}_{r,n}^{(j+1)} - \hat{p}_{\varrho,n}^{(j+1)}\right), \tag{4.52}$$

$$\varrho \in \mathcal{N}_r,\ r = 1, \ldots, N_r$$

Now, consider (4.43), which can be re-written as

$$\begin{aligned}
&\{\hat{p}_{r,n}^{(j+1)}\} \\
&= \arg \min_{\{\hat{p}_{r,n}\geq 0\}} \sum_{r=1}^{N_r} \left[\tilde{\mathcal{J}}_{r,t}(\hat{p}_{r,n}) + \sum_{\varrho\in\mathcal{N}_r} \xi_{r,\varrho}^{(j)}\hat{p}_{r,n} + c\sum_{\varrho\in\mathcal{N}_r}(\hat{p}_{r,n} - q_{r,\varrho}^{(j)})^2\right] \qquad (4.53)\\
&= \arg \min_{\{\hat{p}_{r,n}\geq 0\}} \sum_{r=1}^{N_r} \left[\left(-\tilde{r}_{r,n} + \frac{\lambda_t}{N_r} + \sum_{\varrho\in\mathcal{N}_r}\xi_{r,\varrho}^{(j)} - 2c\sum_{\varrho\in\mathcal{N}_r} q_{r,\varrho}^{(j)}\right)\hat{p}_{r,n}\right. \\
&\qquad\qquad \left. + \left(\frac{1}{2}R_{r,n,n} + c|\mathcal{N}_r|\right)\hat{p}_{r,n}^2\right]. \qquad (4.54)
\end{aligned}$$

Clearly, $\{\hat{p}_{r,n}^{(j+1)}\}$ can be obtained in closed-form as

$$\hat{p}_{r,n}^{(j+1)} = \frac{\left[\tilde{r}_{r,n} - \frac{\lambda_t}{N_r} - \sum_{\varrho\in\mathcal{N}_r}\xi_{r,\varrho}^{(j)} + 2c\sum_{\varrho\in\mathcal{N}_r} q_{r,\varrho}^{(j)}\right]_+}{R_{r,n,n} + 2c|\mathcal{N}_r|} \tag{4.55}$$

$$r = 1, 2, \ldots, N_r.$$

Upon defining $\zeta_r^{(j)} := \sum_{\varrho\in\mathcal{N}_r}\xi_{r,\varrho}^{(j)}$, and substituting (4.51) to (4.55), (4.27) is obtained. Finally, (4.28) follows from the definition of $\zeta_r^{(j)}$ and (4.52).

Chapter 5

Power Allocation Under Channel Gain Uncertainty

Due to lack of mechanisms between CR and PU systems, sensing algorithms face difficulty in acquiring CR-to-PU users channels. Moreover, the sensing algorithms cannot detect silent licensed receivers, which nevertheless have to be obligatorily protected. To make spatio-temporal spectrum re-use even in such challenging scenarios, a power control problem with probabilistic interference constraints is thus well-motivated. Based on primary coverage map and channel gain cartography, the approach presented in this chapter exploits statistical knowledge of the CR-to-PU channels to maximize a given secondary network utility function under chance constraints that ensure protection to any potential licensed user. In addition to the CR-to-PU channel, the channel between the CR transceivers may contain uncertainty. Then, a probabilistic approach encompassing channel knowledge uncertainty on both secondary-to-primary and secondary-to-secondary links is also presented.

5.1 Preliminaries

Compared to the broadly-investigated power control for ad hoc networks [83], [84], [85], [86], [87], several additional challenges need to be considered for channel-adaptive resource allocation schemes to be employed by CRs. In particular, power allocation for underlay (ad hoc) CR networks demands

for instantaneous CR-to-PU CG knowledge, information that is critical in order to ensure protection to the licensed PU system from secondary transmissions [59], [15] and, thus, effectively reuse the spectrum resources in a non-intrusive manner.

Recently, power control in an underlay CR scenario has been studied essentially under the assumption of *perfect* CR-to-PU CG knowledge. See, e.g., [88], [89], [90], [91], [92]. The classical problems inherent to ad hoc networks such as, e.g., rate maximization [88], [89] and admission control [90] have been tailored to the application in context, where the additional constraint on the amount of interference that would be caused to the PU receivers must be present. A scenario comprising a single primary link and a single CR link, i.e., a revisitation of the "Z"-channel, was considered in [88], [91]; also, a CR transmitter equipped with multiple antennas was considered in [92]. An ad hoc setting was considered in, e.g., [89] and [90].

Assumptions of *perfect* knowledge of the *instantaneous* CGs might be unrealistic for many practical systems, especially when mobile nodes as well as ad hoc infrastructure of the CR systems are considered. Recent research effort has been devoted on adaptive schemes that rely on quantization of the CG information, where a quantized version of the channel is pragmatically acquired via a limited-rate receiver-to-transmitter feedback link [93]. A robust power control approach encompassing error-corrupted and outdated channel estimates was proposed in [94], where cellular networks were considered. Focusing on the so called "X"-channel, the achievable capacity of a single CR link under interference constraints that protect ongoing transmissions on a single PU link was analyzed under imperfect channel gain information in [95]. However, typically due to lack of collaboration mechanisms between PU and CR systems, especially between PU *receivers* and CRs, even the assumption of partial CR-to-PU receiver CG knowledge might not be adequate in a CR setup.

Reliably detecting the presence of PU transmissions, and estimating the CR-to-PU channels require considerable effort. More challenging is acquiring passive PU *receivers*, which do not transmit RF energy but just listen. Nonetheless, those receivers still need to be protected under the PU-CR hierarchy. One way to estimate the *potential* PU receiver locations, and

eventually their channel gains, is to rely on the idea of *channel gain cartography*. As shown in chapter 4, once the locations of the PU transmitters are acquired through CR sensing, the channel gain maps allow estimation of the corresponding PU coverage regions, in which the PU receivers must reside.

Based on location information of the (potential) PU receivers and, possibly, an estimate of the PU receivers CG maps, the approach pursued here is to exploit the statistical channel knowledge of the CR-to-PU channels. Since the wireless channel involves shadow fading as well as small-scale fading, both sources of uncertainty must be taken into account. As PU protection constraints must be enforced with high reliability, probabilistic constraints will be imposed in order to guarantee that the interference power experienced by PU receivers falls below a tolerable level with a given high probability.

The randomness of the composite shadowed Nakagami fading can be well-captured by a log-Normal r.v., as shown in section 3.2. See, also, [42, Ch. 2],[46] and [47]. Since exact computation of the aggregate interference is not tractable due to a lack of closed form expression for the *pdf* of a sum of correlated log-Normal r.v.'s, approximation techniques are employed. Specifically, the sum of the CR interfering signal powers is approximated as log-Normal through the use of Fenton-Wilkinson method [96]. Although a multiplicity of methods were proposed to approximate a sum of correlated log-Normal r.v.'s, the Fenton-Wilkinson method may be the most appealing approach thank to its accuracy over a wide range of parameters that are of practical interest [97] and the low computational burden required to get closed-form expressions for mean and variance of the resultant approximating log-Normal r.v.

With a statistical characterization of the potential interference that would be caused to the PUs, a secondary network utility maximization framework comprising probabilistic constraints on the instantaneous interference power is proposed. Specifically, specifications about the probability of exceeding a prescribed interference temperature threshold at the PUs are embraced by the proposed optimization problem. The resulting chance-constrained network utility maximization problem is non-convex, but can be re-formulated so that its Karush-Kuhn-Tucker (KKT) solutions are obtained via sequen-

tial geometric programming (GP). This is remarkable considering the fact that the power allocation problem with *perfect* channel knowledge is also typically non-convex and requires a sequential GP approach [85]. The sequential GP formulation can also benefit from the availability of efficient interior-point solvers [98, Ch. 11] optimized for GPs.

Perfect knowledge of the instantaneous CR-to-CR CGs is required in the utility maximization process. However, error-corrupted measurements and missing and/or outdated channel gain estimates may compromise the accomplishment of the power control task. Acquisition of instantaneous channel state information is rendered challenging by, e.g., mobility of the nodes and fast variation of the CR environment. Even more dramatically, the power gains might not be even estimated in an hierarchical cognitive setup. In fact, a prolonged occupancy of the primary bands might render impossible the communication among all the other secondary devices; or, simply, CRs might not want to waste precious primary resources by performing a time-consuming any-to-any time domain multiple access (TDMA)-based channel training.

To address this case, a robust network utility maximization problem is considered, where the SINR thresholds for CR links are optimized under prescribed outage probabilities. Again, the log-normal approximation of the SINR statistics proves to be vital for tractability of such formulations.

5.2 System Model and Problem Formulation

Consider a CR network comprising $K \leq N_r$ transmitter-receiver pairs[1], sharing spectrum licensed to a PU system. It is assumed that the locations of the CR transmitters and receivers are known to the CR system. Let $\mathbf{x}_k$ and $\mathbf{u}_k$ denote the locations of the k-th CR transmitter and receiver, respectively, where $k \in \{1, 2, \ldots, K\}$.

In order to make opportunistic use of the spectrum under PU-CR hierarchy, the CR system first employs spectrum sensing algorithms to detect

[1]For the sake of exposition simplicity, each CR transmitter is assumed to serve a unique secondary receiver per time instant; however, generalization to point-to-multipoint transmissions is straightforward.

the PU system activity in space and time domains, as the PU state tracker presented in chapter 4. See also, e.g., [81], [99]. Based on the sensing results, power control is performed to prevent excessive interference to the PU system, and to maximize the CR network performance. The CR network is supposed to operate in a time-block fashion.

Recall from section 3.2 that[2] $\dot{g}_{\mathbf{x_k}\to\mathbf{u_k}}$ denotes the instantaneous CG of link $\mathbf{x}_k \to \mathbf{u}_k$ i.e., $\dot{g}_{\mathbf{x_k}\to\mathbf{u_k}} = g_{0,\mathbf{x}_k\to\mathbf{u}_k}||\mathbf{x}_k - \mathbf{u}_k||_2^{-\eta} s_{\mathbf{x_k}\to\mathbf{u_k}}|h_{\mathbf{x_k}\to\mathbf{u_k}}|^2$. Let $p_k \in (0, p_k^{\max}]$ denote the transmission power of CR k, capped by $p_k^{\max}$, and $\mathbf{p} := [p_1, \ldots, p_K]^T$ collect the transmit-powers of all K CRs. Let also $\dot{\pi}_k$ denote the instantaneous received PU signal power as well as other interference measured at the k-th CR receiver. Then, the instantaneous signal-to-interference-plus-noise power ratio (SINR) at CR receiver k can be expressed as

$$\gamma_k := \frac{p_k \dot{g}_{\mathbf{x_k}\to\mathbf{u_k}}}{\sum_{i=1, i\neq k}^{K} p_i \dot{g}_{\mathbf{x_i}\to\mathbf{u_k}} + \dot{\pi}_k + \sigma_k^2}, \quad k = 1, 2, \ldots, K \tag{5.1}$$

where σ_k^2 is the receiver noise statistical power at CR receiver k, which can be in general different from receiver to receiver if the CR network comprises heterogeneous devices. Define $\boldsymbol{\gamma} := [\gamma_1, \ldots, \gamma_K]^T$.

Denote as $\mathcal{U}(\boldsymbol{\gamma}(\mathbf{p}))$ a continuous (possibly non-concave) CR network utility function. Specifically, the following utility functions are of interest [84].

i) **(Weighted) Sum-rate utility**:

$$\mathcal{U}(\gamma(\mathbf{p})) = \sum_{k=1}^{K} w_k \log_2\left(1 + \gamma_k(\mathbf{p})\right) . \tag{5.2}$$

with $\{w_k \geq 0\}_{k=1}^K$ weighting factors.

ii) **Proportional fair utility**:

$$\mathcal{U}(\gamma(\mathbf{p})) = \sum_{k=1}^{K} \log_2\left(\log_2\left(1 + \gamma_k(\mathbf{p})\right)\right) . \tag{5.3}$$

iii) **Harmonic-rate utility**:

$$\mathcal{U}(\gamma(\mathbf{p})) = \left[\sum_{k=1}^{K} \frac{1}{\log_2(1 + \gamma_k(\mathbf{p}))}\right]^{-1} . \tag{5.4}$$

[2]Hereafter, the time slot index t is dropped for brevity.

iv) **Min-rate utility**:

$$\mathcal{U}(\gamma(\mathbf{p})) = \min_k \log_2(1+\gamma_k(\mathbf{p}))\,. \tag{5.5}$$

Note that, in terms of user fairness, the order is reversed.

If no PUs were present in the area where the CR network is operating, the power control problem would consist in finding the set of transmission powers $\mathbf{p}$ such that $\mathcal{U}(\boldsymbol{\gamma}(\mathbf{p}))$ is maximized [85], [100]. However, the CR underlay paradigm envisions an opportunistic spatio-temporal reuse of the primary bands by the secondary system provided that the amount of interference caused to *any* PU *receiver* is kept below a given prescribed threshold [59], [15]. Then, consider R (potential) PU receivers located at $\{\mathbf{r}_r\}_{r=1}^R \subset \mathcal{A}$ and denote as i_r the instantaneous *aggregate* interference caused to the PU receiver r due to the incoherent superimposition of K interfering CR transmissions [46]. Specifically, i_r can be expressed as

$$i_r(\mathbf{p}) = \sum_{k=1}^{K} p_k \dot{g}_{\mathbf{x_k}\to\mathbf{r_r}}\,. \tag{5.6}$$

Remark 5.2.1. A set of R (potential) PU receivers are considered and their locations are assumed to be known to the CR network. If the knowledge of $\{\mathbf{r}_r\}_{r=1}^R$ is not directly available, the coverage region of the primary system can be alternatively considered. See chapter 4. With the estimate of the PU coverage region close at hand, the set $\{\mathbf{r}_r\}_{r=1}^R$ may be chosen upon discretizing its boundary. By forcing the interference constraints to be fulfilled on the boundary, it is essentially guaranteed that potential PU receivers are not interfered in the whole PU coverage region. □

If the CR-to-CR channel gains $\{\dot{g}_{\mathbf{x_k}\to\mathbf{u_k}}\}$ as well as the CR-to-PU channel gains $\{\dot{g}_{\mathbf{x_k}\to\mathbf{r_r}}\}$ were perfectly known to the CR network, the optimal transmission power vector $\mathbf{p}$ that maximizes a given network utility without causing harmful interference to the PU system would be obtained by solving

$$\text{(P1)} \qquad \max_{\mathbf{p}\succeq\mathbf{0}} \ \mathcal{U}(\boldsymbol{\gamma}(\mathbf{p})) \tag{5.7}$$

$$\text{subject to } p_k \le p_k^{\max}, \qquad k=1,\ldots,K \tag{5.8}$$

$$i_r(\mathbf{p}) \le i_r^{\max}, \qquad r=1,\ldots,R \tag{5.9}$$

where $i_r^{\max}$ denotes the maximum interference power that can be tolerated by PU receiver r. Problem (P1) is in general non-convex; however, as will be shown later on, a successive convex approximation technique can be employed to obtain a locally optimal solution efficiently [85].

In consistency with the cognitive radio philosophy, *any* sort of collaboration between PU system and CRs is *not* assumed here. As a consequence, the instantaneous gains $\{\dot{g}_{\mathbf{x_k}\to\mathbf{r_r}}\}$ are *not known* at the CR network side and, thus, problem (5.7) can not be actually solved in practice. A naïve tentative to sidestep this hurdle would be to evaluate the linear constraint (5.9) by relying on a crude path loss-only model. Clearly, the solution of (5.7) that would be obtained by merely neglecting the randomness of channels does not guarantee the actual fulfillment of the interference bounds (5.9).

Instead, statistical knowledge of $\{\dot{g}_{\mathbf{x_k}\to\mathbf{r_r}}\}$ may be collected and used. In this case, to protect the PU transmissions under channel uncertainty, probabilistic interference constraints are well motivated. Then, the problem of interest becomes

$$\text{(P2)} \qquad \max_{\mathbf{p}\succ\mathbf{0}} \ \mathcal{U}(\boldsymbol{\gamma}_k(\mathbf{p})) \tag{5.10}$$

$$\text{subject to } p_k \le p_k^{\max}, \qquad k=1,\ldots,K \tag{5.11}$$

$$\Pr\{i_r(\mathbf{p}) > i_r^{\max}\} \le \epsilon_r, \qquad r=1,\ldots,R \tag{5.12}$$

where $\epsilon_r \in (0,1)$ is a prescribed parameter representing the upper-bound on the probability that the interference due to CR transmissions exceeds a given threshold $i_r^{\max}$ at PU receiver r. On top of the non-convexity issue, an additional challenge in solving (P2) is the chance constraint (5.12). A suitable approximation method will be employed in section 5.3 to first address the challenge associated with (5.12).

In addition to the CR-to-PU channel uncertainty, the channel between the CR transceivers may contain uncertainty. Error-corrupted or outdated CG estimates can happen due to, e.g., mobility of the CR nodes or insufficient time for training owing to prolonged PU activity. Or, simply, CR might not want to waste precious primary resources in a cumbersome time-consuming TDMA-based training.

To incorporate CR-to-CR channel uncertainty, the idea pursued here is

to resort to a chance-constrained utility maximization problem encompassing outage probability specification on a per-CR link basis. Define as $\bar{\gamma}_k > 0$ the SINR threshold on the CR link $\mathbf{x}_k \rightarrow \mathbf{u}_k$. Also, denote as $\nu_k \in (0,1)$ a per-CR receiver parameter capping the outage probability. Then, the following $\{\nu_k\}$-outage utility maximization problem is formulated:

$$\text{(P3)} \qquad \max_{\substack{\mathbf{p} \succ \mathbf{0} \\ \bar{\boldsymbol{\gamma}} \succ \mathbf{0}}} \ \mathcal{U}(\bar{\boldsymbol{\gamma}}_k) \tag{5.13}$$

$$\text{subject to } p_k \leq p_k^{\max}, \qquad k = 1, \ldots, K \tag{5.14}$$

$$\Pr\{i_r(\mathbf{p}) > i_r^{\max}\} \leq \epsilon_r, \qquad r = 1, \ldots, R \tag{5.15}$$

$$\Pr\{\gamma_k(\mathbf{p}) < \bar{\gamma}_k\} \leq \nu_k, \qquad k = 1, \ldots, K \tag{5.16}$$

where utility $\mathcal{U}(\cdot)$ is here a function of $\bar{\boldsymbol{\gamma}} := [\bar{\gamma}_1, \ldots, \bar{\gamma}_K]^T$ rather than of $\boldsymbol{\gamma}$. System parameters $\{\nu_k\}$ might be selected a priori according to CR QoS policies.

In section 5.4, a statistical approximation for the SINR will be derived to first address the extra challenge represented by constraint (5.16). Then, (P3) will be re-formulated and a successive GP approximation technique will be employed in order to obtain an optimal (at least locally) solution of the surrogate chance-constrained problem.

5.3 Power Control Under Interference Probability Constraints

In order to solve (P2), the chance constraints (5.12) must be written explicitly in terms of the optimization variable $\mathbf{p}$. As the r.v. i_r involves summation of powers affected by possibly correlated shadow fading and small-scale fading, direct characterization of its distribution will not lead to a tractable optimization formulation. To sidestep this hurdle, the distribution of i_r is first approximated in the sequel.

5.3.1 Approximation of Interference Constraints

As shown in section 3.2, the composite fading $a_{\mathbf{x_k} \rightarrow \mathbf{r_r}}$ can be approximated by a log-Normal density. See [42, Ch. 2], [45]. The overall channel gain

$\dot{g}_{\mathbf{x_k}\to\mathbf{r_r}}$ is thus also approximately log-normal [cf. (3.6)], and the corresponding CG in dB $\dot{G}_{\mathbf{x_k}\to\mathbf{r_r}}$ is approximately Gaussian with mean and variance given by [cf. (3.4), (3.5)]

$$\begin{aligned}\mu_{\dot{G}_{\mathbf{x_k}\to\mathbf{r_r}}} &= \mu_{A_{\mathbf{x_k}\to\mathbf{r_r}}} + G_{0,\mathbf{x_k}\to\mathbf{r_r}} - 10\eta\log_{10}\|\mathbf{x}_k-\mathbf{r}_r\|_2 \\ &= \kappa^{-1}\left(-\ln m - C + \sum_{m'=1}^{m-1}\frac{1}{m'}\right) + \mu_{S_{\mathbf{x_k}\to\mathbf{r_r}}} + G_{0,\mathbf{x_k}\to\mathbf{r_r}} \\ &\quad - 10\eta\log_{10}\|\mathbf{x}_k-\mathbf{r}_r\|_2 \end{aligned} \tag{5.17}$$

and

$$\begin{aligned}\sigma^2_{\dot{G}_{\mathbf{x_k}\to\mathbf{r_r}}} &= \sigma^2_{A_{\mathbf{x_k}\to\mathbf{r_r}}} \\ &= \kappa^{-2}\zeta(2,m) + \sigma^2_{S_{\mathbf{x_k}\to\mathbf{r_r}}}\end{aligned} \tag{5.18}$$

respectively. Also, let

$$\begin{aligned}C_{\dot{G}_{\mathbf{x_k}\to\mathbf{r_r}},\dot{G}_{\mathbf{x_j}\to\mathbf{r_n}}} &:= \mathbb{E}\{(\dot{G}_{\mathbf{x_k}\to\mathbf{r_r}} - \mu_{\dot{G}_{\mathbf{x_k}\to\mathbf{r_r}}})(\dot{G}_{\mathbf{x_j}\to\mathbf{r_n}} - \mu_{\dot{G}_{\mathbf{x_j}\to\mathbf{r_n}}})\} \\ &= \mathbb{E}\{S_{\mathbf{x_k}\to\mathbf{r_r}} S_{\mathbf{x_j}\to\mathbf{r_n}}\}\end{aligned} \tag{5.19}$$

denote the cross-covariance of $\dot{G}_{\mathbf{x_k}\to\mathbf{r_r}}$ and $\dot{G}_{\mathbf{x_j}\to\mathbf{r_n}}$ for $(k,r)\neq(j,n)$. Note that $C_{\dot{G}_{\mathbf{x_k}\to\mathbf{r_r}},\dot{G}_{\mathbf{x_j}\to\mathbf{r_n}}}$ collects the spatial correlation of the only shadow fading, being processes $\{h_{\mathbf{x_k}\to\mathbf{r_r}}\}_{k,m}$ assumed to be mutually uncorrelated.

Thus, the r.v. i_r can be viewed as a sum of (possibly correlated) log-Normal r.v.'s. The statistical characterization of i_r encounters a nuisance difficulty that happen due to a lack of an exact closed form expression for the *pdf* of a sum of correlated log-Normal r.v.'s. However, considerable effort has been devoted to find an accurate statistical approximation for the log-Normal sum and powerful tools have been devised. The Fenton-Wilkinson method [96] and the Schwartz-Yeh method [101] were used to approximate the pdf of a sum of *independent* log-Normal r.v.'s with the pdf of a *single* log-Normal r.v. The matching cumulant approach was also proposed in [102]. The aforementioned approaches were extended to the case of sum of *correlated* lognormal r.v.'s in [97] and their ability in approximating the complementary cumulative distribution function (*c.c.d.f.*) of the resultant random variable with the one of a single log-Normal random variable was

numerically evaluated. The Fenton-Wilkinson method may be the most appealing approach thank to its accuracy over a wide range of parameters that are of practical interest [97] and the low computational effort required to get close-form expressions for mean and variance of the resultant approximated log-Normal process. Henceforth, it will be considered here to get statistical characterization of i_r. It is worth mentioning that the approach presented in [103] may have superior accuracy than the Fenton-Wilkinson but, unfortunately, might be too complex for the optimization framework proposed here.

Define as $I_r := 10 \cdot \log_{10} i_r$ the instantaneous aggregate interference perceived at PU receiver r in dB. Note that each single interferer $I_{r,k} := 10 \cdot \log_{10}(p_k \dot{g}_{\mathbf{x_k} \to \mathbf{r_r}})$, $k \in \{1, \ldots, K\}$, is Gaussian with mean $P_k + \mu_{\dot{G}_{\mathbf{x_k} \to \mathbf{r_r}}}$ and variance $\sigma^2_{\dot{G}_{\mathbf{x_k} \to \mathbf{r_r}}}$, where $P_k := 10 \cdot \log_{10} p_k$. Retracing the Fenton-Wilkinson method, first rewrite (5.6) as

$$i_r = \sum_{k=1}^{K} e^{\kappa I_{r,k}} \tag{5.20}$$

and then, to approximate i_r in (5.6) with a single log-Normal random variable $\tilde{i}_r$, set

$$\sum_{k=1}^{K} e^{\kappa I_{r,k}} \cong e^{\kappa \tilde{I}_r} \tag{5.21}$$

where $\tilde{I}_r := 10 \cdot \log_{10} \tilde{i}_r$ is the Gaussian random variable that approximates I_r. Denote as $\mu_{\tilde{I}_r}$ and $\sigma^2_{\tilde{I}_r}$ the mean and the variance of $\tilde{I}_r$, respectively. By matching the first two moments of i_r and $e^{\kappa \tilde{I}_r}$ one can readily get a close form expression for $\mu_{\tilde{I}_r}$ and $\sigma^2_{\tilde{I}_r}$. Setting $\mathbb{E}\{e^{\kappa \tilde{I}_r}\} = \mathbb{E}\{i_r\}$ gives (cf. (5.20))

$$\begin{aligned} e^{\kappa \mu_{\tilde{I}_r} + \frac{\kappa^2}{2} \sigma^2_{\tilde{I}_r}} &= \sum_{k=1}^{K} e^{\kappa P_k + \kappa \mu_{\dot{G}_{\mathbf{x_k} \to \mathbf{r_r}}} + \frac{\kappa^2}{2} \sigma^2_{\dot{G}_{\mathbf{x_k} \to \mathbf{r_r}}}} \\ &= \sum_{k=1}^{K} p_k e^{\kappa \mu_{\dot{G}_{\mathbf{x_k} \to \mathbf{r_r}}} + \frac{\kappa^2}{2} \sigma^2_{\dot{G}_{\mathbf{x_k} \to \mathbf{r_r}}}} \end{aligned} \tag{5.22}$$

where the identity $\kappa P_k = \ln p_k$ was used to get (5.22). Matching the second

moment, i.e., setting $\mathbb{E}\{e^{2\kappa\tilde{I}_r}\} = \mathbb{E}\{i_r^2\}$, one obtains

$$\begin{aligned} e^{2\kappa\mu_{\tilde{I}_r}+2\kappa^2\sigma^2_{\tilde{I}_r}} &= \sum_{k=1}^{K} e^{2\kappa P_k+2\kappa\mu_{\dot{G}_{\mathbf{x_k}\to\mathbf{r_r}}}+2\kappa^2\sigma^2_{\dot{G}_{\mathbf{x_k}\to\mathbf{r_r}}}} + \\ &\quad + 2\sum_{k=1}^{K-1}\sum_{i=k+1}^{K} e^{\kappa P_k+\kappa\mu_{\dot{G}_{\mathbf{x_k}\to\mathbf{r_r}}}+\kappa P_i+\kappa\mu_{\dot{G}_{\mathbf{x_i}\to\mathbf{r_r}}}} \\ &\quad \cdot e^{\frac{\kappa^2}{2}(\sigma^2_{\dot{G}_{\mathbf{x_k}\to\mathbf{r_r}}}+\sigma^2_{\mathbf{x_i}\to\mathbf{r_r}}+2C_{\dot{G}_{\mathbf{x_k}\to\mathbf{r_r}},\dot{G}_{\mathbf{x_i}\to\mathbf{r_r}}})} \\ &= \sum_{k=1}^{K} p_k^2 e^{2\kappa\mu_{\dot{G}_{\mathbf{x_k}\to\mathbf{r_r}}}+2\kappa^2\sigma^2_{\dot{G}_{\mathbf{x_k}\to\mathbf{r_r}}}} + \\ &\quad + 2\sum_{k=1}^{K-1}\sum_{i=k+1}^{K} p_k p_i e^{\kappa\mu_{\dot{G}_{\mathbf{x_k}\to\mathbf{r_r}}}+\kappa\mu_{\dot{G}_{\mathbf{x_i}\to\mathbf{r_r}}}} \\ &\quad \cdot e^{\frac{\kappa^2}{2}(\sigma^2_{\dot{G}_{\mathbf{x_k}\to\mathbf{r_r}}}+\sigma^2_{\dot{G}_{\mathbf{x_i}\to\mathbf{r_r}}}+2C_{\dot{G}_{\mathbf{x_k}\to\mathbf{r_r}},\dot{G}_{\mathbf{x_i}\to\mathbf{r_r}}})}. \end{aligned} \tag{5.23}$$

The system of equations (5.22)-(5.23) can now be solved for $\mu_{\tilde{I}_r}$ and $\sigma^2_{\tilde{I}_r}$. Upon defining the following real and positive quantities

$$a_{r,k} := e^{\kappa\mu_{\dot{G}_{\mathbf{x_k}\to\mathbf{r_r}}}+\frac{\kappa^2}{2}\sigma^2_{\dot{G}_{\mathbf{x_k}\to\mathbf{r_r}}}} \tag{5.24}$$

$$b_{r,k} := e^{2\kappa\mu_{\dot{G}_{\mathbf{x_k}\to\mathbf{r_r}}}+2\kappa^2\sigma^2_{\dot{G}_{\mathbf{x_k}\to\mathbf{r_r}}}} \tag{5.25}$$

$$b'_{r,k,i} := e^{\kappa\mu_{\dot{G}_{\mathbf{x_k}\to\mathbf{r_r}}}+\kappa\mu_{\dot{G}_{\mathbf{x_i}\to\mathbf{r_r}}}} e^{\frac{\kappa^2}{2}(\sigma^2_{\dot{G}_{\mathbf{x_k}\to\mathbf{r_r}}}+\sigma^2_{\dot{G}_{\mathbf{x_i}\to\mathbf{r_r}}}+2C_{\dot{G}_{\mathbf{x_k}\to\mathbf{r_r}},\dot{G}_{\mathbf{x_i}\to\mathbf{r_r}}})} \tag{5.26}$$

it can be shown that mean and variance of $\tilde{I}_r$ are given by

$$\mu_{\tilde{I}_r} = \kappa^{-1}\ln\left(\frac{\xi_{I_r,1}}{\xi^{1/2}_{I_r,2}}\right) \tag{5.27}$$

and

$$\sigma^2_{\tilde{I}_r} = \kappa^{-2}\ln\left(\frac{\xi_{I_r,2}}{\xi_{I_r,1}}\right) \tag{5.28}$$

with

$$\xi_{I_r,1} := \left(\sum_{k=1}^{K} p_k a_{r,k}\right)^2 \tag{5.29}$$

$$\xi_{I_r,2} := \sum_{k=1}^{K} p_k^2 b_{r,k} + 2\sum_{k=1}^{K-1}\sum_{i=k+1}^{K} p_k p_i b'_{r,k,i} \tag{5.30}$$

respectively. Thus, given the first- and the second-order statistics of the shadow fading processes in dB scale, and the m parameter of the Nakagami-m-distributed small-scale fading, the distribution of the dB-scale interference powers $\{I_r\}$ at PU locations $\{\mathbf{r}_r\}$ can be approximated as Gaussian with mean and variance given in terms of the optimization variable $\mathbf{p}$.

Based on the foregoing discussion, and with $I_r^{\max} := 10\log_{10} i_r^{\max}$, the interference constraints (5.12) can be approximated by

$$\begin{aligned}\Pr\left\{\tilde{i}_r(\mathbf{p}) > i_r^{\max}\right\} &= \Pr\left\{e^{\kappa\tilde{I}_r(\mathbf{p})} > i_r^{\max}\right\} \\ &= \Pr\left\{\tilde{I}_r(\mathbf{p}) > I_r^{\max}\right\} \\ &= Q\left(\frac{I_r^{\max} - \mu_{\tilde{I}_r}(\mathbf{p})}{\sigma_{\tilde{I}_r}(\mathbf{p})}\right) \end{aligned} \tag{5.31}$$

where $Q(x) := \int_x^\infty \frac{1}{\sqrt{2\pi}} e^{-\frac{t^2}{2}} dt$ is the standard Gaussian tail function. Constraints (5.31) can be equivalently written as

$$\mu_{\tilde{I}_r}(\mathbf{p}) + Q^{-1}(\epsilon_r)\sigma_{\tilde{I}_r}(\mathbf{p}) \leq I_r^{\max}, \quad r = 1, 2, \ldots, R. \tag{5.32}$$

Next, (P2) with (5.12) replaced by (5.32) will be tackled by employing a successive convex approximation method.

5.3.2 Problem re-formulation

Plugging (5.27)-(5.28) directly into (5.32) does not lead to a tractable formulation. Instead, upon introducing a set of positive auxiliary variables $\mathbf{z}_r := [z_{r,1}, z_{r,2}]^T$, $r = 1, 2, \ldots, R$, the following set of constraints equivalent to (5.32) is considered:

$$\mu_{\tilde{I}_r}(\mathbf{p}) \leq \ln(z_{r,1}), \quad r = 1, \ldots, R \tag{5.33}$$

$$\sigma^2_{\tilde{I}_r}(\mathbf{p}) \leq \ln(z_{r,2}), \quad r = 1, \ldots, R \tag{5.34}$$

$$\phi_r(\mathbf{z}_r) := \ln(z_{r,1}) + Q^{-1}(\epsilon_r)\sqrt{\ln(z_{r,2})} - I_r^{\max} \leq 0, \quad r = 1, \ldots, R. \tag{5.35}$$

Using (5.27)-(5.28), it is possible to express after some manipulations (5.33) and (5.34) as the following ratios of posynomials

$$\frac{\xi_{I_r,1}^2(\mathbf{p})}{\xi_{I_r,2}(\mathbf{p})z_{r,1}^{2\kappa}} \leq 1, \quad r = 1, \ldots, R \tag{5.36}$$

$$\frac{\xi_{I_r,2}(\mathbf{p})}{\xi_{I_r,1}(\mathbf{p})z_{r,2}^{\kappa^2}} \leq 1, \quad r = 1, \ldots, R\,. \tag{5.37}$$

The objective functions also need to be re-formulated. Next, convenient surrogates for the utility functions listed in section 5.2 are derived.

i) *(Weighted) Sum-rate utility.* Maximizing the sum-rate (5.2) is equivalent to minimizing the function $\prod_{k=1}^{K}(1+\gamma_k(\mathbf{p}))^{-w_k}$. Then, upon introducing auxiliary variables $\mathbf{t} := [t_1, \ldots, t_K]^T \succ \mathbf{0}$, minimization of

$$\mathcal{U}'(\mathbf{t}) = \prod_{k=1}^{K} t_k^{w_k} \tag{5.38}$$

with the extra constraints

$$\xi_{\mathcal{U},k}(\mathbf{p},\mathbf{t}) = \frac{\sum_{i=1,i\neq k}^{K} p_k \dot{g}_{\mathbf{x_i}\to\mathbf{u_k}} + \dot{\pi}_k + \sigma_k^2}{\sum_{i=1}^{K} p_k \dot{g}_{\mathbf{x_i}\to\mathbf{u_k}} + \dot{\pi}_k + \sigma_k^2}\, t_k^{-1} \leq 1, \quad k = 1, \ldots, K \tag{5.39}$$

yields maximization of the network (weighted) sum-rate.

ii) *Proportional fair utility.* Maximization of utility (5.3) is attained in an equivalent manner by minimizing $\sum_{k=1}^{K} -\log_2(\log_2(1+\gamma_k(\mathbf{p})))$ and, hence, function $\prod_{k=1}^{K}(\log_2(1+\gamma_k(\mathbf{p}))^{-1}$. Next, consider approximation [104]

$$\ln(x) \approx a(x^{1/a} - 1), \quad x > 0 \tag{5.40}$$

with $a \gg 1$. Using (5.40) and employing auxiliary variables $\mathbf{t}$, yield the following utility

$$\mathcal{U}'(\mathbf{t}) = \prod_{k=1}^{K} t_k \tag{5.41}$$

which has to be minimized, with the K associated extra constraints [cf. (5.1)]:

$$\xi_{\mathcal{U},k}(\mathbf{p},\mathbf{t}) = (1+t_k^{-1})^a \frac{\sum_{i=1,i\neq k}^{K} p_k \dot{g}_{\mathbf{x_i}\to\mathbf{u_k}} + \dot{\pi}_k + \sigma_k^2}{\sum_{i=1}^{K} p_k \dot{g}_{\mathbf{x_i}\to\mathbf{u_k}} + \dot{\pi}_k + \sigma_k^2} \leq 1\,. \tag{5.42}$$

iii) *Harmonic-rate utility.* Consider minimizing function $\sum_{k=1}^{K} \frac{1}{\log(1+\gamma_k(\mathbf{p}))}$. Making use of (5.40) and, again, employing auxiliary variables $\mathbf{t}$, maximization of the harmonic-rate utility can be achieved by minimizing

$$\mathcal{U}'(\mathbf{t}) = \sum_{k=1}^{K} t_k \tag{5.43}$$

under constraints (5.42).

iv) *Min-rate utility.* Note, first, that maximization of (5.5) and minimization of the cost $\max_k \frac{1}{1+\gamma_k(\mathbf{p})}$ are equivalent. Then, upon introducing a real auxiliary variable $t > 0$, maximization of (5.5) can be equivalently attained by minimizing utility

$$\mathcal{U}'(t) = t \tag{5.44}$$

under the K extra constraints expressed by means of rational functions of posynomials [cf. (5.1)]

$$\xi_{\mathcal{U},k}(\mathbf{p}, t) = \frac{\sum_{i=1, i\neq k}^{K} p_k \dot{g}_{\mathbf{x_i}\to\mathbf{u_k}} + \dot{\pi}_k + \sigma_k^2}{\sum_{i=1}^{K} p_k \dot{g}_{\mathbf{x_i}\to\mathbf{u_k}} + \dot{\pi}_k + \sigma_k^2} t^{-1} \leq 1, \quad k = 1, \ldots, K. \tag{5.45}$$

Based on the preceding discussion, the surrogate problem for (P2) that is to be solved here becomes

$$\text{(P2b)} \qquad \min_{\mathbf{p}\succ\mathbf{0}, \{\mathbf{z}_r\succ\mathbf{0}\}, \mathbf{t}\succ\mathbf{0}} \mathcal{U}'(\mathbf{t}) \tag{5.46}$$

$$\text{subject to } \xi_{\mathcal{U},k}(\mathbf{p}, \mathbf{t}) \leq 1, \qquad k = 1, \ldots, K \tag{5.47}$$

$$p_k \leq p_k^{\max}, \qquad k = 1, \ldots, K \tag{5.48}$$

$$\frac{\xi_{I_r,1}^2(\mathbf{p})}{\xi_{I_r,2}(\mathbf{p}) z_{r,1}^{2\kappa}} \leq 1, \qquad r = 1, \ldots, R \tag{5.49}$$

$$\frac{\xi_{I_r,2}(\mathbf{p})}{\xi_{I_r,1}(\mathbf{p}) z_{r,2}^{\kappa^2}} \leq 1, \qquad r = 1, \ldots, R \tag{5.50}$$

$$\phi_r(\mathbf{z}_r) \leq 0, \qquad r = 1, \ldots, R. \tag{5.51}$$

Problem (P2b) involves constraints expressed as ratio-of-posynomials in (5.47) and (5.49)–(5.50), which are in general non-convex. Another manifest source of non-convexity is (5.51).

Thus, a globally optimal solution of (P2b) is in general difficult to obtain. Recall nonetheless that this is true even for the case of perfect channel knowledge in (P1) [85]. Therefore, we resort to a successive convex approximation method to obtain (at least locally) optimal solutions [105]. Remarkably, it can be shown that this approach boils down to sequential GP as in the *perfect* channel knowledge case [85].

5.3.3 Successive Convex Approximation

Here, the general successive convex approximation method is briefly described [105]. Consider an optimization problem

$$\min_{\mathbf{p}\in\mathcal{P}} f_0(\mathbf{p}) \tag{5.52}$$

$$\text{subject to } f_k(\mathbf{p}) \leq 0, \quad k = 1, 2, \ldots, K \tag{5.53}$$

where $f_0(\mathbf{p})$ is convex and differentiable, $f_k(\mathbf{p})$, $k = 1, \ldots, K$, are differentiable functions, and the feasible region $\mathcal{F} := \{\mathbf{p} \in \mathcal{P} | f_k(\mathbf{p}) \leq 0, k = 1, \ldots, K\}$ is compact[3]. Then, starting from a feasible point $\mathbf{p}^{(0)} \in \mathcal{F}$, a series of approximate problems is solved to locate a KKT point of the original (non-convex) problem. For each $k = 1, \ldots, K$, let $\tilde{f}_k(\mathbf{p}; \mathbf{p}^{(j)})$ denote the surrogate function for $f_k(\mathbf{p})$, which may depend on the solution $\mathbf{p}^{(j)}$ to the problem of the (previous) $(j-1)$-st iteration. The approximate problem to solve per iteration j is

$$\min_{\mathbf{p}\in\mathcal{P}} f_0(\mathbf{p}) \tag{5.54}$$

$$\text{subject to } \tilde{f}_k(\mathbf{p}; \mathbf{p}^{(j)}) \leq 0, \quad k = 1, 2, \ldots, K \tag{5.55}$$

and its feasible region is denoted by $\mathcal{F}^{(j)}$. Provided that $\tilde{f}_k(\mathbf{p}; \mathbf{p}^{(j)})$ satisfies the following conditions

c1) $f_k(\mathbf{p}) \leq \tilde{f}_k(\mathbf{p}; \mathbf{p}^{(j)}), \quad \forall \mathbf{p} \in \mathcal{F}^{(j)}$

c2) $f_k(\mathbf{p}^{(j)}) = \tilde{f}_k(\mathbf{p}^{(j)}; \mathbf{p}^{(j)})$

[3]If function $f_0(\mathbf{p})$ is non-convex, the objective function can be moved to the constraints by introducing an auxiliary scalar variable q and writing $\min_{\mathbf{p}\in\mathcal{P},q} q$ subject to the additional constraint $f_0(\mathbf{p}) \leq q$.

c3) $\nabla f_k(\mathbf{p}^{(j)}) = \nabla \tilde{f}_k(\mathbf{p}^{(j)}; \mathbf{p}^{(j)})$

for each $k = 1, \ldots, K$, the series of solutions to the approximate problems converge to the KKT point of the original problem.

5.3.4 Sequential GP

In order to apply the successive convex approximation method to (P2b), appropriate surrogate constraints for the non-convex constraints need to be determined.

The single condensation method [106] can be effectively used to cope with the non-convexity of constraints expressed by means of a rational function of posynomials. Such method entails the approximation of the posynomial at the denominator with a monomial, leading to a constraint in posynomial form[4]. Let $\frac{n(\mathbf{p})}{d(\mathbf{p})}$, with $n(\mathbf{p}) = \sum_i n_i(\mathbf{p})$ and $d(\mathbf{p}) = \sum_i d_i(\mathbf{p})$, be a rational function of posynomials. Then, exploiting the arithmetic-geometric mean inequality, the best local monomial approximation of $d(\mathbf{p})$ around a point $\mathbf{p}^{(j)}$ in the sense of first order Taylor approximation reads

$$d(\mathbf{p}) \leq \tilde{d}(\mathbf{p}; \mathbf{p}^{(j)}) = \prod_i \left(\frac{d_i(\mathbf{p})}{\alpha_i} \right)^{\alpha_i} \tag{5.56}$$

with

$$\alpha_i := \frac{d_i(\mathbf{p}^{(j)})}{\sum_l d_l(\mathbf{p}^{(j)})} \,. \tag{5.57}$$

Then, a constraint given by

$$\frac{\sum_i n_i(\mathbf{p})}{\sum_i d_i(\mathbf{p})} \leq 1 \tag{5.58}$$

can be is approximated as

$$\frac{\sum_i n_i(\mathbf{p})}{\prod_i \left(\frac{d_i(\mathbf{p})}{\alpha_i} \right)^{\alpha_i}} \leq 1 \,. \tag{5.59}$$

By viewing the left hand side of (5.58) and (5.59) as $f_k(\mathbf{p})$ and $\tilde{f}_k(\mathbf{p}; \mathbf{p}^{(j)})$, respectively, it can be readily shown that they satisfy conditions **c1)**–**c3)** in Sec. 5.3.3 [85].

[4] A posynomial divided by a monomial is a posynomial.

To handle the non-convexity in (5.51), it is first noted that $\phi_r(\mathbf{z}_r)$ is a concave function for $\mathbf{z}_r \succ \mathbf{0}$, which can be easily verified by examining the second-order derivatives of each term [cf. (5.35)], and recalling that the sum of concave functions is concave. Thus, an upper-bound of $\phi_r(\mathbf{z}_r)$ that satisfies **c1)**–**c3)** can be obtained via the supporting hyperplane as

$$\tilde{\phi}_r(\mathbf{z}_r; \mathbf{z}_r^{(j)}) := \frac{z_{r,1}}{z_{r,1}^{(j)}} + \frac{Q^{-1}(\epsilon_r) z_{r,2}}{2 z_{r,2}^{(j)} \sqrt{\ln z_{r,2}^{(j)}}} - c_r(\mathbf{z}_r^{(j)}) \tag{5.60}$$

$$c_r(\mathbf{z}_r^{(j)}) := 1 + \frac{Q^{-1}(\epsilon_r)}{2\sqrt{\ln z_{r,2}^{(j)}}} - \phi_r(\mathbf{z}_r^{(j)}). \tag{5.61}$$

It is apparent from (5.61) and (5.51) that $c_r(\mathbf{z}_r^{(j)}) > 0$ provided that $\mathbf{z}_r^{(j)}$ is a feasible point, and $\epsilon_r < 0.5$. Therefore, a surrogate constraint for (5.51) is

$$\frac{1}{c_r(\mathbf{z}_r^{(j)})} \tilde{\phi}'_r(\mathbf{z}_r; \mathbf{z}_r^{(j)}) \leq 1, \quad r = 1, \ldots, R. \tag{5.62}$$

with

$$\tilde{\phi}'_r(\mathbf{z}_r; \mathbf{z}_r^{(j)}) := \frac{z_{r,1}}{z_{r,1}^{(j)}} + \frac{Q^{-1}(\epsilon_r) z_{r,2}}{2 z_{r,2}^{(j)} \sqrt{\ln z_{r,2}^{(j)}}}\,. \tag{5.63}$$

The left hand side is affine, and thus it is a posynomial.

Overall, the successive approximation algorithm consists in solving at the j-th iteration the following problem:

$$(\mathrm{P2b}^{(j)}) \qquad \min_{\mathbf{p} \succ \mathbf{0}, \{\mathbf{z}_r \succ \mathbf{0}\}, \mathbf{t} \succ \mathbf{0}} \mathcal{U}'(\mathbf{p}, \mathbf{t}) \tag{5.64}$$

$$\text{subject to } \tilde{\xi}_{\mathcal{U},k}(\mathbf{p}, \mathbf{t}; \mathbf{p}^{(j-1)}, \mathbf{t}^{(j-1)}) \leq 1, \qquad k = 1, \ldots, K \tag{5.65}$$

$$p_k \leq p_k^{\max}, \qquad k = 1, \ldots, K \tag{5.66}$$

$$\frac{\xi_{I_r,1}^2(\mathbf{p})}{\tilde{\xi}_{I_r,2}(\mathbf{p}; \mathbf{p}^{(j-1)}) z_{r,1}^{2\kappa}} \leq 1, \qquad r = 1, \ldots, R \tag{5.67}$$

$$\frac{\xi_{I_r,2}(\mathbf{p})}{\tilde{\xi}_{I_r,1}(\mathbf{p}; \mathbf{p}^{(j-1)}) z_{r,2}^{\kappa^2}} \leq 1, \qquad r = 1, \ldots, R \tag{5.68}$$

$$\frac{1}{c_r(\mathbf{z}_r^{(j)})} \tilde{\phi}'_r(\mathbf{z}_r; \mathbf{z}_r^{(j)}) \leq 1, \qquad r = 1, \ldots, R. \tag{5.69}$$

with $\mathbf{p}^{(j-1)}, \{\mathbf{z}_r^{(j-1)}\}, \mathbf{t}^{(j-1)}$ the solution of (P2b$^{(j-1)}$), (5.65) and (5.67)–(5.68) computed by using the single condensation method, and (5.69) given by (5.62).

Proposition 5.3.1. *Given an initial feasible starting point* $\mathbf{p}^{(0)}, \{\mathbf{z}_r^{(0)}\}$, $\mathbf{t}^{(0)}$, *the sequence* $\mathbf{p}^{(j)}, \{\mathbf{z}_r^{(j)}\}$, $\mathbf{t}^{(j)} j = 1, 2, \ldots$ *converges to a KKT point of (P2b).*

Proof: see [105, Theorem 1]. □

It is immediate that this problem is a GP problem, which involves minimizing a posynomial subject to posynomial inequality constraints. GP problems can be solved efficiently through optimized interior-point methods [98, Ch. 11]. Although GP problems are not convex in their original form, their globally optimal solution can be obtained by convex re-formulation through a log change of variables [104].

Remark 5.3.2. From a practical perspective, the sequential GP algorithm requires a stopping criterion. Upon defining an error tolerance $\upsilon > 0$, a simple stopping rule may consist in checking whether condition $\mathcal{U}'(\mathbf{t}^{(j-1)}) - \mathcal{U}'(\mathbf{t}^{(j)}) \leq \upsilon$ is satisfied at each iteration. □

5.3.5 Addressing Power Consumption Concerns

Hardware limitations or battery consumption concerns may invoke a trade off between network utility maximization and transmission power limitation. Denote first as $\mathcal{C}(\mathbf{p})$ a cost inherent to the CR transmission power $\mathbf{p}$ that would be spent. To limit the power consumption, it would be desirable to minimize $\mathcal{C}(\mathbf{p})$. As an example, $\mathcal{C}(\mathbf{p})$ can be simply set to [83]

$$\mathcal{C}(\mathbf{p}) = \|\mathbf{p}\|_1 = \sum_{k=1}^{K} p_k \,. \tag{5.70}$$

Then, a joint power minimization and utility maximization of a given network utility $\mathcal{U}(\mathbf{p})$ can be attained by setting in (P2) the following objective function

$$\check{\mathcal{U}}(\mathbf{p}) = \epsilon\, \mathcal{C}(\mathbf{p}) - (1-\epsilon)\, \mathcal{U}(\mathbf{p}) \;, \tag{5.71}$$

which has to be minimized, with $\epsilon \in [0, 1)$ a pre-determined CR system parameter. In (P2b), the objective function amounts to

$$\check{\mathcal{U}}'(\mathbf{p}) = \epsilon\, \mathcal{C}(\mathbf{p}) - (1-\epsilon)\, \mathcal{U}'(\mathbf{p}) \;, \tag{5.72}$$

with the additional auxiliary constraints, depending on the specific utility considered.

If a pure power minimization is targeted [83], [90], i.e., if ϵ would be set to 1, a constraint imposing a minimum value for $\mathcal{U}(\mathbf{p})$ has to added to (P2) (a minimum value for $\mathcal{U}'(\mathbf{p})$ in (P2b), respectively). As an example, minimum per-link rate requirements can be set.

5.4 Extensions to Uncertain CR-to-CR Channels

Fast variations of the CR environment, insufficient time for training owing to prolonged PU activity, or difficulty in acquiring instantaneous channel power estimates lead to uncertain CR-to-CR CGs. Problem (P3) addresses the consequent difficulties in evaluating the actual SINRs by considering network utilities that depends on the outage thresholds; CR-to-CR CG uncertainty is incorporated by explicitly adding outage probability constraints on a per-CR link basis. Clearly, interference constraints enforcing protection of the PU system are still present.

In section 5.3.2 a Gaussian approximation for $\{I_r\}$ was derived and a proper re-formulation of interference constraints (5.15) was obtained in order to solve (P2). Likewise, here the solution of (P3) is approached by re-writing the outage constraints (5.16) in terms of the optimization variables $\mathbf{p}$ and $\bar{\boldsymbol{\gamma}}$. To this end, a suitable approximation for r.v.'s $\{\gamma_k\}$ is devised next.

Remark 5.4.1. Upon disabling the constraints on the probability of interference, problem (P3) - and, thus (P3b) - may find a place in the ad hoc network context as well. Compared to prior works, see, e.g. [83], [85], [87], the attracting feature of (P3) consists in the possibility of obtaining the powers $\mathbf{p}$ maximizing $\mathcal{U}(\mathbf{p})$ in either a channel-agnostic setup (if channel gain maps are not used) or a semi channel-agnostic (if shadowing is estimated) way. In the first case, only information about receivers' locations is needed and, thus, extensive any-to-any channel gain measurement is avoided. Note that updates of the transmission powers can be carried out at a time scale that is way larger than the coherence time of the fast-time varying small-scale fading; precisely, an update is needed every time that the location of either a transmitter or a receiver is changed. In the second case, the problem

inherent to the use of outdated estimates of the (instantaneous) channels is sidestepped; in fact, since the estimate of average CG is contained in the CG maps used, power updates can be carried out at a time scale of the shadow fading rather than of the small-scale fading. □

5.4.1 Approximation of the Distribution of SINRs

Express first γ_k^{-1} as

$$\gamma_k^{-1} = \sum_{j=1, j\neq k}^{K} p_k^{-1} p_j \dot{g}^{-1}_{\mathbf{x_k}\to\mathbf{u_k}} \dot{g}_{\mathbf{x_j}\to\mathbf{u_k}} + p_k^{-1} \dot{g}^{-1}_{\mathbf{x_k}\to\mathbf{u_k}} (\dot{\pi}_k + \sigma^2_{w,k}) \,. \tag{5.73}$$

and notice that $\{p_k^{-1} p_j \dot{g}^{-1}_{\mathbf{x_k}\to\mathbf{u_k}} \dot{g}_{\mathbf{x_i}\to\mathbf{u_k}}\}$ and $p_k^{-1} \dot{g}^{-1}_{\mathbf{x_k}\to\mathbf{u_k}}$ are still log-Normal. Specifically, using lemmas 5.7.1 and 5.7.2 in Appendix 5.7, one can show that

$$\begin{aligned} p_k^{-1} p_j \dot{g}^{-1}_{\mathbf{x_k}\to\mathbf{u_k}} \dot{g}_{\mathbf{x_j}\to\mathbf{u_k}} \sim \\ log\mathcal{N}\Big(-P_k + P_j - \mu_{\dot{G}_{\mathbf{x_k}\to\mathbf{u_k}}} + \mu_{\dot{G}_{\mathbf{x_j}\to\mathbf{u_k}}}, \\ \sigma^2_{\dot{G}_{\mathbf{x_j}\to\mathbf{u_k}}} + \sigma^2_{\dot{G}_{\mathbf{x_k}\to\mathbf{u_k}}} - 2C_{\dot{G}_{\mathbf{x_k}\to\mathbf{u_k}}, \dot{G}_{\mathbf{x_j}\to\mathbf{u_k}}} \Big) \end{aligned} \tag{5.74}$$

and, as a sub-case of (5.74),

$$\begin{aligned} p_k^{-1} \dot{g}^{-1}_{\mathbf{x_k}\to\mathbf{u_k}} (\dot{\pi}_k + \sigma^2_{w,k}) \sim \\ log\mathcal{N}\Big(-P_k - \mu_{\dot{G}_{\mathbf{x_k}\to\mathbf{u_k}}} + 10\log_{10}(\dot{\pi}_k + \sigma^2_{w,k}), \sigma^2_{\dot{G}_{\mathbf{x_k}\to\mathbf{u_k}}} \Big) \end{aligned} \tag{5.75}$$

The r.v. γ_k^{-1} thus involves summation of correlated log-Normal r.v.'s. Again, the Fenton-Wilkinson method can be employed to find a log-Normal approximation for r.v. γ_k^{-1} and, thus, for r.v. γ_k (see lemma (5.7.1)). Let $\Gamma_k := 10\log_{10}\gamma_k$ be the SINR at CR receiver k in dB, and consider a Gaussian r.v. $\tilde{\Gamma}_k := 10\log_{10}\tilde{\gamma}_k$ with mean $\mu_{\tilde{\Gamma}_k}$ and variance $\sigma^2_{\tilde{\Gamma}_k}$. By matching the first two moments of γ_k^{-1} and $\tilde{\gamma}_k^{-1} = e^{-\kappa\tilde{\Gamma}_k}$, one can establish (see, also, lemma (5.7.1))

$$\mu_{\tilde{\Gamma}_k} := \kappa^{-1} \ln\left(\frac{\xi^{1/2}_{\tilde{\Gamma}_k,2}}{\xi_{\tilde{\Gamma}_k,1}} \right) \tag{5.76}$$

$$\sigma^2_{\tilde{\Gamma}_k} := \kappa^{-2} \ln\left(\frac{\xi_{\tilde{\Gamma}_k,2}}{\xi_{\tilde{\Gamma}_k,1}} \right) \tag{5.77}$$

where

$$\xi_{\tilde{\Gamma}_k,1} := \left(\sum_{j=1,j\neq k}^{K} p_k^{-1} p_j \alpha_{k,j} + p_k^{-1} \alpha_{k,K+1} \right)^2 \tag{5.78}$$

$$\begin{aligned} \xi_{\tilde{\Gamma}_k,2} :=& \sum_{\substack{j=1 \\ j\neq k}}^{K} p_k^{-2} p_j^2 \beta_{k,j} + p_k^{-2} \beta_{k,K+1} + 2 \sum_{\substack{j=1 \\ j\neq k}}^{K-1} \sum_{\substack{i=j+1 \\ i\neq k}}^{K} p_k^{-2} p_j p_i \beta'_{k,j,i} \\ &+ 2 \sum_{\substack{j=1 \\ j\neq k}}^{K-1} p_k^{-2} p_j \beta''_{k,j,K+1} \end{aligned} \tag{5.79}$$

and

$$\begin{aligned} \alpha_{k,j} :=& e^{\kappa\left(\mu_{\dot{G}_{\mathbf{x_j}\to\mathbf{u_k}}} - \mu_{\dot{G}_{\mathbf{x_k}\to\mathbf{u_k}}}\right)} \cdot \\ & \cdot e^{\frac{\kappa^2}{2}\left(\sigma^2_{\dot{G}_{\mathbf{x_j}\to\mathbf{u_k}}} + \sigma^2_{\dot{G}_{\mathbf{x_k}\to\mathbf{u_k}}} - 2C_{\dot{G}_{\mathbf{x_j}\to\mathbf{u_k}},\dot{G}_{\mathbf{x_k}\to\mathbf{u_k}}}\right)} \end{aligned} \tag{5.80}$$

$$\alpha_{k,K+1} := (\dot{\pi}_k + \sigma^2_{w,k}) e^{-\kappa\mu_{\dot{G}_{\mathbf{x_k}\to\mathbf{u_k}}} + \frac{\kappa^2}{2}\sigma^2_{\dot{G}_{\mathbf{x_k}\to\mathbf{u_k}}}} \tag{5.81}$$

$$\begin{aligned} \beta_{k,j} :=& e^{2\kappa\left(\mu_{\dot{G}_{\mathbf{x_j}\to\mathbf{u_k}}} - \mu_{\dot{G}_{\mathbf{x_k}\to\mathbf{u_k}}}\right)} \cdot \\ & \cdot e^{2\kappa^2\left(\sigma^2_{\dot{G}_{\mathbf{x_j}\to\mathbf{u_k}}} + \sigma^2_{\dot{G}_{\mathbf{x_k}\to\mathbf{u_k}}} - 2C_{\dot{G}_{\mathbf{x_j}\to\mathbf{u_k}},\dot{G}_{\mathbf{x_k}\to\mathbf{u_k}}}\right)} \end{aligned} \tag{5.82}$$

$$\beta_{k,K+1} := (\dot{\pi}_k + \sigma^2_{w,k})^2 e^{-2\kappa\mu_{\dot{G}_{\mathbf{x_k}\to\mathbf{u_k}}} + 2\kappa^2\sigma^2_{\dot{G}_{\mathbf{x_k}\to\mathbf{u_k}}}} \tag{5.83}$$

$$\begin{aligned} \beta'_{k,j,i} :=& e^{\kappa\left(\mu_{\dot{G}_{\mathbf{x_j}\to\mathbf{u_k}}} + \mu_{\dot{G}_{\mathbf{x_i}\to\mathbf{u_k}}} - 2\mu_{\dot{G}_{\mathbf{x_k}\to\mathbf{u_k}}}\right)} \cdot \\ & \cdot e^{\frac{\kappa^2}{2}\left(\sigma^2_{\dot{G}_{\mathbf{x_j}\to\mathbf{u_k}}} + \sigma^2_{\dot{G}_{\mathbf{x_i}\to\mathbf{u_k}}} + 4\sigma^2_{\dot{G}_{\mathbf{x_k}\to\mathbf{u_k}}} - 4C_{\dot{G}_{\mathbf{x_j}\to\mathbf{u_k}},\dot{G}_{\mathbf{x_k}\to\mathbf{u_k}}} - \right.} \\ & \left. - 4C_{\dot{G}_{\mathbf{x_i}\to\mathbf{u_k}},\dot{G}_{\mathbf{x_k}\to\mathbf{u_k}}} + 2C_{\dot{G}_{\mathbf{x_i}\to\mathbf{u_k}},\dot{G}_{\mathbf{x_j}\to\mathbf{u_k}}}\right) \end{aligned} \tag{5.84}$$

$$\begin{aligned} \beta''_{k,j,K+1} :=& (\pi_k + \sigma^2_{w,k}) e^{\kappa\left(\mu_{\dot{G}_{\mathbf{x_j}\to\mathbf{u_k}}} - 2\mu_{\dot{G}_{\mathbf{x_k}\to\mathbf{u_k}}}\right)} \cdot \\ & \cdot e^{\frac{\kappa^2}{2}\left(\sigma^2_{\dot{G}_{\mathbf{x_j}\to\mathbf{u_k}}} + 4\sigma^2_{\dot{G}_{\mathbf{x_k}\to\mathbf{u_k}}} - 4C_{\dot{G}_{\mathbf{x_j}\to\mathbf{u_k}},\dot{G}_{\mathbf{x_k}\to\mathbf{u_k}}}\right)}. \end{aligned} \tag{5.85}$$

Thus, the SINRs in dB $\{\Gamma_k\}$ can be approximated as Gaussian, with mean and variance that solely depend on the CR transmission powers $\mathbf{p}$ provided that $\{\mu_{\dot{G}_{\mathbf{x_i}\to\mathbf{u_k}}}\}$, $\{\sigma^2_{\dot{G}_{\mathbf{x_i}\to\mathbf{u_k}}}\}$ and covariances $\{C_{\dot{G}_{\mathbf{x_j}\to\mathbf{u_k}},\dot{G}_{\mathbf{x_i}\to\mathbf{u_k}}}\}$ are known to the CR system.

Using the Gaussian approximation for the dB-scale SINRs, constraint (5.16) can be re-expressed as follows

$$\begin{aligned}\Pr\{\tilde{\gamma}_k(\mathbf{p}) < \bar{\gamma}_k\} &= \Pr\left\{e^{\kappa\tilde{\Gamma}_k(\mathbf{p})} < \bar{\gamma}_k\right\} \\ &= \Pr\left\{\tilde{\Gamma}_k(\mathbf{p}) < \kappa^{-1}\ln(\bar{\gamma}_k)\right\} \\ &= 1 - Q\left(\frac{\kappa^{-1}\ln(\bar{\gamma}_k) - \mu_{\tilde{\Gamma}_k}(\mathbf{p})}{\sigma_{\Gamma_k}(\mathbf{p})}\right) \leq \nu_k \end{aligned} \tag{5.86}$$

which can be further re-written as

$$-\mu_{\tilde{\Gamma}_k}(\mathbf{p}) - Q^{-1}(1-\nu_k)\sigma_{\tilde{\Gamma},k}(\mathbf{p}) + \kappa^{-1}\ln(\bar{\gamma}_k) \leq 0\ . \tag{5.87}$$

5.4.2 Solution Approach

To overcome the cumbersome intractability of the expression that one would obtain by plugging (5.76)–(5.77) directly into (5.87), consider the following equivalent set of constraints:

$$-\mu_{\tilde{\Gamma}_k}(\mathbf{p}) \leq \ln(y_{k,1}), \quad r = 1,\ldots,R \tag{5.88}$$

$$\sigma^2_{\tilde{\Gamma}_k}(\mathbf{p}) \leq \ln(y_{k,2}), \quad r = 1,\ldots,R \tag{5.89}$$

$$\psi_k(\mathbf{y}_k,\bar{\gamma}_k) := \ln(y_{k,1}) - Q^{-1}(1-\nu_k)\sqrt{\ln(y_{k,2})} + \kappa^{-1}\ln(\bar{\gamma}_k) \leq 0, \quad k = 1,\ldots,K. \tag{5.90}$$

where the set of positive real variables $\mathbf{y}_k := [y_{k,1}, y_{k,2}]^T$, $k = 1,\ldots,K$, is employed. Note that $-Q^{-1}(1-\eta_k) > 0$ preserves the concavity of $\psi_k(\mathbf{y}_k,\bar{\gamma}_k)$. Then, using (5.76)–(5.77), constraints (5.88)–(5.89) can be re-written as

$$\frac{\xi^2_{\tilde{\Gamma}_k,1}(\mathbf{p})}{\xi_{\tilde{\Gamma}_k,2}(\mathbf{p})y^{2\kappa}_{k,1}} \leq 1, \quad k = 1,\ldots,K \tag{5.91}$$

$$\frac{\xi_{\tilde{\Gamma}_k,2}(\mathbf{p})}{\xi_{\tilde{\Gamma}_k,1}(\mathbf{p})y^{\kappa^2}_{k,2}} \leq 1, \quad k = 1,\ldots,K\,. \tag{5.92}$$

Before stating a surrogate problem for (P3), a proper reformulation of the outage-based utility functions is provided next.

i) *(Weighted) Outage sum-rate utility.* Maximizing the (weighted) sum-outage-rate $\sum_k w_k \log_2(1+\bar{\gamma}_k)$ is equivalent to minimizing the function $\prod_{k=1}^K (1+\bar{\gamma}_k)^{-w_k}$. Consider introducing K auxiliary variables

$\mathbf{t} := [t_1, \ldots, t_K]^T \succ \mathbf{0}$. Then, the (weighted) sum-outage-rate can be maximized by minimizing

$$\mathcal{U}'(\mathbf{t}) = \prod_{k=1}^{K} t_k^{w_k} \tag{5.93}$$

with the extra constraints

$$\xi_{\mathcal{U},k}(\bar{\gamma}_k, t_k) = \frac{1}{(1+\bar{\gamma}_k)t_k} \leq 1, \quad k = 1, \ldots, K. \tag{5.94}$$

ii) *Proportional fair utility.* Consider cost $\sum_{k=1}^{K} -\log_2(\log_2(1+\bar{\gamma}_k))$, which has to be minimized. Noticing that one can equivalently minimize $\prod_{k=1}^{K}(\log_2(1+\bar{\gamma}_k)^{-1}$ and using (5.40), proportional fair utility is maximized upon minimization of

$$\mathcal{U}'(\mathbf{t}) = \prod_{k=1}^{K} t_k \tag{5.95}$$

subject to

$$\xi_{\mathcal{U},k}(\bar{\gamma}_k, t_k) = \frac{(1+t_k^{-1})^a}{1+\bar{\gamma}_k} \leq 1\,. \tag{5.96}$$

iii) *Harmonic-outage-rate utility.* Based on the foregoing re-formulations, maximization of the harmonic-outage-rate utility can be attained by minimizing

$$\mathcal{U}'(\mathbf{t}) = \sum_{k=1}^{K} t_k \tag{5.97}$$

under constraints (5.96).

iv) *Min-outage-rate utility.* Introduce an auxiliary variable $t > 0$. Then, maximization of $\min_k \log_2(1+\bar{\gamma}_k)$ can be attained by minimizing

$$\mathcal{U}'(t) = t \tag{5.98}$$

under the following K extra constraints

$$\xi_{\mathcal{U},k}(\mathbf{p}, t) = \frac{1}{(1+\bar{\gamma}_k)t} \leq 1, \quad k = 1, \ldots, K. \tag{5.99}$$

With the re-formulation the outage constraints (5.16) as well as of the outage-based network utilities, the surrogate problem for (P3) becomes:

$$\text{(P3b)} \quad \min_{\mathbf{p}\succ\mathbf{0},\{\mathbf{z}_r\succ\mathbf{0}\},\{\mathbf{y}_k\succ\mathbf{0}\},\bar{\boldsymbol{\gamma}}\succ\mathbf{0},\mathbf{t}\succ\mathbf{0}} \mathcal{U}'(\mathbf{t}) \tag{5.100}$$

$$\text{subject to } \xi_{\mathcal{U},k}(\bar{\gamma}_k, t_k) \leq 1, \qquad k = 1,\ldots,K \tag{5.101}$$

$$p_k \leq p_k^{\max}, \qquad k = 1,\ldots,K \tag{5.102}$$

$$\frac{\xi^2_{I_r,1}(\mathbf{p})}{\xi_{I_r,2}(\mathbf{p}) z_{r,1}^{2\kappa}} \leq 1, \qquad r = 1,\ldots,R \tag{5.103}$$

$$\frac{\xi_{I_r,2}(\mathbf{p})}{\xi_{I_r,1}(\mathbf{p}) z_{r,2}^{\kappa^2}} \leq 1, \qquad r = 1,\ldots,R \tag{5.104}$$

$$\phi_r(\mathbf{z}_r) \leq 0, \qquad r = 1,\ldots,R. \tag{5.105}$$

$$\frac{\xi^2_{\tilde{\Gamma}_k,1}(\mathbf{p})}{\xi_{\tilde{\Gamma}_k,2}(\mathbf{p}) y_{k,1}^{2\kappa}} \leq 1, \qquad k = 1,\ldots,K \tag{5.106}$$

$$\frac{\xi_{\tilde{\Gamma}_k,2}(\mathbf{p})}{\xi_{\tilde{\Gamma}_k,1}(\mathbf{p}) y_{k,2}^{\kappa^2}} \leq 1, \qquad k = 1,\ldots,K \tag{5.107}$$

$$\psi_k(\mathbf{y}_k, \bar{\gamma}_k) \leq 0, \qquad k = 1,\ldots,K. \tag{5.108}$$

where (5.106)–(5.108) have been added to the constraints (5.103)–(5.105) that cap the probability of interfering the PU system. Clearly, (P3b) is non-convex. On top of the non-convexity of problem (5.100)–(5.105), it is easy to recognize that (5.103) and (5.104) are expressed by means of rational functions of posynomials. Also, the function $\psi_k(\mathbf{y}_k, \bar{\gamma}_k)$ is concave for $\mathbf{y}_k \succ \mathbf{0}$ and $\bar{\gamma}_k > 0$, as can be verified by computing the second-order derivatives with respect to each optimization variable. Next, it will be shown that a KKT point of (P3b) can be obtained by resorting to the sequential GP approach.

5.4.3 Sequential GP for outage-based utility maximization

Appropriate surrogate constraints for the non-convex interference constraints (5.103)–(5.105) was derived in section 5.3.4.

Here, in order to use the successive GP method to solve (P3b), proper approximating GP-consistent constraints for (5.101) and (5.106)–(5.108) need to be determined.

Note that (5.101) and (5.91)–(5.92) are rational functions of posynomials. Thus, the single condensation method (5.59) can be employed. Also, since $\psi_k(\mathbf{y}_k, \bar{\gamma}_k)$ is concave for $\mathbf{y}_k \succ \mathbf{0}$ and $\bar{\gamma}_k > 0$, the supporting hyperplane at a given point $\mathbf{y}_k^{(j)}, \bar{\gamma}_k^{(j)}$ can be used to obtain an upper bound on $\psi_k(\mathbf{y}_k, \bar{\gamma}_k)$. This leads to

$$\tilde{\psi}_k(\mathbf{y}_k, \bar{\gamma}_k; \mathbf{y}_k^{(j)}, \bar{\gamma}_k^{(j)}) := \frac{y_{k,1}}{y_{k,1}^{(j)}} + \frac{y_{k,2}\, Q^{-1}(\eta_k)}{2\, y_{k,2}^{(j)} \sqrt{\ln(y_{k,2}^{(j)})}} + \frac{\bar{\gamma}_k}{\kappa \bar{\gamma}_k^{(j)}} - c_{k,y}(\mathbf{y}_k^{(j)}, \bar{\gamma}_k^{(j)}) \tag{5.109}$$

with

$$c_{y,k}(\mathbf{y}_k^{(j)}, \bar{\gamma}_k^{(j)}) = (1 + \kappa^{-1}) + \frac{Q^{-1}(\eta_k)}{2\sqrt{\ln(y_{k,2}^{(j)})}} - \phi_{y,k}(\mathbf{y}_k^{(j)}, \bar{\gamma}_k^{(j)}) \tag{5.110}$$

and it satisfies **c1)**–**c3)**. Note from (5.108) and (5.109) that, for points $\mathbf{y}_k^{(j)}, \bar{\gamma}_k^{(j)}$ that are feasible and for $\nu_k < 0.5$, $c_{y,k}(\mathbf{y}_k^{(j)}, \bar{\gamma}_k^{(j)}) > 0$ holds. Then, upon defining

$$\tilde{\psi}'_k(\mathbf{y}_k, \bar{\gamma}_k; \mathbf{y}_k^{(j)}, \bar{\gamma}_k^{(j)}) := \frac{y_{k,1}}{y_{k,1}^{(j)}} + \frac{y_{k,2}\, Q^{-1}(\eta_k)}{2\, y_{k,2}^{(j)} \sqrt{\ln(y_{k,2}^{(j)})}} + \frac{\bar{\gamma}_k}{\kappa \bar{\gamma}_k^{(j)}}\,, \tag{5.111}$$

an appropriate surrogate of constraints (5.108) is

$$\frac{1}{c_{k,y}(\mathbf{y}_k^{(j)}, \bar{\gamma}_k^{(j)})} \tilde{\psi}'_k(\mathbf{y}_k, \bar{\gamma}_k; \mathbf{y}_k^{(j)}, \bar{\gamma}_k^{(j)}) \leq 1\,. \tag{5.112}$$

Wrapping up, the successive GP approach for solving (P2b) entails the solution of the following GP at each iteration $j = 1, 2, \ldots$

$$(\text{P3b}^{(j)}) \quad \min_{\mathbf{p}\succ\mathbf{0},\{\mathbf{z}_r\succ\mathbf{0}\},\{\mathbf{y}_k\succ\mathbf{0}\},\bar{\boldsymbol{\gamma}}\succ\mathbf{0},\mathbf{t}\succ\mathbf{0}} \mathcal{U}'(\mathbf{t}) \tag{5.113}$$

$$\text{subject to } \tilde{\xi}_{\mathcal{U},k}(\bar{\gamma}_k, t_k; \bar{\gamma}_k^{(j-1)}, t_k^{(j-1)}) \leq 1, \quad k=1,\ldots,K \tag{5.114}$$

$$p_k \leq p_k^{\max}, \qquad k=1,\ldots,K \tag{5.115}$$

$$\frac{\xi_{I_r,1}^2(\mathbf{p})}{\tilde{\xi}_{I_r,2}(\mathbf{p};\mathbf{p}^{(j-1)}) z_{r,1}^{2\kappa}} \leq 1, \quad r=1,\ldots,R \tag{5.116}$$

$$\frac{\xi_{I_r,2}(\mathbf{p})}{\tilde{\xi}_{I_r,1}(\mathbf{p};\mathbf{p}^{(j-1)}) z_{r,2}^{\kappa^2}} \leq 1, \quad r=1,\ldots,R \tag{5.117}$$

$$\frac{1}{c_r(\mathbf{z}_r^{(j-1)})} \tilde{\phi}_r'(\mathbf{z}_r;\mathbf{z}_r^{(j-1)}) \leq 1, \quad r=1,\ldots,R. \tag{5.118}$$

$$\frac{\xi_{\tilde{\Gamma}_k,1}^2(\mathbf{p})}{\tilde{\xi}_{\tilde{\Gamma}_k,2}(\mathbf{p};\mathbf{p}^{(j-1)}) y_{k,1}^{2\kappa}} \leq 1, \quad k=1,\ldots,K \tag{5.119}$$

$$\frac{\xi_{\tilde{\Gamma}_k,2}(\mathbf{p})}{\tilde{\xi}_{\tilde{\Gamma}_k,1}(\mathbf{p};\mathbf{p}^{(j-1)}) y_{k,2}^{\kappa^2}} \leq 1, \quad k=1,\ldots,K \tag{5.120}$$

$$\frac{1}{c_{k,y}(\mathbf{y}_k^{(j)}, \bar{\gamma}_k^{(j-1)})} \tilde{\psi}_k'(\mathbf{y}_k, \bar{\gamma}_k; \mathbf{y}_k^{(j-1)}, \bar{\gamma}_k^{(j-1)}) \leq 1, \quad k=1,\ldots,K. \tag{5.121}$$

with $\mathbf{p}^{(j-1)}, \{\mathbf{z}_r^{(j-1)}\}, \{\mathbf{y}_k^{(j-1)}\}, \bar{\boldsymbol{\gamma}}^{(j-1)}, \mathbf{t}^{(j-1)}$ the solution carried out at the $(j-1)$-th iteration.

Proposition 5.4.2. *Given an initial feasible starting point* $\mathbf{p}^{(0)}$, $\{\mathbf{z}_r^{(0)}\}$, $\{\mathbf{y}_k^{(0)}\}$, $\bar{\boldsymbol{\gamma}}^{(0)}$, $\mathbf{t}^{(0)}$, *the sequence of solutions* $\mathbf{p}^{(j)}$, $\{\mathbf{z}_r^{(j)}\}$, $\{\mathbf{y}_k^{(j)}\}$, $\bar{\boldsymbol{\gamma}}^{(j)}$, $\mathbf{t}^{(j)}$ *of (P3b*$^{(j)}$*)* $j=1,2,\ldots$, *converges to a KKT point of (P3b).* □

5.5 A Method to Obtain a Feasible Starting Point

Initial points that lie in the feasible region of (P2b) and (P3b), respectively, are required at the first iteration of the sequential GP method. Next, a method to obtain feasible points for (P2b) and (P3b) is devised. See, also, [107].

Denote as $\xi_{j,i}(\mathbf{p})$ a generic posynomial in the variables $\mathbf{p}$; also, let $\phi_l(\mathbf{z})$ be a concave function. Then, the aforementioned feasibility problem entails the computation of a solution $\mathbf{p}^*, \mathbf{z}^*$ of the following set of non-convex

constraints:

$$\frac{\xi_{j,1}(\mathbf{p})}{\xi_{k,2}(\mathbf{p})} \leq 1 \qquad j = 1, \ldots, J \tag{5.122}$$

$$\phi_l(\mathbf{z}) \leq 0 \qquad l = 1, \ldots, L\,. \tag{5.123}$$

To find $\mathbf{p}^*, \mathbf{z}^*$, pick first an arbitrary point $\mathbf{p}' \succ \mathbf{0}, \mathbf{z}' \succ \mathbf{0}$, where $0 < p'_k \leq p_k^{\max}\ \forall\, k$. Then, compute the following quantities $\{\omega_j\}$:

$$\omega_j := \max\left\{1, \frac{\xi_{j,1}(\mathbf{p}')}{\xi_{k,2}(\mathbf{p}')}\right\} \qquad j = 1, \ldots, J \tag{5.124}$$

$$\omega_{l+J} := \max\left\{1, \phi_l(\mathbf{z}')\right\} \qquad l = 1, \ldots, L. \tag{5.125}$$

If $\omega_j = 1\ \forall\, j$, then $\mathbf{p}^* = \mathbf{p}', \mathbf{z}^* = \mathbf{z}'$ is a feasible solution for (5.122)–(5.123). Hence, can be used as a starting point for the sequential GP algorithm. If $\omega_j \neq 1$ for at least one $j \in \{1, \ldots, J+L\}$, then a feasible point for (5.122)–(5.123) can be found by solving the following problem:

$$\text{(P4)} \qquad \min_{\mathbf{p}\succ\mathbf{0}, \mathbf{z}\succ\mathbf{0}, \boldsymbol{\omega}\succ\mathbf{0}} \prod_{j=1}^{J+L} \omega_j \tag{5.126}$$

$$\text{subject to}: \ p_k \leq p_k^{\max} \qquad k = 1, \ldots, K \tag{5.127}$$

$$\omega_j \geq 1 \qquad j = 1, \ldots, J+L \tag{5.128}$$

$$\frac{\xi_{j,1}(\mathbf{p})}{\xi_{k,2}(\mathbf{p})}\omega_j^{-1} \leq 1 \qquad j = 1, \ldots, J \tag{5.129}$$

$$\phi_l(\mathbf{z}_i)\omega_{l+J}^{-1} \leq 1 \qquad l = 1, \ldots, L \tag{5.130}$$

where $\boldsymbol{\omega} := [\omega_1, \ldots, \omega_{J+L}]^T$. Clearly, problem (P4) is non-convex, being (5.129) ratios of posynomials and (5.130) concave in $\mathbf{z}$.

However, an optimal (at least locally) solution for (P4) can be attained by using the sequential GP approach. Specifically, GP-consistent surrogate constraints can be obtained by applying the single condensation and the hyperplane-based approximation to (5.129) and (5.130), respectively. If the solution $\mathbf{p}'', \mathbf{z}'', \boldsymbol{\omega}''$ of (P4), obtained via sequential GP, satisfies condition $\prod_{j=1}^{J+L} \omega''_j = 1$, then $\mathbf{p}^* = \mathbf{p}'', \mathbf{z}^* = \mathbf{z}''$. Conversely, if $\prod_{j=1}^{J+L} \omega''_j > 1$ the sequential GP algorithm failed to converge to a global optimum point for (P4) and, then, the routine described in this section has to be repeated.

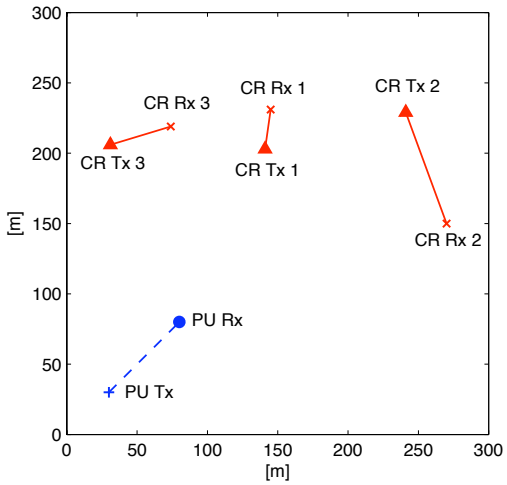

Figure 5.1: Test scenario.

5.6 Numerical Tests

Consider the scenario depicted in Fig. 5.1, where $K = 3$ CR links (shown in solid red lines) are present in a geographical area of 300×300m. Also, a single ($R = 1$) PU link is active (dashed blue line), with a transmit-power of 0.1W. The path loss parameters were set to $g_{0,\mathbf{x}\to\mathbf{u}} = 1$, for all $\mathbf{x}, \mathbf{u}$, and $\gamma = 3.5$; $m = 10$ was chosen for the Nakagami-m fading. The spatially-correlated shadow fading was generated according to the loss fileld-based model seth forth in [26]. Specifically, the parameters of the isotropic and exponentially decaying covariance function (3.21) were set to $\sigma_\ell = 12$dB and $d_\ell = 30$m. This led to a generated shadow fading with zero mean and standard deviation of approximately 10dB. The maximum transmission power was fixed to $p_k^{\max} = 5$W for all the CR transmitters. The interference temperature threshold at the PU receiver was assumed to be $I_r^{\max} = -80$dB, and the probability of exceeding such value was limit to $\epsilon_r = 0.01$. In order to terminate the iterations of the sequential GP algorithm, the threshold υ was set to 10^{-4}. Also, to make the feasible set compact and avoid computational problems while performing the single-condensation method (5.59), transmission powers were lower bounded by $p_k \geq 10^{-10}$.

Consider maximizing the sum-rate (5.2) of the CR network. Set unitary

weighting coefficients in (5.2), i.e., $w_k = 1 \ \ \forall k = 1, \ldots, K$. Also, consider first the case in which the CR-to-CR CGs are perfectly known. Thus power control via (P2) is firstly analyzed.

Evaluation of the actual interference that is perceived at the PU receiver when CRs make use of the transmission powers obtained by solving (P2b) is critical in order to assess the quality of the statistical approximations employed and the effectiveness of the proposed algorithm. For this purpose, the complementary cumulative distribution function (*c.c.d.f.*) of the interference caused at the PU receiver is plotted in Fig. 5.2. The curve with square markers corresponds to the case where only the location information was utilized to obtain the channel gain statistics; in this case, the mean of shadow fading is set to 0 dB, and the correlations were computed based on (3.23). The curve with 'X' markers represents the case where shadowing measurements were used to estimate the CR-PU channel gain via channel gain maps, as shown in chapter 3. Thus, the channel gain was estimated reliably with error standard deviation of 4 dB. In these two cases, (P2b) was solved to obtain the CR transmission powers. As a benchmark, the curve with the circle markers depicts the case of perfect CR-to-PUchannel knowledge; in this case, (P1) was solved to obtain optimal powers. Also, the curve with the '+' markers represent the case when (P1) is solved by resorting to a path loss-only model, with shadowing and small-scale fading completely neglected. $5,000$ independent realizations were used to generate the plot.

From Fig. 5.2, it is seen that with perfect CR-to-PU CG information is available, the CRs push the interference $i_r(\mathbf{p})$ to the limit $I_r^{\max}$ in order to maximize the network sum-rate. This explains the sharp transition at $I_r^{\max}$, point that is never exceeded. Conversely, the fulfillment of the linear interference bound in (P1) is seriously jeopardized when the randomness of the CG is completely neglected; in this case, the CRs unduly harm the PU receiver. Fig. 5.2 clearly shows that solving (P2b) enforces the desired interference constraint, which also verifies the accuracy of the associated approximations. In fact, with crude channel gain statistics, the interference constraint is seen to be over-satisfied, while channel gain cartography leads to a tightly met constraint.

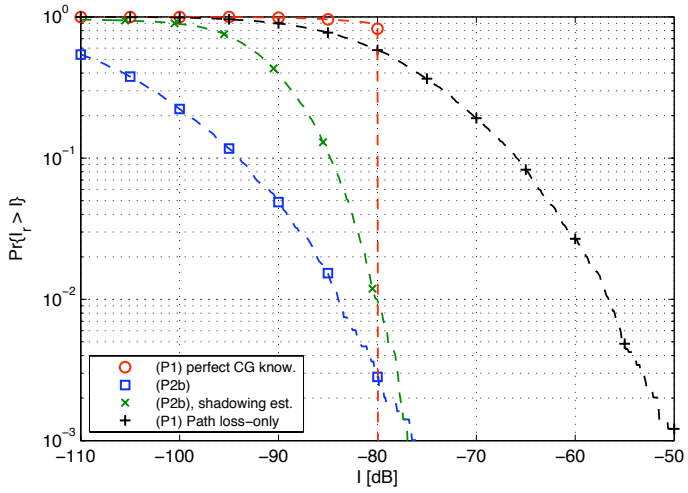

Figure 5.2: Sum-rate maximization. Interference power *c.c.d.f.*.

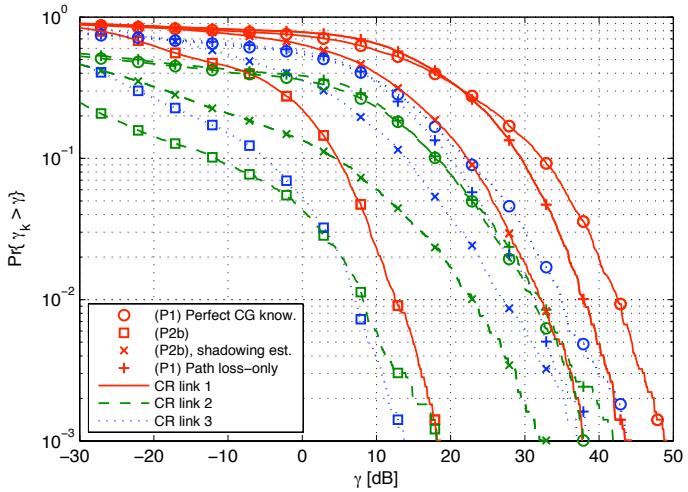

Figure 5.3: Sum-rate maximization. CR SINR *c.c.d.f.*

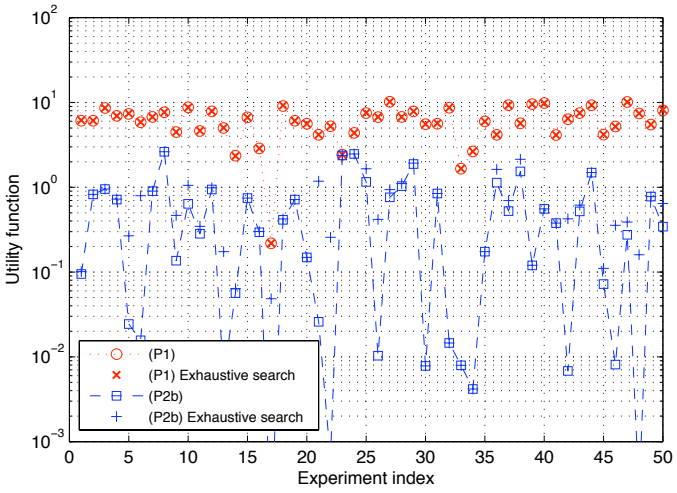

Figure 5.4: Sum-rate maximization. Achieved sum-rates.

Fig. 5.3 shows the *c.c.d.f.*'s of the SINRs $\{\gamma_k\}$ of the CR links. The solid, dashed, and dotted curves represent different CR links, and the markers are used in the same manner as in Fig. 5.2. It can be seen that especially when the channel gains are estimated from measurements, the performance degradation from the perfect channel gain case is not too large. The path loss-only case exhibits better SINRs than the proposed schemes, but only at severe interference to the PU system.

To see how close the obtained KKT solutions are to the globally optimal solution, an exhaustive grid-based search was performed. Fig. 5.4 depicts the weighted sum-rate objectives obtained by solving (P1) and (P2b) for 50 different channel realizations. It is seen that the sequential GP-based objectives very often coincide with the globally optimal objectives even in the case with channel uncertainty.

Finally, Table 5.1 collects the average number of GPs (rounded up) that were solved up until the stopping condition for the sequential GP was met. See remark 5.3.2. Also, the average number of iterations (rounded up) of the sequential GP that were required to solve the feasibility problem (P4) is reported. The computational burden required to solve (P2b) without employing the CG maps is not exorbitantly higher than that for solving

Table 5.1: Average number of iterations required to solve (P1) and (P2b) via sequential GP, for scenario in Fig. 5.1

	Feasible problem	Power control
(P1) - perfect CG	1	8
(P1) - path loss-only	1	8
(P2b) - without CG maps	6	9
(P2b) - with CG maps	3	17

(P1). With the use of the CG maps, more GPs are required; however, in this case, the profit from using CG maps is to achieve firmly higher sum-rates.

Then, consider the case of imperfectly known CR-to-CR CGs and target the maximization of the $\{\nu_k\}$-outage network sum rate. Set the weighting coefficients in (5.93) to 1 and limit the probability of exceeding the outage threshold $\bar{\gamma}_k$ to $\nu_k = 0.01$ for all the CRs. Also, $\upsilon = 10^{-4}$. Finally, to make the feasible set compact, variables $\bar{\gamma}_k$ were lower bounded as $\bar{\gamma}_k \geq 10^{-10}$.

To test out the quality of the statistical approximations for the SINRs and, consequently, verify observation of the outage constraints, the variables $\{\bar{\gamma}_k\}$ solving (P3b) in 50 different experiments are plotted in Fig. 5.5; these are compared with the actual values of the outage thresholds, which were computed by employing the set of powers obtained from (P3b), by generating $5,000$ independent fading realizations (shadowing and small scale-fading were generated to obtain Fig. 5.5(a), only small-scale fading was generated to obtain Fig. 5.5(b)), and, finally, by computing the cumulative distribution function (*c.d.f.*) of the received SINR at the CR receivers.

From Fig. 5.5(a), where only the location information was utilized to obtain the CR-to-CR channel statistics, it is seen that solving (P3b) always ensures observation of the desired outage constraints. In fact, the actual SINR outage thresholds for users "2" and "3" are higher than $\bar{\gamma}_k$ for each CR link, thus indicating that the outage constraints are over-satisfied. In Fig. 5.5(b), channel gain maps were used to obtain the channel gain statistics. In this case, approximation errors sometimes cause a slight violation

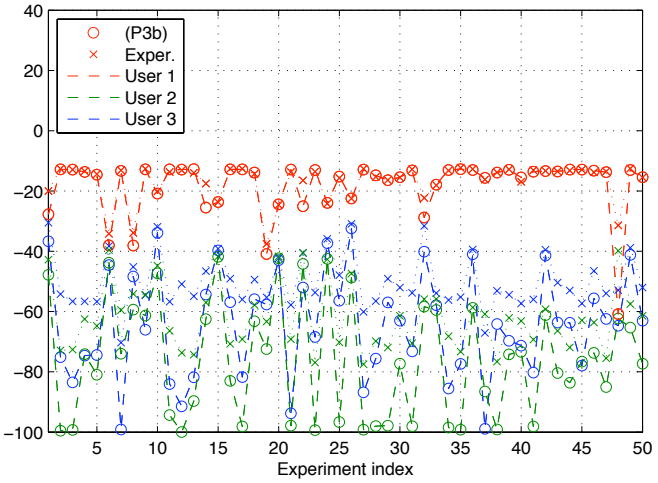

(a) CG statistics based on only users' locations

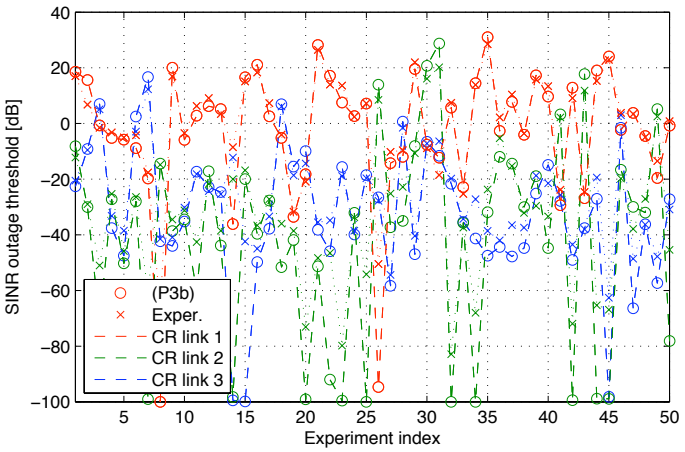

(b) CG map-aided

Figure 5.5: Users' SNR outage thresholds. Variables $\{\bar{\gamma}_k\}$ carried out by (P3b) are compared with the actual SNR outage thresholds obtained by using the set of powers $\{\mathbf{p}\}$.

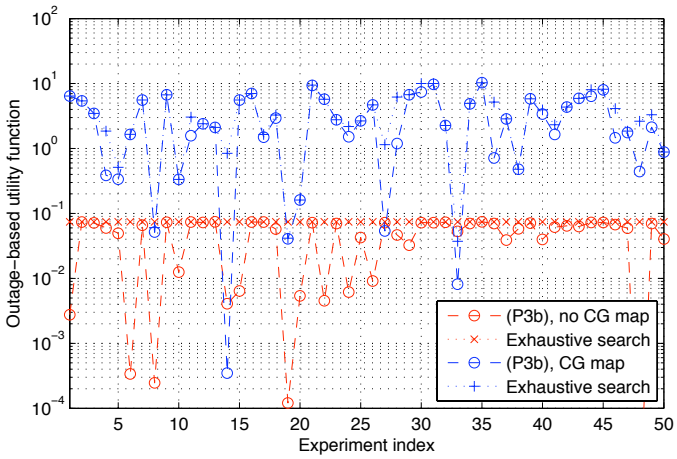

Figure 5.6: Sum-outage-rate maximization. Achieved sum-outage-rates.

Table 5.2: Average number of iterations required to solve (P3b) via sequential GP, for scenario in Fig. 5.1

	Feasible problem	Power control
(P3b) - without CG maps	20	26
(P3b) - with CG maps	11	32

of the outage constraints, which are nevertheless profusely fulfilled most of the time.

Again, an exhaustive grid-based search was performed to check whether the KKT solutions are globally optimal. The sum-outage-rate achieved in 50 different experiments are plotted in Fig. 5.6. The solutions of (P3b) obtained via sequential GP, with and without CG maps, often coincide with the globally optimal objectives. Note that without CG maps, the optimal objective is always the same, being the solution dependent on only the locations of the users.

Table 5.2 reports the average number of GPs (rounded up) that were solved up until the stopping condition was met. As general remark, solution of (P3b) requires a higher number of iterations of the sequential GP algorithm compared to (P2b); a higher computational burden is the price to pay

for not being able to estimate the instantaneous CR-to-CR CGs reliably.

5.7 Appendix

The following lemmas were used to devise a statistical approximation for the SINRs $\{\gamma_k\}$.

Lemma 5.7.1. *Let $x \sim log\mathcal{N}(\mu_x, \sigma_x^2)$, with μ_x and σ_x^2 the mean and the variance of the Gaussian-distributed random variable $X := \ln(x)$. Then, x^{-1} is log-Normally-distributed and $x^{-1} \sim log\mathcal{N}(-\mu_x, \sigma_x^2)$.*

Proof. Rewrite x^{-1} as $x^{-1} = (e^X)^{-1} = e^{-X}$ and recall that $\mathcal{N}(\mu_x, \sigma_x^2)$. Then, it can be readily shown that $-X \sim \mathcal{N}(-\mu_x, \sigma_x^2)$. □

Lemma 5.7.2. *Let $x \sim log\mathcal{N}(\mu_x, \sigma_x^2)$ and $y \sim log\mathcal{N}(\mu_y, \sigma_y^2)$ be two correlated log-Normal random variables. Then, xy^{-1} is log-Normally-distributed and $xy^{-1} \sim log\mathcal{N}(\mu_x - \mu_y, \sigma_x^2 + \sigma_x^2 - 2\text{cov}\{X, Y\})$, where $X := \ln(x)$ and $Y := \ln(y)$.*

Proof. Rewrite first xy^{-1} as $xy^{-1} = e^X e^{-Y} = e^{X-Y}$. Recall that $X \sim \mathcal{N}(\mu_x, \sigma_x^2)$ and $Y \sim \mathcal{N}(\mu_y, \sigma_y^2)$. The statistical description of xy^{-1} is complete upon computing the first two central moments of $Z := X - Y$. From the linearity of the expectation operator, $\mathbb{E}\{Z\} = \mu_x - \mu_y$. The variance of Z is obtained as follows.

$$\begin{aligned}
\sigma_Z^2 &:= \mathbb{E}\{(Z - \mathbb{E}\{Z\})^2\} \\
&= \mathbb{E}\left\{((X - Y) - (\mu_x - \mu_y))^2\right\} \\
&= \text{var}\{X\} + \text{var}\{Y\} - 2\mathbb{E}\{XY\} + 2\mu_x\mu_y \\
&= \sigma_x^2 + \sigma_x^2 - 2\text{cov}\{X, Y\}\,.
\end{aligned}$$

□

Chapter 6

Conclusions

In an effort that strives for addressing the ambitious challenges involved by the emerging hierarchical spectrum access setup, where continuous situational awareness is unceasingly demanded for opportunistic and non-intrusive CR spectrum reuse purposes, the present thesis introduced innovative large-scale collaborative algorithms for accurate RF ambient characterization and spectrum opportunity detection. These were complemented by novel resource allocation techniques, which allow to circumvent the hurdles that a lack of explicit coordination between primary and secondary systems has engendered.

A consistent portion of the work concentrated on the channel gain cartography framework. The problem addressed entailed tracking the evolution of the channel gains on arbitrary transmitter-receiver pairs starting from channel gain measurements among collaborating CRs. In a sense, the aim was to enable acquisition of a consistent, global, multidimensional view of the RF ambient viewed from arbitrary points in space, thereby involving a significant departure from the conventional cooperative point-to-point channel estimation philosophy. To do so, a spatio-temporal evolution of shadow fading was first characterized by judiciously extending an experimentally verified model in order to capture both spatial and temporal correlations. Then, a novel KKF-based algorithm was shown to be capable of obtaining the distribution of unknown CGs of wireless links at arbitrary transceiver locations, conditioned on measurements taken by the collaborating CRs. To

address scalability and robustness concerns, a distributed version of the KKF algorithm was derived using the ADMoM framework. The proposed collaborative map tracking algorithm showed excellent performance, especially when compared to the non-collaborative counterpart in terms of channel gain map MSE.

The problem of monitoring the activity of the primary system jointly in the spatial, temporal and frequency domains was addressed. Based on a parsimonious model accounting for mutual interference concerns among primary transmitters, a sparsity-exploiting linear regression problem was formulated to estimate the PU locations and transmit power levels in real-time. In the derivation of the sparsity-cognizant algorithm, tools with well-appreciated merits in sparse linear regression and optimization theory, namely, Lasso and cyclic coordinate descent, were adapted to the problem at hand. Both centralized and distributed implementations of the sensing algorithm were developed. In particular, the latter was derived by using the ADMoM framework. Extensive numerical experiments were performed to show the considerable improvement in estimating not only the positions of the PUs but also their power levels compared to the sparsity-agnostic RLS algorithm. Also, the CG atlas was shown to remarkably improve both localization and power estimation accuracy with respect to a simple model based on only the deterministic path loss. Then, based on the CG maps, the outcome of the sensing algorithm was used to reconstruct the actual PSD map of the primary system and, thus, the PU system coverage region. In other words, complementing the sensing algorithm with the CG maps is it possible to reveal the locations where potential PU receivers can reside. In this context, CG atlas was shown to constitute an invaluable means to overcome a disk-shaped time-invariant over-simplification of the per-PU coverage region.

Then, resource allocation under constraints that limit the interference perceived by the incumbent PU system was considered. In this context, the major issue is represented by the impossibility of getting an estimate of the channels between CRs and PUs. Moreover, conventional sensing algorithms can detect PU transmitters but cannot localize silent licensed receivers, which nevertheless have to be obligatorily protected. Based on location information of the potential PU receivers provided by the proposed

sensing algorithm and on an estimate of the PU CG maps, a CR power allocation algorithm was developed under CR-to-PU channel gain uncertainty arising from shadowing and small-scale fading effects. As PU protection constraints must be enforced with high reliability, probabilistic constraints were imposed in order to guarantee that the interference power experienced by any PU receiver falls below a tolerable level with a given high probability. Fenton-Wilkinson-type approximations were employed to model the received interference power at the PUs as log-normal, which led to a tractable network utility maximization formulation. Due to the truly non-convexity of the problem, a successive convex approximation technique was adopted to obtain a KKT solution. This approach was shown to boils down to a sequential GP algorithm as in the perfect channel knowledge case. Uncertain CR-to-CR channels were also considered, and an outage-based utility maximization with per-CR link outage probability requirements was proposed. Fenton-Wilkinson method was used again to approximate the distribution of the SINRs as log-normal, leading to a formulation where a sequential GP-based solution still applied.

The main results of the present Ph.D. Thesis have been submitted for publication to journals and international conferences; the list of the papers already accepted for publication and currently under revision is provided in the following.

1. E. Dall'Anese, S.-J. Kim, G. B. Giannakis, and S. Pupolin, "Chance-Constrained Power Allocation for Cognitive Radio Networks Under Channel Uncertainty", *IEEE Trans. on Wireless Communications*, in preparation.

2. E. Dall'Anese, S.-J. Kim, and G. B. Giannakis, "Channel Gain Map Tracking via Distributed Kriging", *IEEE Trans. on Vehicular Technology*, submitted May 2010, revised December 2010.

3. S.-J. Kim, E. Dall'Anese, and G. B. Giannakis, "Cooperative Spectrum Sensing for Cognitive Radios Using Kriged Kalman Filtering ", *IEEE Journal of Selected Topics in Signal Processing (JSTSP)*, February 2011.

4. E. Dall'Anese, S.-J. Kim, G. B. Giannakis, and S. Pupolin, "Power Allocation for Cognitive Radio Networks Under Channel Uncertainty", *IEEE International Conference on Communications 2011*, submitted, September 2010.

5. S.-J. Kim, E. Dall'Anese, G. B. Giannakis, and S. Pupolin, "Collaborative Channel Gain Map Tracking for Cognitive Radios," in *Proc. of The Second International Workshop on Cognitive Information Processing (CIP)*, Elba Island, Italy, June 2010.

6. E. Dall'Anese, "Geostatistics-Inspired Sparsity-Aware Cooperative Spectrum Sensing for Cognitive Radio Networks," *Proc. of The Second International Workshop on Mobile Opportunistic Networking (Ph.D. Forum)*, Pisa, Italy, Feb. 2010.

7. S.-J. Kim, E. Dall'Anese, and G. B. Giannakis, "Spectrum Sensing for Cognitive Radios Using Kriged Kalman Filtering," *Proc. of The Third International Workshop on Computational Advances in Multi-Sensor Adaptive Processing*, Aruba, Dutch Antilles, Dec. 2009 (invited paper).

8. S.-J. Kim, E. Dall'Anese, and G. B. Giannakis, "Sparsity-Aware Cooperative Cognitive Radio Sensing Using Channel Gain Maps," *Proc. of Asilomar Conference on Signal, Systems and Computers*, Pacific Groove, CA, USA, Nov. 2009.

Indeed, there could be several extensions of the work presented in this dissertation that would be worth investigating. Beyond the CR setup, CG atlas is envisioned as a tool that can help cross-layer design and assessment of the system-level performance of wireless networks and to enhance handoff, localization, routing, and resource allocation. It would be interesting to analyze the actual applicability of the maps to the aforementioned problems and corroborate their potential benefits.

As for the sensing algorithm, actual design of PU detection strategies is of interest; in other words, it would be desirable to devise a thresholding-based rule in order to decide whether a non-zero entry of the estimand

corresponds to a PU transmitter or it is just corrupted by some spurious power. Unfortunately, the derivation of an optimal decision rule encounters insurmountable difficulties arising from a lack of exact statistical characterization of Lasso-like estimates; however, sub-optimal heuristic decision criteria may be devised. Also, an approach similar to the one pursued in the total least-squares (T-LS) framework may be taken to cope with errors introduces by a grid-based discretization of the geographical area and errors in reconstructing the CG maps.

When QoS policies impose minimum-rate requirements on the CR-to-CR links, the power control problem may encounter feasibility concerns; i.e., all the per-CR QoS constraints may not be simultaneously satisfied. In this case, an admission control scheme is advocated. It is thus worth investigating an extension of the proposed power allocation algorithm that incorporates prior minimum CR transmission rates constraints and, eventually, user selection techniques that cope with the possible infeasibility of the problem.

Bibliography

[1] *Report of the spectrum efficiency working group*, FCC Spectrum Policy Task Force, 2002. [Online]. Available: http://www.fcc.gov/sptf/reports.htm

[2] M. A. McHenry, P. A. Tenhula, D. McCloskey, D. A. Roberson, and C. S. Hood, "Chicago spectrum occupancy measurements & analysis and a long-term studies proposal," in *Proceedings of the first international workshop on Technology and policy for accessing spectrum*, ser. TAPAS '06, 2006.

[3] C. Ghosh, S. Roy, M. B. Rao, and D. P. Agrawal, "Spectrum occupancy validation and modeling using real-time measurements," in *Proceedings of the 2010 ACM workshop on Cognitive radio networks*, ser. CoRoNet '10, 2010, pp. 25–30.

[4] C. Schiphorst, R. Slump, "Evaluation of spectrum occupancy in Amsterdam using mobile monitoring vehicles," in *Proceedings of the IEEE 71st Vehicular Technology Conference (VTC 2010-Spring)*, May 2010.

[5] M. Lòpez-Benìtez, A. Umbert, and F. Casadevall, "Evaluation of spectrum occupancy in Spain for cognitive radio applications," in *Proceedings of the IEEE 69th Vehicular Technology Conference (VTC 2010-Spring)*, Sep. 2009.

[6] Q. Zhao and B. Sadler, "A survey of dynamic spectrum access," *IEEE Sig. Proc. Mag.*, vol. 24, no. 3, pp. 79–89, May 2007.

[7] J. M. Peha, "Approaches to spectrum sharing," *IEEE Commun. Mag.*, vol. 43, no. 2, pp. 10–12, Feb. 2005.

[8] R. Coase, "The federal communications commission," *J. Law and Economics*, pp. 1–40, 1959.

[9] D. Hatfield and P. Weiser, "Property rights in spectrum: Taking the next step," in *Proceedings of the 1st IEEE Symp. New Frontiers Dynamic Spectrum Access Networks*, Nov. 2005, pp. 43–55.

[10] R. T. L. Xu, T. Paila, W. Hansmann, M. Frank, and M. Albrecht, "DRiVE-ing to the internet: Dynamic radio for ip services in vehicular environments," in *Proceedings of the 25th Annual IEEE Conf. Local Computer Networks*, Nov. 2000, pp. 281–289.

[11] W. Lehr and J. Crowcroft, "Managing shared access to a spectrum commons," in *Proceedings of the 1st IEEE Symp. New Frontiers Dynamic Spectrum Access Networks*, Nov. 2005, pp. 420–444.

[12] R. Etkin, A. Parekh, and D. Tse, "Spectrum sharing for unlicensed bands," in *Proceedings of the 1st IEEE Symp. New Frontiers Dynamic Spectrum Access Networks*, Nov. 2005, pp. 251–258.

[13] J. I. Mitola and G. J. Maguire, "Cognitive radio: Making software radios more personal," *IEEE Personal Communications*, no. 4, pp. 13–18, Aug. 2002.

[14] S. Haykin, "Cognitive radio: Brain-empowered wireless communications," *IEEE J. Sel. Areas Commun.*, no. 2, pp. 201–220, Feb. 2007.

[15] X. Hong, C. Wang, H. Chen, and Y. Zhang, "Secondary spectrum access networks," *IEEE Veh. Technol. Mag.*, vol. 4, no. 2, pp. 36–43, Jun. 2009.

[16] U. Berthold and F. Jondral, "Guidelines for designing ofdm overlay systems," in *Proceedings of the 1st IEEE Symp. New Frontiers Dynamic Spectrum Access Networks*, Nov. 2005, pp. 626–629.

[17] M. Abdallah, A. Salem, M.-S. Alouini, and K. Qaraqe, "Discrete rate and variable power adaptation for underlay cognitive networks," in *Proceedings of the 2010 European Wireless Conference*, Lucca, Italy, Apr. 2010, pp. 733–737.

[18] W. Q. Malik and D. J. Edwards, "Cognitive techniques for ultrawideband communications," in *Proceedings of IET Seminar on Ultra Wideband Systems, Technologies and Applications*, London, UK, Apr. 2006, pp. 81–86.

[19] Y. Zhao, L. Morales, J. Gaeddert, K. K. Bae, J.-S. Um, and J. H. Reed, "Applying radio environment maps to cognitive wireless regional area networks," in *Proc. of the DySPAN Conf.*, Dublin, Ireland, Apr. 2007, pp. 115–118.

[20] A. B. MacKenzie, J. H. Reed, P. Athanas, C. W. Bostian, R. M. Buehrer, L. A. DaSilva, S. W. Ellingson, Y. T. Hou, J.-M. Park, C. Patterson, S. Raman, C. R. C. M. da Silva, and M. Hsiao, "Cognitive radio and networking research at Virginia Tech," *Proc. IEEE*, vol. 97, no. 4, pp. 660–688, Apr. 2009.

[21] A. Fette, *Cognitive Radio Technology.* Communications Engineering Series, Newnes, 2006.

[22] T. S. Rappaport, *Wireless Communications: Principles & Practice.* Prentice Hall, 1996.

[23] M. Gudmundson, "Correlation model for shadow fading in mobile radio systems," *Elec. Lett.*, vol. 27, no. 23, pp. 2145–2146, Nov. 1991.

[24] F. Graziosi and F. Santucci, "A general correlation model for shadow fading in mobile radio systems," *IEEE Commun. Lett.*, vol. 6, no. 3, pp. 102–104, Mar. 2002.

[25] Z. Wang, E. K. Tameh, and A. Nix, "Simulating correlated shadowing in mobile multihop relay/ad hoc networks," IEEE 802.16 Broadband Wireless Access Working Group, Tech. Rep. IEEE C802.16j-06/060, Jul. 2006.

[26] P. Agrawal and N. Patwari, "Correlated link shadow fading in multihop wireless networks," *IEEE Trans. Wireless Commun.*, vol. 8, no. 9, pp. 4024–4036, Aug. 2009.

[27] C. Oestges, N. Czink, B. Bandemer, P. Castiglione, F. Kaltenberger, and A. J. Paulraj, "Experimental characterization and modeling of outdoor-to-indoor and indoor-to-indoor distributed channels," *IEEE Trans. Veh. Technol.*, vol. 59, pp. 2253–2265, Jun. 2010.

[28] K. S. Butterworth, K. W. Sowerby, and A. G. Williamson, "Base station placement for in-building mobile communication systems to yield high capacity and efficiency," *IEEE Trans. Commun.*, vol. 48, no. 4, pp. 658–669, Apr. 2000.

[29] K. Kumaran, S. E. Golowich, and S. Borst, "Correlated shadow-fading in wireless networks and its effect on call dropping," *Wireless Networks*, vol. 8, no. 1, pp. 61–71, Jan. 2002.

[30] J. Cho and Z. J. Haas, "On the throughput enhancement of the downstream channel in cellular radio networks through multihop relaying," *IEEE J. Sel. Areas Commun.*, vol. 22, no. 7, pp. 1206–1219, Sep. 2004.

[31] S.-J. Kim, E. Dall'Anese, and G. Giannakis, "Cooperative spectrum sensing for cognitive radios using Kriged Kalman filtering," *IEEE J. Sel. Topics Sig. Proc.*, Feb. 2011, to appear.

[32] B. Mark and A. Nasif, "Estimation of maximum interference-free power level for opportunistic spectrum access," *IEEE Trans. Commun.*, vol. 8, no. 5, pp. 2505–2513, May 2009.

[33] A. B. H. Alaya-Feki, S. B. Jemaa, B. Sayrac, P. Houze, and E. Moulines, "Informed spectrum usage in cognitive radio networks: interference cartography," in *Proc. of the PIMRC Conf.*, Cannes, France, Sep. 2008, pp. 1–5.

[34] J. Riihijärvi, P. Mähönen, M. Wellens, and M. Gordziel, "Characterization and modelling of spectrum for dynamic spectrum access with spatial statistics and random fields," in *Proc. of the PIMRC Conf.*, Cannes, France, Sep. 2008, pp. 1–6.

[35] N. Cressie, "The origins of Kriging," *Math. Geol.*, vol. 22, no. 3, pp. 239–252, Apr. 1990.

[36] S. K. Sahu and K. V. Mardia, "A Bayesian kriged Kalman model for short-term forecasting of air pollution levels," *J. Royal Stat. Soc. Series C (Appl. Statist.)*, vol. 54, no. 1, pp. 223–244, Jan. 2005.

[37] D. Avidor and S. Mukherjee, "Estimation and prediction of the local mean signal power in mobile systems," in *Proc. of the Veh. Tech. Conf.*, vol. 4, Rhodes, Greece, May 2001, pp. 2751–2755.

[38] S. Barbarossa, G. Scutari, and T. Battisti, "Cooperative sensing for cognitive radio using decentralized projection algorithms," in *Proc. of the SPAWC Conf.*, Perugia, Italy, Jun. 2009, pp. 116–120.

[39] J.-A. Bazerque and G. B. Giannakis, "Distributed spectrum sensing for cognitive radio networks by exploiting sparsity," *IEEE Trans. Sig. Proc.*, vol. 58, no. 3, pp. 1847–1862, Mar. 2010.

[40] G. Mateos, J.-A. Bazerque, and G. B. Giannakis, "Spline-based spectrum cartography for cognitive radios," in *Proc. of 43nd Asilomar Conf. on Signals, Systems, and Computers*, Pacific Grova, CA, Nov. 2009.

[41] E. Dall'Anese, S.-J. Kim, and G. Giannakis, "Global channel gain tracking using distributed Kriged Kalman filtering," *IEEE Trans. Veh. Technol.*, Jun. 2010, submitted.

[42] G. L. Stüber, *Principles of Mobile Communication*, 2nd ed. Boston, MA: Kluwer Academic Publishers, 2001.

[43] M. Nakagami, "The m-distribution, a general formula of intensity of rapid fading," *In William C. Hoffman, editor, Statistical Methods in Radio Wave Propagation: Proceedings of a Symposium*, pp. 3–36, Jun. 1958, Permagon Press, 1960.

[44] U. Charash, "Reception through nakagami fading multipath channels with random delays," *IEEE Trans. Commun.*, vol. 27, pp. 657–670, Apr. 1979.

[45] M.-J. Ho and G. L. Stüber, "Co-channel interference of microcellular systems on shadowed Nakagami fading channels," in *Proc. of the IEEE Veh. Tech. Conf.*, Secaucus, NJ, May 1993, pp. 568–571.

[46] R. Prasad and A. Kegel, "Improved assessment of interference limits in cellular radio performance," *IEEE Trans. Veh. Technol.*, vol. 40, no. 2, pp. 412–419, May 1991.

[47] X. Hong, C.-X. Wang, and J. Thompson, "Interference modeling of cognitive radio networks," in *Proc. of the IEEE Veh. Tech. Conf.*, Singapore, May 2008, pp. 1851–1855.

[48] A. J. Goldsmith, L. J. Greenstain, and G. J. Foschini, "Error statistics of real-time power measurements in cellular channels with multipath and shadowing," *IEEE Trans. Veh. Technol.*, vol. 43, no. 3, pp. 439–446, Aug. 1994.

[49] C. K. Wikle and N. Cressie, "A dimension-reduced approach to space-time Kalman filtering," *Biometrika*, vol. 86, no. 4, pp. 815–829, 1999.

[50] J. Cortés, "Distributed Kriged Kalman filter for spatial estimation," *IEEE Trans. Auto. Control*, vol. 54, no. 12, pp. 2816–2827, Dec. 2009.

[51] B. D. Ripley, *Spatial Statistics*. John Wiley & Sons, 1981.

[52] B. D. O. Anderson and J. B. Moore, *Optimal Filtering*. Prentice Hall, 1979.

[53] B. Sinopoli, L. Schenato, M. Franceschetti, K. Poolla, M. I. Jordan, and S. S. Sastry, "Kalman filtering with intermittent observations," *IEEE Trans. Auto. Contr.*, vol. 49, no. 9, pp. 1453–1464, Sep. 2004.

[54] P. K. Suetin, *Orthogonal Polynomials in Two Variables*. CRC Press, 1999.

[55] R. Olfati-Saber, "Distributed Kalman filtering and sensor fusion in sensor networks," in *Proc. of the 44th Conf. on Decision and Control*, Sevilla, Spain, Dec. 2005, pp. 5492–5498.

[56] I. D. Schizas, A. Ribeiro, and G. B. Giannakis, "Consensus in *ad hoc* WSNs with noisy links—part I: distributed estimation of deterministic signals," *IEEE Trans. Sig. Proc.*, vol. 56, no. 1, pp. 350–364, Jan. 2008.

[57] D. P. Bertsekas and J. N. Tsitsiklis, *Parallel and Distributed Computation: Numerical Methods.* Englewood Cliffs, NJ: Prentice Hall, 1989.

[58] S. M. Kay, *Fundamentals of Statistical Signal Processing, Estimation Theory.* Prentice Hall, 1993.

[59] Q. Zhao and B. M. Sadler, "A survey of dynamic spectrum access," *IEEE Sig. Proc. Magazine*, pp. 79–89, 2007.

[60] H. Urkowitz, "Energy detection of unknown deterministic signals," *Proc. IEEE*, vol. 55, no. 4, pp. 523–531, Apr. 1967.

[61] D. Cabric, A. Tkachenko, and R. W. Brodersen, "Spectrum sensing measurements of pilot, energy, and collaborative detection," in *Proc. of the MILCOM Conf.*, Washington, D.C., Oct. 2006, pp. 1–7.

[62] Z. Quan, S. Cui, H. V. Poor, and A. H. Sayed, "Collaborative wideband sensing for cognitive radios," *IEEE Sig. Proc. Mag.*, vol. 25, no. 6, pp. 60–73, Nov. 2008.

[63] S.-J. Kim and G. B. Giannakis, "Rate-optimal and reduced-complexity sequential sensing algorithms for cognitive ofdm radios," *EURASIP J. Adv. Signal Process*, vol. 2009, pp. 2:1–2:11, March 2009.

[64] P. D. Sutton, K. E. Nolan, and L. E. Doyle, "Cyclostationary signature in practical cognitive radio applcations," *IEEE J. Sel. Areas Commun.*, vol. 26, no. 1, pp. 13–24, Jan. 2008.

[65] E. Visotsky, S. Kuffner, and R. Peterson, "On collaborative detection of TV transmissions in support of dynamic spectrum sharing," in *Proc. of the DySPAN Conf.*, Baltimore, MD, Nov. 2005, pp. 338–345.

[66] G. Ganesan, Y. Li, B. Bing, and S. Li, "Spatio-temporal sensing in cognitive radio networks," *IEEE J. Sel. Areas Commun.*, vol. 26, no. 1, pp. 5–12, Jan. 2008.

[67] J. Unnikrishnan and V. V. Veeravalli, "Cooperative sensing for primary detection in cognitive radio," *IEEE J. Sel. Topics Sig. Proc.*, vol. 2, no. 1, pp. 18–27, Feb. 2008.

[68] J. Ma, G. Zhao, and Y. Li, "Soft combination and detection for cooperative spectrum sensing in cognitive radio networks," *IEEE Trans. Wireless Commun.*, vol. 7, no. 11, pp. 4502–4507, Nov. 2008.

[69] N. Cressie, "The origin of Kriging," *Mathematical Geology*, vol. 22, no. 3, pp. 239–252, 1990.

[70] M. Wellens, J. Riihijärvi, M. Gordziel, and P. Mähönen, "Spatial statistics of spectrum usage: From measurements to spectrum models," in *Proc. of the ICC Conf.*, Dresden, Germany, Jun. 2009, pp. 1–6.

[71] R. Tibshirani, "Regression shrinkage and selection via the Lasso," *J. Royal Stat. Soc.*, vol. 58, no. 1, pp. 267–288, 1996.

[72] E. Candès and T. Tao, "Near optimal signal recovery from random projections: Universal encoding strategies?" *IEEE Trans. Info. Theory*, vol. 52, no. 12, pp. 5406–5425, 2006.

[73] S. S. Chen, D. L. Donoho, and M. A. Saunders, "Atomic decomposition by basis pursuit," *SIAM J. Sci. Comput.*, vol. 20, no. 1, pp. 33–61, 1998.

[74] G. Taubock and F. Hlawatsch, "A compressed sensing technique for ofdm channel estimation in mobile environments: exploiting channel sparsity for reducing pilots," in *Int. Conf. Acoust., Speech, Signal Process.*, Las Vegas, NV, Apr. 2008.

[75] T. Hastie, R. Tibshirani, and J. Friedman, *The Elements of Statistical Learning*, 2nd ed. New York: Springer, 2009, 2009.

[76] T. T. Wu and K. Lange, "Coordinate descent algorithms for lasso penalized regression," *Ann. Appl. Statist.*, vol. 2, pp. 224–244, 2008.

[77] P. Tseng, "Convergence of block coordinate descent method for non-differentiable minimization," *J. Optimiz. Theory Appl.*, vol. 109, pp. 475–494, Jun 2001.

[78] J. Friedman, T. Hastie, H. Höfling, and R. Tibshirani, "Pathwise coordinate optimization," *Ann. Appl. Statist.*, vol. 1, pp. 302–332, Dec 2007.

[79] D. Angelosante, J.-A. Bazerque, and G. B. Giannakis, "Online adaptive estimation of sparse signals: Where RLS meets the ℓ_1-norm," *IEEE Trans. Sig. Proc.*, vol. 58, no. 7, pp. 3436–3447, Jul. 2009.

[80] M. F. Catedra and J. Perez, *Cell Planning for Wireless Communications*, 1st ed. Norwood, MA, USA: Artech House, Inc., 1999.

[81] J.-A. Bazerque and G. B. Giannakis, "Distributed spectrum sensing for cognitive radio networks by exploiting sparsity," *IEEE Trans. Sig. Proc.*, vol. 58, no. 3, pp. 1847–1862, Mar. 2010.

[82] A. Goldsmith, *Wireless Communications.* Cambridge University Press, 2005.

[83] T. ElBatt and A. Ephremides, "Joint scheduling and power control for wireless ad hoc networks," *IEEE Trans. Wireless Commun.*, vol. 3, no. 1, pp. 74–85, 2004.

[84] Z.-Q. Luo and S. Zhang, "Dynamic spectrum management: Complexity and duality," *IEEE J. Sel. Topics Sig. Proc.*, vol. 2, no. 1, pp. 57–73, Feb. 2008.

[85] M. Chiang, C. W. Tan, D. P. Palomar, D. O'Neill, and D. Julian, "Power control by geometric programming," *IEEE Trans. Wireless Commun.*, vol. 6, no. 7, pp. 2640–2651, Jul. 2007.

[86] J. Huang, R. Berry, and M. L. Honig, "Spectrum sharing with distributed interference," in *Proc. of IEEE Symp. New Frontiers in Dynamic Spectrum Access Networks (DySPAN)*, Nov. 2005.

[87] M. Charafeddine and A. Paulraj, "Sequential geometric programming for 2×2 interference channel power control," in *Proc. CISS*, Mar. 2007, pp. 185–189.

[88] A. Ghasemi and E. S. Sousa, "Fundamental limits of spectrum-sharing in fading environments," *IEEE Trans. Wireless Commun.*, vol. 6, no. 2, pp. 649–658, Feb. 2007.

[89] J.-S. Pang, G. Scutari, D. P. Palomar, and F. Facchinei, "Design of cognitive radio systems under temperature-interference constraints: a variational inequality approach," in *Proc. of IEEE ICASSP*, Mar. 2010.

[90] I. Mitliagkas, N. Sidiropoulos, and A. Swami, "Convex approximation-based joint power and admission control for cognitive underlay networks," in *Proc. of the IEEE IWCMC Conf.*, Crete, Greece, 2008, pp. 28–32.

[91] R. Zhang, "Optimal power control over fading cognitive radio channel by exploiting primary user CSI," in *Proc. of IEEE Globecom*, Nov.–Dec. 2008.

[92] R. Zhang and Y. C. Liang, "Exploiting multi-antennas for opportunistic spectrum sharing in cognitive radio networks," *IEEE J. Sel. Topics Sig. Proc.*, vol. 2, no. 1, pp. 88–102, Feb. 2008.

[93] A. G. Marques, X. Wang, and G. B. Giannakis, "Dynamic resource management for cognitive radios using limited-rate feedback," *IEEE Trans. Sig. Proc.*, vol. 57, no. 9, pp. 3651–3666, Sep. 2009.

[94] M. Biguesh, S. Shahbazpanahi, and A. B. Gershman, "Robust downlink power control in wireless cellular systems," *EURASIP Journal on Wireless Communications and Networking*, pp. 261–272, Dec. 2004.

[95] H. A. Suraweera, P. J. Smith, and M. Shafi, "Capacity limits and performance analysis of cognitive radio with imperfect channel knowledge," *IEEE Trans. Veh. Technol.*, vol. 59, no. 4, pp. 1811–1822, May 2010.

[96] L. F. Fenton, "The sum of lognormal probability distributions in scatter transmission systems," *IRE Trans. Commun. Syst.*, vol. 8, no. 1, pp. 57–67, Mar. 1960.

[97] A. A. Abu-Dayya and N. C. Beaulieu, "Outage probabilities in the presence of correlated lognormal interferers," *IEEE Trans. Veh. Technol.*, vol. 43, no. 1, pp. 164–173, Feb. 1994.

[98] S. Boyd and L. Vandenberghe, *Convex Optimization*. Cambridge University Press, 2004.

[99] A. Nasif and B. Mark, "Opportunistic spectrum sharing with multiple cochannel primary transmitters," *IEEE Trans. Commun.*, vol. 8, no. 11, pp. 5702–5710, May 2009.

[100] S. Kandukuri and S. Boyd, "Optimal power control in interference-limited fading wireless channels with outage-probability specifications," *IEEE Trans. Wireless Commun.*, vol. 1, no. 1, pp. 46–55, Jan. 2002.

[101] S. Schwartz and Y. Yeh, "On the distribution function and moments of power sums with lognormal components," *Bell Syst. Tech. J.*, vol. 61, no. 7, pp. 1441–1462, Sep. 1982.

[102] D. C. Schleher, "Generalized Gram-Charlier series with application to the sum of log-normal variates," *IEEE Trans. Info. Theory*, vol. 23, no. 2, pp. 275–280, Mar. 1977.

[103] N. B. Mehta, J. Wu, A. F. Molisch, and J. Zhang, "Approximating a sum of random variables with a lognormal," *IEEE Trans. Wireless Commun.*, vol. 6, no. 7, pp. 2690–2699, Jul. 2007.

[104] S. Boyd, S.-J. Kim, L. Vandenberghe, and A. Hassibi, "A tutorial on geometric programming," *Optim. Eng.*, vol. 8, pp. 67–127, 2007.

[105] B. R. Marks and G. P. Wright, "A general inner approximation algorithm for nonconvex mathematical programs," *Oper. Res.*, vol. 26, no. 4, pp. 681–683, Jul.-Aug. 1978.

[106] M. Avriel and A. C. Williams, "Complementary geometric programming," *SIAM Journal on Applied Mathematics*, vol. 19, no. 1, pp. 125–141, Jul. 1970.

[107] M. Avriel, R. Dembo, and U. Passy, "Solution of generalized geometric programs," *International Journal for Numerical Methods in Engineering*, vol. 9, pp. 149–168, 1975.